April 2018

Remote Control Aircraft for SAE Aero Design West Competition

Andrew Hunter Libby
Worcester Polytechnic Institute

Blake Rice
Worcester Polytechnic Institute

Clifford Edward Smith
Worcester Polytechnic Institute

Elio G. Daci
Worcester Polytechnic Institute

Emily Chretien
Worcester Polytechnic Institute

See next page for additional authors

Follow this and additional works at: https://digitalcommons.wpi.edu/mqp-all

Author

Andrew Hunter Libby, Blake Rice, Clifford Edward Smith, Elio G. Daci, Emily Chretien, John Russell, Kamyar Sajjadi, Nabeel J. Tokatli, Ryan Capozzi, Shintaro N. Clanton, Stephen J. Peccerillo, and Timothy Liam Jones

Remote Control Aircraft for the SAE Aero Design West Competition

A Major Qualifying Project Report
Submitted to the Faculty of the
WORCESTER POLYTECHNIC INSTITUTE
in Partial Fulfillment of the Requirements for the
Degree of Bachelor of Science
in Aerospace Engineering

by

_____ _____ _____

Ryan Capozzi Emily Chretien Shintaro Clanton

_____ _____ _____

Elio Daci Timothy Jones Andrew Libby

_____ _____ _____

Stephen Peccerillo Blake Rice John Russell

_____ _____ _____

Kamyar Sajjadi Clifford Smith Nabeel Tokatli

April 26, 2018

Approved by: _____

David J. Olinger, Advisor
Aerospace Engineering Program
Mechanical Engineering Department, WPI

_____

Raghvendra V. Cowlagi, Co-Advisor
Aerospace Engineering Program
Mechanical Engineering Department, WPI

Abstract

The purpose of this project was to design a remote controlled aircraft for the Society of Automotive Engineers 2018 Aero Design West competition. Students were asked to employ knowledge of aerodynamics, structural mechanics, control systems, electrical engineering, and design principles to create an airworthy submission. Using various analysis tools, the team designed, constructed, and tested an aircraft capable of carrying 7 pounds of payload for the prescribed competition flight pattern, which limited the takeoff distance to 200 feet and required a circular flight pattern followed by a controlled landing and stop. The 12-foot wingspan aircraft is constructed mostly from foam and aluminum, and conforms to all competition specifications, with the exception of the electric motor power.

Acknowledgements

We would like to thank the following individuals and groups for their help and support throughout the entirety of this project.

Project Advisor   Professor David J. Olinger

Project Co-Advisor   Professor Raghvendra V. Cowlagi

Millis RC Club Pilots   Scott Annis & Mickey Callahan

Financial Administrator   Barbara Furhman

Table of Authorship

Section	Author(s) of Section	Project Work Completed By
Introduction and Background		
I.1, I.2	CS, EC	CS, EC
I.3	CS, EC, JR, KS, NT, ED	all
Literature Review		
II.1	CS, EC	
II.2	CS, EC	EC, ED
II.3	AL, CS, EC, SP	AL, SP
II.4	CS, EC, KS, RC	RC, KS
II.5	CS, EC, SC, TJ	TJ, SC
II.6	CS, EC, JR	CS, JR
System Design		
III.1.1	CS, EC	EC, ED
III.1.2	AL, SP, CS, EC, JR	AL, SP
III.1.3	KS, RC, EC	RC, KS
III.1.4	NT, CS, EC	NT, BR
III.1.5	CS, EC, JR	CS, JR
III.2	CS, EC	
III.3	SP, AL, EC	AL, SP, JR
III.4	CS, EC, ED, KS	EC, CS, ED, KS
III.5	KS, JR, EC	KS, CS, JR
III.6	KS, EC, ED	EC, NK, BR, ED
Fabrication		
IV.1	EC	BR, EC
IV.2	EC, TJ, RC	TJ, NK, JR

IV.3	TJ, EC	TJ, EC, ED, NK, BR, CS, RC, SC, AL, JR
IV.4	ED, EC	all
IV. 5	ED, EC	EC, NK, BR, CS
Aircraft Testing and Modifications		
V.1	EC	NK, BR, EC
V.2	JR, EC	all
V.3	EC, JR, ED	all
V.4.1	KS, EC	KS, EC, CS, NK, BR
V.4.2	EC, CS, KS	EC, CS, KS
V.4.3	EC	EC, CS
V.4.4	SP, AL, JR, EC, ED	SP, AL, JR, NK, BR, TJ
V.4.5	BR, EC	BR, NK
V.5	EC, JR, ED	JR, SC, ED, RC, AL, NK
Results and Conclusions		
VI.1, VI.2	TJ, RC, ED, EC	all

Student initials shown.

Contents

List of Figures

List of Tables

Part I
Introduction and Background

The purpose of this Major Qualifying Project (MQP) was to enter a remote controlled (RC) aircraft into the Society of Automotive Engineers (SAE) 2018 Aero Design West competition. Students were tasked to employ knowledge of aerodynamics, structural mechanics, control systems, electrical engineering, and design principles to create an airworthy submission. In general, the three main phases of the design process aligned with each seven week term at Worcester Polytechnic Institute (WPI). The initial design phase occurred during A Term, B Term was reserved for the construction of multiple design iterations, and final development and testing resided during C Term.

1 Project Objective and Design Goals

As defined in the 2018 Collegiate Design Series - SAE Aero Design Rules (included in Appendix A), the objective of the competition was to score as many overall points as possible in order to achieve the highest overall score, called the Final Flight Score (FFS). Points toward the FFS were awarded in a number of separate flight rounds. During each flight round, a team accumulated points toward an individual Flight Score (FS) for that round. In each round, the aircraft needed to successfully takeoff, complete a simple flight circuit, and land in order to score points. For successful flights, teams accumulated points based on the number of "passengers," represented by tennis balls, and additional "luggage," or cargo weight. The aircraft was configured to hold a pre-specified number of passengers in designated "seats" as well as 0.5 pounds or more of "luggage" per passenger, bolted into a single mass and secured in a "cargo bay." Flying with fewer passengers and associated luggage than the number of seats for which the aircraft is designed resulted in a lower score.

The 2018 Collegiate Design Series - SAE Aero Design Rules provided the following two equations for the calculation of the FFS and each FS:

$$FFS = Final\ Flight\ Score = \frac{1}{40N}\left[\sum_{1}^{N}(FS)\right] \tag{1}$$

and

$$FS = Flight\ Score = 100P + 50C - 100E \tag{2}$$

Where P is the number of seated passengers on the flight, C is the cargo weight in pounds, E is the number of empty seats, and N is the number of flight attempts.

1.1 Competition Rules and Design Constraints

Some restrictions placed on the aircraft resulted from FAA regulations as well as other rules to increase safety and equalize the competitive aspect of the event. New restrictions for the 2018 competition reduced the maximum wingspan to 144 inches, the maximum total aircraft power to 1000 Watts, and a battery to 6 cell lithium polymer battery with a minimum of 3000 mAh. At the competition, teams were allotted one minute to fully load the passengers and associated cargo for the flight and one minute to unload afterwards. The aircraft needed to take off within 200 feet of a designated start line on the runway and make its initial turn no sooner than 400 feet from the start line. The landing constraints were similar, requiring the aircraft to fly an oval flight path to land on the runway in the same direction as takeoff, and come to a controlled stop within 400 feet. A complete set of rules are in the 2018 Collegiate Design Series - SAE Aero Design Rules, included in Appendix A of this report.

2 Project Timeline

The project ran from early September 2017 through April 2018. WPI's seven-week academic terms formed the time frame for the three main phases of the project. During A Term, which spanned the last week of August through mid-October, the team focused on research and began the initial design of the aircraft. Team members used textbooks and other references to develop an index of key equations as well as spreadsheets, software, and analysis tools that could be used later in the design process. Project advisor Professor Cowlagi provided a constructed Horizon Hobby plane that the team used to confirm the accuracy of these analysis tools and equations.

SAE International released the official rules for the 2018 Aero Design Competition on September 14, 2017. The team studied these rules in detail, then used them to help make initial design decisions. The last three weeks of the A Term consisted of developing initial designs for the propulsion system, wings, and fuselage structure. Official registration for the SAE Aero Design West competition occurred on October 2, 2018.

During B Term (mid-October through mid-December) the team constructed and tested prototypes from the initial designs. An iterative process of prototyping, analyzing, and adjusting refined the aircraft designs and developed detailed designs for the payload arrangement, controls surfaces, and electronics layout. After selecting materials and fabrication methods, the team began constructing the full aircraft.

C Term ran from mid-January to the first week of March and involved final manufacturing of the aircraft, test flights, and adjustments. The faculty advisers set a date of February 23, 2018 in C Term as the deadline for a successful test flight in order for the team to travel to compete in the Aero Design West competition in D Term. D Term began in mid-March and consisted of final preparations for the competition. The Aero Design West competition was April 6 through April 8, 2018 in Van Nuys, California.

Figure 1 summarizes the major phases and milestones of the project.

MQP Lifecycle

A-term
- Design and analysis. DESIGN
- MQP Report: Intro, Literature review, preliminary design.
- Online registration for SAE AERO events will open on October 2, 2017 at 10:00 AM EDT.

B-term
- Development and design iterations. BUILD
- MQP Report: Final design, fabrication, preliminary testing.

C-term
- Development and testing. TEST
- MQP Report: Final testing, conclusions + SAE Design Report.
- REQUIRED SUCCESSFUL TEST FLIGHT BY READING DAY FEBRUARY 23, 2018 to attend competition.

D-term
- SAE Aero Design West Competition, April 6-8, 2018 (start of D term)
- Project presentation day. PRESENT/COMPETE
- MQP Report: finish; sign eCDR to complete MQP
- AIAA student paper competition ?

Figure 1: MQP timeline and important dates [1]

3   Team Organization

The project team divided into sub-groups for each of the three phases of the design process. Each sub-group met several times each week and focused on a particular area of research or work. Twice a week, the entire project team met with the project advisors to report on progress and share important information across sub-groups.

3.1   Sub-Groups for Research and Initial Design (A Term)

At the first full project team meeting with advisors, the advisors proposed a set of six sub-groups for the first phase of the project. These sub-groups were aerodynamics, stability controls, propulsion, Computer Aided Design (CAD) structures, hardware structures, and software/simulations. Each project member ranked their preference of the six sub-groups through a Google Form, and one project member used the survey results to assign project members to groups. Each sub-group consisted of two team members and focused on researching their particular area of aircraft design. Teams developed research and design tools and began making preliminary design decisions. The following sections describe the six sub-groups and their roles in the first design phase.

3.1.1   Aerodynamics

The aerodynamics team consisted of Emily Chretien and Elio Daci. This team investigated the aerodynamic forces that act on an aircraft in flight, different measures of aerodynamic performance, and what design parameters influence the forces and performance of an aircraft. Selecting the airfoil, designing the wing shape, and creating preliminary tail designs were among the tasks this team completed during the first phase of the project. This team worked closely with the CAD structures and software teams to validate design tools and decisions.

3.1.2   Propulsion

The propulsion team consisted of Stephen Peccerillo and Hunter Libby. This team was responsible for the design of the aircraft's electric prop-motor systems. They researched the fundamentals of batteries and electric motors to optimize thrust within the given power restrictions. In addition, they utilized a wind tunnel to run static and dynamic thrust tests to validate the theoretical capabilities of the propulsion system.

3.1.3   Stability and Control

Team members Ryan Capozzi and Kamyar Sajjadi formed the stability and controls team. This team analyzed aircraft dynamics, performance, and control systems to achieve stability of the design. They investigated the effects of center of gravity, neutral point, and static margin, and evaluated dynamical stability using stability derivatives by accounting for total moments. The tasks of the controls team included analyzing various controls parameters and applying control surfaces and hinge equations for a stable aircraft.

3.1.4   Computer Aided Design (CAD) Structures

The CAD structures team consisted of Nabeel Tokatli and Blake Rice. This team focused on the structural design and analysis of the aircraft. They specifically utilized computer-based software such as SOLIDWORKS to create 3-dimensional (3D) models and perform preliminary stress and deflection analyses of components. When designing the full aircraft, the team also ran full body analyses to ensure structural integrity.

3.1.5 Hardware Structures

The hardware structures team, composed of Shintaro Clanton and Timothy Jones, focused on the materials and fabrication portion of the design process. They used software such as ANSYS and CES EduPak to investigate appropriate materials and material properties for the fabrication of the aircraft. They tested and evaluated potential materials, adhesives, and manufacturing methods for the construction of the fuselage, wings, and wing spars. Properties such as strength, yield stress, young's modulus, cost, and manufacturability factored into material decisions.

3.1.6 Software Analysis

The software team, Clifford Smith and John Russell, were tasked with researching and learning computer-based tools that would help the team validate and test different designs and plane configurations. Working closely with the aerodynamics team, the software team used tools such as XFLR5 to analyze potential airfoils, wing shapes, tail shapes, and other design considerations the aerodynamics team suggested.

3.2 Sub-Groups for Final Design and Construction (B and C Terms)

The team restructured in B Term in order to better distribute remaining tasks and ensure that team members had the opportunity to work on multiple areas of the project and were not restricted to just one element. The team divided into two primary sub-teams, design and manufacturing. The design team, led by Nabeel Tokatli, was responsible for the developing the final design of the plane, ensuring all flight characteristics and calculations were accurate. The manufacturing team, led by John Russell, was responsible for identifying and testing fabrication methods for different aircraft parts, as well as manufacturing aircraft prototypes as prescribed by the design team. The two teams worked closely to ensure all aspects of the aircraft were designed in a way that could be fabricated with the available supplies, and that prototypes and aircraft parts were correctly built.

The two team leaders were responsible for identifying and delegating tasks to team members, setting deadlines, and assessing progress for their team. In addition, the two team leaders reported to a third sub-group, the logistics committee. The logistics committee, led by Emily Chretien, included members from both the design and manufacturing teams and served as an interface between the two teams. In addition to facilitating communication between all team members, this committee was responsible for overall project management and any auxiliary needs or functions that arose, such as travel arrangements and budgeting. This committee set weekly goals for both the design and manufacturing team and delegated tasks to ensure the project stayed on schedule.

Figure 2 depicts the B Term team organizational structure.
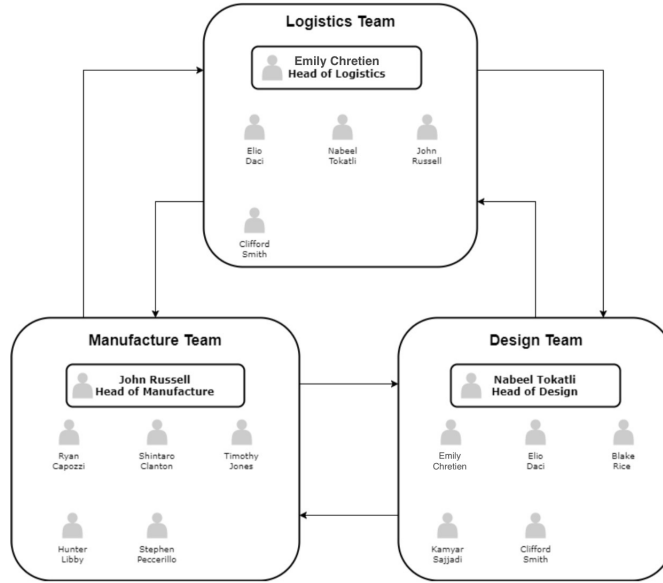
Figure 2: Team organizational structure for B Term, which consists of the manufacturing and design sub-teams reporting to the logistics committee

Part II
Literature Review

Background investigation began with the review of previous MQP reports from teams competing in similar model aircraft competitions. While most of these teams competed in the micro class of the SAE Aero Design or Design/Build/Fly (DBF) competition events, the MQP reports gave general guidelines for the model aircraft design and build processes. The team frequently referred to the 2014 DBF MQP report, as this recent report contained similar design goals and restrictions to the 2018 competition.

Another type of reference material resided in student notes from controls, aerodynamics, and aircraft design classes at WPI. These notes also provided a general timeline for the design process, but also gave specific equations, design trends, and optimizations. Textbooks provided additional theory and equations for reference during the design process.

1 Describing Aircraft Motion

In order to design an aircraft to achieve specific performance goals, the team needed to establish a method for describing aircraft design and performance parameters. It is simplest to describe the shape of an aircraft and aircraft motion using a body-fixed coordinate system. Conventionally, this is a Cartesian Coordinate system with the origin located on a plane of symmetry in the body, typically either at the tip of the nose cone or on the leading edge of the wings. For the purpose of this project, the team chose to center the origin on the leading edge of the wings. The X-axis of this coordinate system points forward toward the nose cone, the Y-axis in the direction of the right wing, and the Z-axis completes the triad by pointing downward through the plane of symmetry.

Aircraft motion is described in terms of translation and rotation about the X, Y, and Z axes. Rotation around the X-axis is called "roll," rotation about the Y-axis is called "pitch," and rotation about the Z-axis is called "yaw" [2]. Figure 3 depicts the body-fixed coordinate system and three axial rotations.
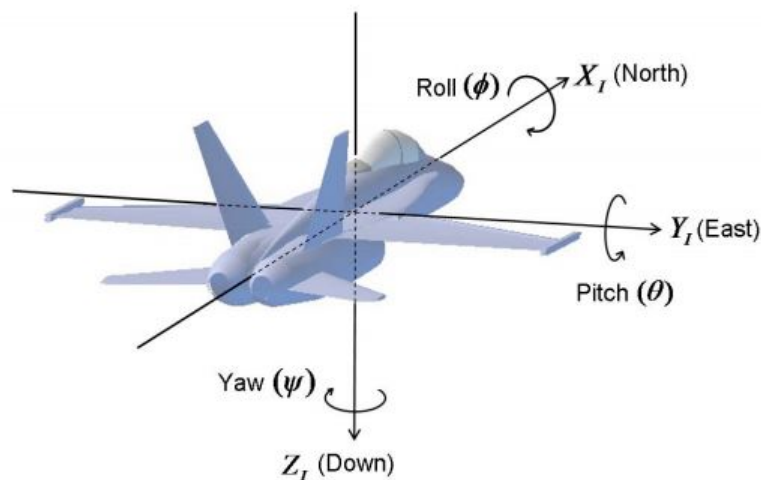
Figure 3: Coordinate system and axial rotations of an aircraft. Copyright: CHRobotics LLC. [2]

2   Aerodynamics

The aerodynamics team sought to gain a general overview of various design parameters and how manipulating these parameters controls the aerodynamic performance of the aircraft. This section introduces the primary aerodynamic forces and moments, the aerodynamic properties of airfoils, and the characteristics of finite-length wings.

2.1   Aerodynamic Forces and Moments

The four fundamental forces that act on an aircraft in flight are:

1. The weight force (W) due to the mass of the body and the gravitational acceleration of the earth. This force is equivalent to the mass of the aircraft (m) multiplied by the gravitational acceleration constant (g), and acts downward toward the center of the earth. It can be approximated as a point-force located on the body's Center of Gravity (CG).

2. The thrust force (T) produced by the aircraft's propulsion system. The magnitude and direction of this force depend on the specific propulsion system, but for most fixed-wing aircraft, the thrust vector is directed forward along the aircraft's X-axis.

3. The lift force (L) generated by the air pressure gradient across the upper and lower lifting surfaces of the aircraft. The magnitude of the lift force is dependent upon many factors, including the shape of the body and the speed of the airflow across the body, and acts in the direction perpendicular to the air-relative velocity. The place on the aircraft at which this force can be approximated as a point-force is called the Center of Lift (CL).

4. The drag force (D), is a result of friction forces between the air molecules and surface molecules of the moving aircraft. The magnitude of the drag force depends on the shape of the body and the speed of the body through the air. The drag vector is antiparallel to the velocity vector of the aircraft relative to the surrounding air.

Additionally, the aerodynamic forces of a moving aircraft produce a moment about the Y-axis. This moment, called the pitch moment (M), is often measured about the leading edge of the wing (X = 0 in the body-fixed coordinates). A positive pitch moment causes a "nose-up" condition [3].

The magnitude of these forces and moments are directly related to the air-relative velocity and the shape of the aircraft's lifting surfaces, as the following sections describe. Figure 4 depicts these primary aerodynamic forces and moments on a fixed-wing aircraft.
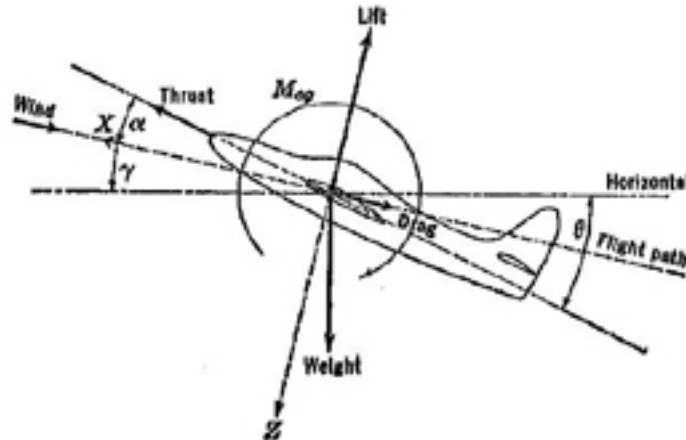
Figure 4: Aerodynamic forces and moments. Copyright: TLG Aerospace, LLC. [4]

2.2 Airfoil Properties

The airfoil, or the cross-section shape of a wing or other lifting surface, guides the flow of air across the upper and lower surfaces to produce a pressure gradient and generate lift for the aircraft [3]. An airfoil can be described by its chord line, thickness, and camber line. The chord line is an imaginary straight line drawn between the leading edge and the tailing edge of an airfoil, with the length of this line being the chord length, or simply the chord [3]. The thickness of an airfoil is the vertical distance between the upper and lower surfaces, and can vary along the airfoil. The camber line is an imaginary curve drawn from the leading edge to the trailing edge of the airfoil, passing through the centerline between the upper and lower surfaces at each point on the airfoil [3]. The camber at a given point, then, is the distance between the chord line and the camber line, and is a measure of the curvature of the airfoil. The maximum thickness and the maximum camber of an airfoil are typically described as a percentage of the airfoil's chord length [3].

The thickness and camber profiles of an airfoil influence the ability of the airfoil to generate lift, drag, and pitch moment during motion. The amount of lift a wing with a particular airfoil cross-section has the ability to produce is characterized by its lift coefficient (C_L). This dimensionless value obeys the following equation[3]:

$$C_L = \frac{L}{qS} \tag{3}$$

where S is the planform surface area of the wing and q is the dynamic pressure [3]. The dynamic pressure (q) is a function of the air density (ρ) and the relative velocity (V) of the wing through the air, and can be found using the following equation [3]:

$$q = \frac{1}{2}\rho V^2 \tag{4}$$

The lift equation shows that for a constant dynamic pressure and wing area, the magnitude of the lift force generated is directly proportional to the coefficient of lift. The lift coefficient for a particular airfoil shape varies with angle of attack, which is the inclination angle between the air-relative velocity vector and the airfoil chordline [3]. Figure 5 shows a plot of lift coefficient as a function of angle of attack (α), which is called the lift curve. At low angles of attack, the lift coefficient increases approximately linearly as the angle of attack increases, until the angle of attack reaches the angle of attack at which the wing stalls (stall). At this point, the wing's lift coefficient reaches its maximum (C_{Lmax}). The wing also has an angle of zero lift (α_{0L}), which is an angle of attack at which the wing does not produce any lift force [5]. The angle of zero lift, maximum lift coefficient, and stall angle of attack are all dependent upon the specific shape of the airfoil profile.
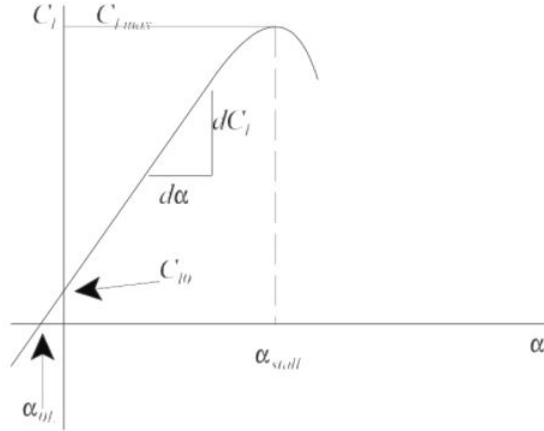
Figure 5: Lift curve. Copyright: Fredrick H. Lutze, 2003 [3]

Similarly, the airfoil shape and angle of attack influences the drag coefficient (C_D) and the drag curve (drag as a function of angle of attack) of the wing. As with lift, the drag generated by an airfoil is a function of dynamic pressure, wing area, and drag coefficient:

$$C_D = \frac{D}{qS} \tag{5}$$

The ratio between the lift force and the drag force is an important quantity that describes the aerodynamic performance of an airfoil or wing [5]. The lift-to-drag ratio ($\frac{L}{D}$) is then also a function of angle of attack, and is equivalent to the ratio of the lift and drag coefficients:

$$\frac{L}{D} = \frac{C_L}{C_D} \tag{6}$$

The final dimensionless coefficient used to characterize and compare airfoils is the pitch moment coefficient (C_M). The following equation relates the pitch moment about the leading edge generated by a wing to the pitch moment coefficient:

$$C_M = \frac{M}{qSc} \tag{7}$$

Unlike the lift and drag forces, the pitch moment is also proportional to the moment arm, or the chord length c [5]. If the reference point for the pitch moment is some location A other than the leading edge, then the following equation is used to calculate the pitch moment coefficient about point A (C_{MA}) from the pitch moment coefficient about the leading edge (C_M):

$$C_{MA} = C_M + C_L l_A \tag{8}$$

in which l_A is the distance between point A and the leading edge [3]. As with the lift and drag coefficients, the moment coefficient varies with angle of attack. However, there is one location on the wing about which the pitch moment coefficient is constant across all angles of attack [3]. This wing location is the aerodynamic center of the wing [3]. For most wings for subsonic aircraft, the aerodynamic center is approximately located at the quarter-chord, or the location one-quarter of the chord length behind the leading edge [3].

Depending on the aircraft application, different combinations of lift, drag, and pitch moment are desired for the required velocity and angle of attack ranges. Therefore, it is important to tailor the airfoil and wing shape to achieve the most applicable properties. Plots such as the lift curve, drag curve, pitch moment curve, and lift-to-drag ratio profile are helpful for comparing different airfoil shapes.

2.3 Wing Properties

As the primary source of lift for the aircraft, the shape of the wings has a significant impact on aerodynamic performance. The equations in the previous section demonstrates how the magnitude of the lift force, drag force, and pitch moment are all directly proportional to the surface area of the wing. Therefore, a larger wing area generates more lift, but at the cost of increased drag. Additionally, a wing with a longer chord length generates a greater pitch moment than a wing of the same surface area with a shorter chord length. Thus the application of the aircraft and the desired lift, drag, and moment properties help determine what wing shape is most appropriate. This investigation focused on wing geometry that are most effective for low-speed, heavy-lifting applications.

2.3.1 Induced Drag and Wingtip Effects

Unlike a simple airfoil, a wing of finite length is 3-dimensional and experiences downwash. Downwash occurs at the ends of the wing, when air of high pressure from below the wing flows to the area of low pressure above the wing by creating vortices about the wing tips [3]. Figure 6 demonstrates this effect. These vortices produce a downward force on the wing, called the downwash force (w), which results in a reduced angle of attack. The amount by which the downwash decreases the angle of attack is called the induced angle of attack (i). Reducing the angle of attack also reduces the lift coefficient, resulting in a smaller lift force. It also offsets the lift force vector by the same angle of induced angle of attack; the component of the offset lift force in the same direction as the drag vector is the induced drag (D_i) [3]. Figure 7 depicts these induced angles and forces. One of the main goals when selecting a wing shape is to minimize this induced drag.
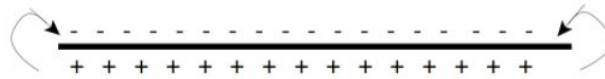
Figure 6: Downwash vortices on a wing of finite length. Copyright: Fredrick H. Lutze, 2003 [3]
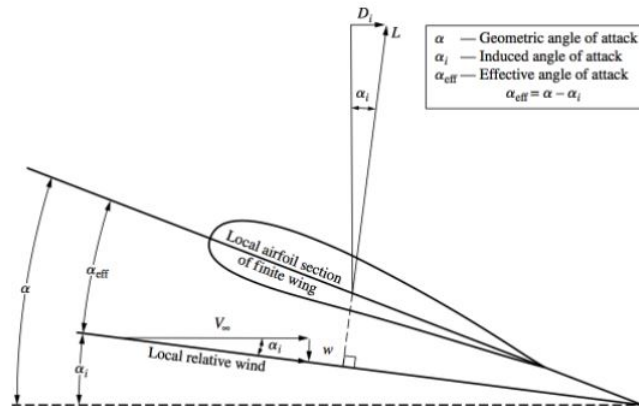
Figure 7: Induced angle of attack and induced drag as a result of downwash. Copyright: John D. Anderson, 2016 [5]

2.3.2 Describing Wing Geometry

The surface area of the wing is defined by the wingspan (b) and the chord length, and is calculated from simple geometric equations. For any wing shape other than a rectangle, the chord length varies along

the length of the wing. It is often useful to describe the wing in terms of the chord length at the fuselage, or the "root" (c_r), and the chord length at the wing tip (c_t) [3]. In a tapered wing, the ratio between these two chord lengths is known as the taper ratio (λ):

$$\lambda = \frac{c_t}{c_r} \tag{9}$$

For non-rectangular wings, other reference chord lengths describe the wing shape and can be used to simplify aerodynamic calculations. One such reference chord length is the mean geometric chord (c_g). The mean geometric chord of a particular wing of any shape is equal to the chord length of a simple rectangular wing of the same wingspan and area [3]. Therefore, for a rectangular wing, this is simply:

$$c_g = \frac{S}{b} \tag{10}$$

and for a straight tapered wing:

$$c_g = \frac{c_r}{2}\left(1 + \lambda\right) \tag{11}$$

More generally, the following equation calculates the mean geometric chord for a wing of any shape [3]:

$$c_g = \frac{2}{b} \int_0^{b/2} c(y)dy \tag{12}$$

Similar to the mean geometric chord is the mean aerodynamic chord, or MAC ($\bar{c}$). The MAC of any shape wing is the chord length of a rectangular wing of the same span that has equivalent pitch moment characteristics as the original wing [3]. The generic MAC equation is:

$$\bar{c} = \frac{2}{S} \int_0^{b/2} \left[c(y)\right]^2 dy \tag{13}$$

and simplifies to

$$\bar{c} = \frac{2}{3}c_r \frac{1 + \lambda + \lambda^2}{1 + \lambda} \tag{14}$$

for a straight tapered wing [3]. These reference chord lengths help to describe non-rectangular wings and simplify geometric and aerodynamic calculations.

A common way to characterize different wing shapes is by aspect ratio (AR). The aspect ratio of a wing is the ratio of the span to the mean geometric chord. For non-rectangular wings, the chord length is not constant along the wing, so it is useful to also define the aspect ratio in terms of the span and wing area [3]:

$$AR = \frac{b}{c_g} = \frac{b^2}{S} \tag{15}$$

A wing with a high aspect ratio wing is long (spanwise) and thin (chordwise), while a low aspect ratio wing is short and wide.

2.3.3 Wing Sizing

Since the lift force, drag force, and pitch moment are all directly proportional to the lifting surface area, the size of the wing – which serves as the primary lifting surface – has a significant impact on the aerodynamic performance of the aircraft. Intuitively, a large wing surface is desirable for maximum lift. However, this comes at the cost of increased drag, weight, and cost. Therefore, the wings should be as large enough to achieve the necessary lift forces for the desired flight maneuvers of the aircraft, but not excessively large in order to curb drag, weight, and cost.

The surface area is adjusted by manipulating the wingspan and mean geometric chord. Manipulating these variables also changes the aspect ratio of the wings. The aspect ratio plays an important role in the aerodynamic performance as well as stability of the aircraft. Wings of higher aspect ratio produce less induced drag than wings of low aspect ratios. Since the pitch moment is directly proportional to the chord length as well as surface area, wings of low aspect ratio also generate a greater pitch moment than high-aspect ratio wings of the same surface area [5]. High-aspect ratio wings are more stable, however at the cost of decreased maneuverability.

2.3.4 Wing Shapes

The shape of the wings further influences the drag characteristics and performance of the aircraft. The simplest wing shape is rectangular. This is easy to manufacture, however it does not have a very efficient drag profile. In theory, the most desirable wing shape generates an elliptical lift and drag distribution [5]. Figure 8 depicts this elliptical distribution, derived using Lifting Line Theory, which is described later in section 6.2.2. The most intuitive wing shape to generate this ideal lift distribution is an ellipse. However, elliptical wings are more expensive and complex to manufacture as compared to rectangular wings. Thus other, simpler wing shapes have been developed to approximate an elliptical lift distribution, as a compromise between high-performance elliptical wings and low-cost rectangular wings [5]. The majority of these wing shapes fall under the category of tapered wings.
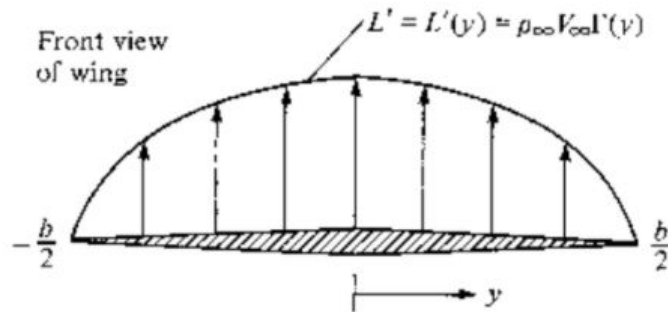
Figure 8: Elliptical lift distribution. Copyright: John D. Anderson, 2016 [5]

Tapered wings, which have a smaller tip chord than root chord, help reduce downwash and induced drag compared to rectangular wings [5]. Figure 9 demonstrates the change in induced drag (in this case, represented by δ) with increasing taper ratio at various aspect ratios. This shows that a taper ratio of approximately 0.3 achieves the minimum induced drag for all aspect ratios, and that the reduction in induced drag due to taper is more significant for higher aspect ratios. It is important to note, however, that large taper ratios result in a shorter mean geometric chord and thus reduced surface area and lift force for a given wingspan. When designing a wing, the correct balance between surface area, aspect ratio, and taper ratio is crucial to achieve the desired aerodynamic characteristics.
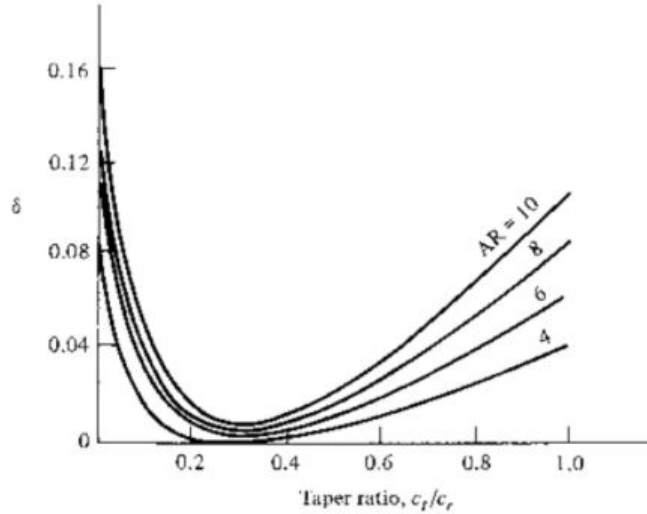
Figure 9: Induced drag as a function of taper ratio for various aspect ratios. Copyright: John D. Anderson, 2016 [5]

Large commercial aircraft often incorporate wing sweep. Swept wings have improved drag characteristics at high flight speeds, but do not exhibit the same behaviors at low speed and thus were not evaluated for this project.

2.3.5 Other Wing Adjustments

Adjustments to the wing such as winglets, dihedral, and control surfaces fine-tune the aerodynamic performance and stability of the aircraft. Aircraft often include winglets to minimize induced drag at the wing tips. Winglets are either vertical plates attached to the ends of the wings or an upward curvature of the wings near the tips that prevent wing tip vortices from applying the downwash force to the upper surface of the wings [6].

2.3.6 Tail Geometries

The tail consists of a horizontal and a vertical stabilizer, and serves to balance the moments from the wings and to achieve stability for the aircraft. The horizontal stabilizer generates lift and a pitch moment, while the vertical stabilizer provides a yaw moment. Each stabilizer typically includes a control surface, usually an elevator to adjust pitch on the horizontal stabilizer and a rudder to adjust yaw on the vertical stabilizer. A variety of configurations for the vertical and horizontal stabilizers are possible, and each tail configuration has different lift and drag properties. Figure 10 displays eight common tail configurations.
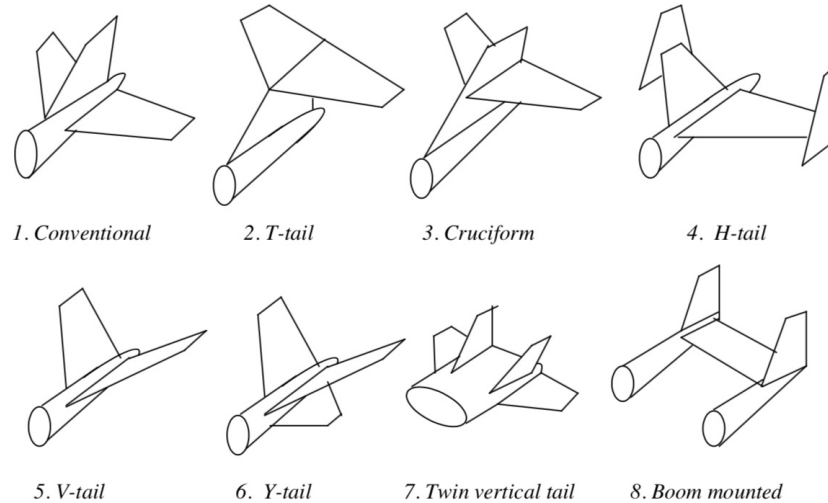
Figure 10: Common tail configurations. Copyright: Mohammad H. Sadraey, 2013 [7]

The surface area and moment arm of the two stabilizers are the two primary factors that influence the effectiveness of the tail at achieving stability [7]. Tail volume coefficients help to identify the ideal surface area and moment arm that will produce the proper moment balance. The horizontal and vertical tail volume coefficients (V_H and V_V, respectively) are dimensionless constants derived from the vertical and horizontal moment balances [7]:

$$V_H = \frac{l_H S_H}{\bar{c} S} \tag{16}$$

$$V_V = \frac{l_V S_V}{b S} \tag{17}$$

In these equations, S is the planform surface area of the wings, S_H is the planform area of the horizontal stabilizer, S_V is the elevation view area of the vertical stabilizer, b is the wingspan, and $\bar{c}$ is the MAC of the wings, and l_H and l_V are the horizontal and vertical stabilizer moment arms. These two moment arms are the distance between the aerodynamic center of the wings and the aerodynamic center of the respective stabilizer, and is typically estimated to be the distance between the wing and respective stabilizer quarter-chords [7].

3   Propulsion

The goal of the propulsion team is to determine the thrust requirements and flight time of the aircraft, and then design a propulsion system that could perform reliably while also minimizing added weight.

3.1   Battery Requirements

According to design rules in appendix A, all batteries used in the design must have the following minimum specifications:

- Lithium polymer

- 6 Cell

- 3000 mAh Capacity

- 25c Draw

Although the 6 cell count could not be changed, it was possible to choose a battery with a larger capacity or maximum draw value. A battery's capacity rating in milliamp hours (mAh) describes the energy charge of the battery and how long it can provide power before needing to be recharged. The c-draw value of the battery is a measure of the rate at which a battery is discharged relative to its maximum capacity [9]. Therefore, dividing the capacity rating in milliamp hours by the c-draw value provides the length of time, in milli-hours, that the battery can sustain the draw and maintain flight. This can be manipulated with simple unit conversions to achieve the following equation, which provides the maximum flight time in minutes [10]:

$$Flight\ Time = \frac{\frac{Capacity}{Draw} \times 60}{1000} \tag{18}$$

From this, the team could evaluate if certain battery specifications were capable of powering the aircraft for a required flight time.

3.1.1 Flight Time

It is important that the battery of the aircraft was able to provide power to the motor for the entire flight, despite the requirements. The team reviewed the flight plan, stated in the design challenge rules to determine the aircraft's approximate travel distance and flight time. The length of the runway and flight course was determined to be approximately 250 meters. Given a low estimate of a flight speed of 5 meters per second, the aircraft would be in flight for approximately one minute, with the motor running for an additional minute during take-off and landing. Including a factor of safety of 2, the battery would support a run time of at least four minutes.

3.2 Thrust

Thrust is produced when a system accelerates or expels mass in one direction, thereby imparting a reactionary force on the system. For a fixed-wing aircraft, thrust is generated when air is pushed in the direction opposing flight, and is proportional to the change in velocity of the airstream [11]. The thrust in Newtons produced by an electric motor and propeller is a function of motor rotation speed in RPM (ω), propeller diameter (d), propeller pitch (p), and forward flight speed (V_0), as the following equation describes [12]:

$$F = 4.392399e^{-8} \times \omega \times \frac{d^{3.5}}{\sqrt{p}} \times [(4.23333e^{-4}) \times \omega \times p - V_0] \tag{19}$$

3.2.1 Motor Properties

An electric motor converts electric energy into rotational mechanical energy through the use of permanent magnets and a series of copper windings. The permanent magnets are mounted around the copper windings and as current is sent through the copper it produces a magnetic field. The two magnetic fields repel each other and cause the copper windings and shaft to rotate. As the two fields begin to align, the current running through the windings is reversed, causing the two fields to repel each other once more and rotate [13].
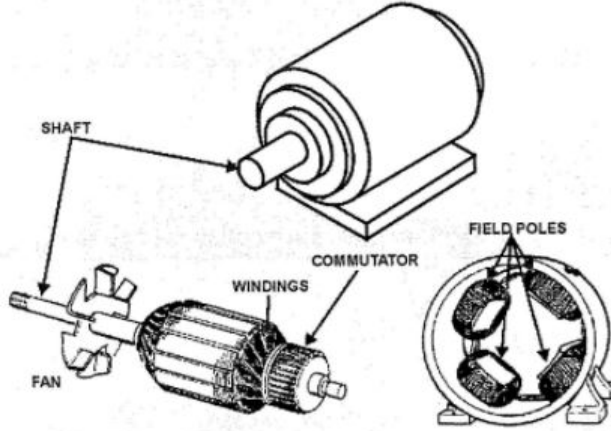
Figure 11: Simplified electric motor. Copyright: Joe Wolfe, 2011 [13]

Electric motors are classified by their KV rating, which is a function of the copper windings themselves. Using a 6-cell LiPo battery, the motor kV, and rated motor efficiency (η), full-throttle motor rotation speed in RPM (ω) can be calculated with the equation:

$$\omega = 21 \times \eta \times kV \tag{20}$$

3.2.2   Propeller Properties

Propellers come in standard sizes and are identified by blade count, diameter, and pitch. Aircraft that utilize a single motor will primarily use a two-blade prop with greater diameter and pitch. Dual-motor craft will often use props with three blades. A propeller's diameter is the length of the prop, in inches, from tip to tip; a larger diameter means more prop surface area but also more weight [8]. A propeller's pitch indicates the distance in inches it will move through the air per single revolution of the propeller shaft. However, the pitch measurement of a prop must only be taken as a theoretical value due to several conditions. These factors may include the material of the prop, its condition, efficiency, air density, and several other factors. [8].

4   Stability and Controls

The stability and controls team aimed to achieve stable flight and maneuvers for the competition aircraft. Stable flight requires both static and dynamic stability, which means that after a disturbance the aircraft returns to its equilibrium state for static stability, or its trim condition for dynamic stability [14]. The team analyzed controls and aerodynamics of the aircraft to calculate desired conditions for aircraft stability.

4.1   Static Stability

The first step toward achieving stability in a moving aircraft is to consider the equilibrium state and static stability. A statically stable aircraft has a positive static stability [15]. To achieve a positive static stability, the aircraft must respond to a disturbance from its equilibrium state by naturally returning to its equilibrium position without pilot input [15]. This occurs when the neutral point of the aircraft is located behind the aircraft's CG [16].

By definition, the neutral point is the CG location which would cause the aircraft to have a neutral or "zero" stability. In this case, the aircraft would neither return to nor be driven away from its equilibrium

position following a disturbance. This location is determined by considering all the pitching moments about the CG, independent of the change in angle of attack [16]. It is calculated from the horizontal tail volume ratio, the lift curve slopes of the wing-body and the tail, and the aerodynamic center of the wing which is approximated at the quarter length of the wing's MAC. The location of the neutral point stays relatively constant during flight and will only vary slightly at different flight speeds due to the change in lift coefficient and lift curve slopes for the wing and tail [16]. The neutral point location, expressed as a fraction of the wing's MAC length, (h_n) is given as [15]:

$$h_n := h_{n,wb} + \frac{a_t}{\bar{a}} \bar{V}_H \left(1 - \frac{\partial \epsilon}{\partial \alpha} \right) \tag{21}$$

The neutral point location as a length x behind the leading edge of the wing is [15]:

$$x := \frac{h_n}{\bar{c}} \tag{22}$$

In these equations, V_H is the horizontal tail volume ratio, a is the wing-body lift curve slope, a_t is the tail lift curve slope, $h_{n,wb}$ is the wing's aerodynamic center expressed as a fraction of the wing's MAC length (typically approximated at 0.25), $\frac{\partial \epsilon}{\partial \alpha}$ is the downwash derivative, and $\bar{c}$ is the MAC length of the wing [15]. The downwash derivative accounts for the change in downwash effects as the angle of attack varies, and is described by the following equation:

$$\frac{\partial \epsilon}{\partial \alpha} := 4.44 \sqrt{1 - Mach^2} \left(\left(\frac{1}{AR} - \frac{1}{1 + AR^{1.7}} \right) \left(\frac{10 - 3\lambda}{7} \right) \left(\frac{1 - \bar{l}_{tv}/b}{(2\bar{l}_t/b)^{0.33}} \right) \sqrt{cos\Lambda} \right)^{1.19} \tag{23}$$

where AR is the aspect ratio of the wing, λ is the taper ratio of the wing, Λ is the sweep angle of the wing from its aerodynamic center, b is the wing span, $\bar{l}_t$ is the distance between the aerodynamic centers of the wing and the tail, and $\bar{l}_{tv}$ is the vertical distance between the aerodynamic centers of the wing and the tail [15].

The static margin (SM) is the distance between the aircraft's CG and neutral point, and is calculated as a percentage of the MAC of the wing:

$$SM\% := \frac{h_n - h}{\bar{c}} * 100\% \tag{24}$$

where h is the CG location of the aircraft as a fraction of the wing's MAC [15]. Increasing the static margin increases the stability of the aircraft, with conventional aircraft tending to use static margins between 5% and 10%. A negative static margin is possible in computer-assisted aircraft and can be useful in fighter airplanes, as being slightly unstable increases responsiveness. A static margin higher than 15% can lead to sensitive aircraft [15]. In order to have a minimal change in static margin, the location change of the CG and the neutral point must remain constant. Thus, it is crucial that the distribution of the payload does not alter the CG location.

4.2   Trim Analysis

Balancing the moments about the center of gravity of the aircraft in flight is crucial for dynamic stability during level, steady trim flight. A total of zero applied moment is required to balance the aircraft based on the location of the center of gravity. A nose-heavy aircraft would usually require a downlifting tail. An aft located center of gravity usually requires an uplifting tail. All the force-induced moments applied such as the lift and weight forces as well as the moments about the aerodynamic centers of the wing and the tail must be taken into calculation. Other forces such as thrust or fuselage lift must also be taken into account if the moments they generate are significant. For most high-wing aircraft with a centered front propeller, the moment created by the lift forces of the wing and the tail are the most significant. The sum of all forces and moments should be near zero to allow for minimal control input to sustain trim flight, so that control inputs may be used to respond to disturbances and return the aircraft to equilibrium.

4.3   Control Surfaces

Control surfaces are portions of the wing and tail stabilizers that the pilot can manipulate independently in order to control the motion of the aircraft. The geometry and movement of these control surfaces affect the aircraft's maneuverability and its ability to evade large disturbances. The primary factors that influence the design of the control surfaces are the forces that the control surfaces must overcome in order to alter the aircraft's flight path [15]. Calculating the required torque of the control surface hinges yields the desired control surface geometries, including areas, spans, and deflection angles

Control surfaces are important for both longitudinal and lateral stability. The most common types of longitudinal-axes control surfaces are elevators, flaps, and slats, while ailerons and rudders influence lateral stability.

Elevators, generally located on the tail of an aircraft, control the aircraft's pitch. These change the wing's angle of attack and can assist in turning and changing altitude. Elevators also manage the airplane's pitch trim. Integration of flaps and slats provide additional longitudinal control. Flaps and slats work to increase lift at high angles of attack. There are many types of flaps, ranging from double slit flaps to plain flaps to split flaps. Double slit flaps produce the most lift at the cost of being most complicated to manufacture. Plain flaps and split flaps produce less lift, but are easier to implement. Slats are small, highly cambered airfoils mounted on the leading edge of the main wing. They work by increasing the pressure differential between the top and bottom surfaces of the wing. Adding slats to the wings improves lift and thus allows for a larger payload and reduced thrust requirements. Figure 12 shows various maximum lift coefficients of different flap designs.
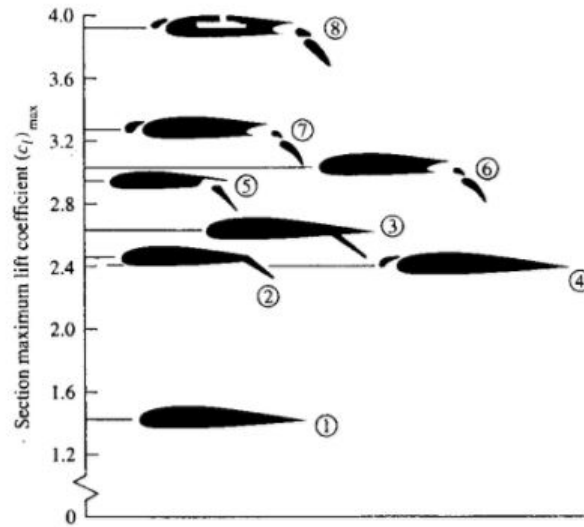
Figure 12: Maximum lift coefficient for high-lift devices. Copyright: John D. Anderson, 1999 [16]

Fixed to the trailing edge of the wing, ailerons are used to control the roll of the airplane. This allows the aircraft to bank and turn by changing the angle of the lift vector from the wing. The rudder gives the airplane yaw control to keep the aircraft in line during a banked turn. In aircraft with multiple engines, the rudder can be used to compensate for a single engine failure or other adverse yaw effects. On some aircraft, the rudder has an additional trim tab to control the attitude without pilot intervention.

5   Structures

The goal of the structures team was to analyze various designs and materials for all components of the aircraft, then select the best options to achieve successful flight while carrying the most passengers. The primary focus of the analyses performed by this team were structural integrity, maximizing factors of safety, and minimizing weight of the aircraft.

5.1   Materials Research

Research done by the team determined certain materials for different applications within the plane. For example, wing spars will carry more weight and will need to deflect less than a fuselage wall. Choosing the specific materials will factor in the density of material, the manufacturing properties, and the cost. Due to competition rule 7.2.1, the use of plastic-reinforced composites are prohibited. With a restriction on composite materials, the search for lightweight, strong, and cost efficient materials remained a challenge.

While many previous MQP aircraft have used balsa wood ribs with a mylar skin for wing construction, the team also identified uniform modeling foam as a potential wing material. Modelling foams for hobby aircraft applications include expanded polyethylene (EPE), expanded polypropylene (EPP), expanded polystyrene (EPS), extruded polystyrene (XPS), and expanded polyurethane (EPU). EPE and EPP are resilient and are less prone to fracturing. EPS, XPS, and EPU are much stronger but are more likely to break on impact. The differences between the various polystyrenes are due to their manufacturing processes. Extrusion gives the material a more consistent structure, making it stronger than its expanded counterpart. EPU is primarily used for expanding foam. Many different types of foam are available for purchasing from specialized suppliers or general hardware stores.

Most RC aircraft use carbon-derivative spars, such as solid carbon or a complex carbon fiber material. While the competition rules state that the use of any carbon fiber materials is strictly disallowed, rods of solid carbon not formed into a matrix are permitted. Therefore, the team limited research on spar materials to carbon rods.

A necessary component in aircraft assembly and design is the adhesive with which various components are secured to each other. Adhesives exist in many available forms with a wide range of properties and material compatibility. Examples of applicable adhesives are hot glue, super glues with name brands such as Gorilla Glue, as well as adhesives designed for securing foams to one another.

Hot glue is an adhesive that is used by many hobbyists in the RC aircraft community for various applications, however some express concern that that material does not bind surfaces together easily and can become brittle in lower temperatures. Super glues are typically a recommended choice, as they can be applied to many different types of material for bonding purposes, and provide a secure, flexible hold when cured properly over the course of several hours. Adhesives designed for binding foams together can range in terms of compatibility, as many will adhere to only specific types of foam. These adhesives become applicable whenever a need is apparent to secure separate components together which are both made from the same or similar types of foam on the aircraft.

5.2   Stress Analysis

As one of the primary tasks of the development of aircraft components by the structural team is structural integrity, research was conducted in general stress analysis applied to the aircraft. It was found that the main forces experienced by aircraft wings are bending, torsion, and shear [18]. The context in which these forces are calculated tend to be on an aircraft wing cell basis, in which the various stringers lining the length of the wing create separable sections along the airfoil shape. In order to retain the ability to perform stress analysis on a wing that may not use the stringer design methods, more general equations for these forces were utilized.

For many wingtip deflection calculations, it would be possible to assume a rectangular airfoil shape and treat the calculation as a cantilever beam problem. In this instance, the typical cantilever beam equation for deflection would be used [19]:

$$\delta = \frac{Pl^3}{EI} \tag{25}$$

In this, the variable (P) represents the applied force, while (l) is the length of the beam being acted upon. (E) and (I) represent Young's Modulus and moment of inertia of the beam, respectively. This equation is beneficial for approximating deflections in wings with assumed shapes, however it was found that there would be a need to more accurately determine wingtip deflection of a real wing shape. However, this too is a calculation typically carried out in the presence of stringers along the wing's cross-section, a case that may not be applied to potential uniform core wing designs. In order to solve for this deflection in a more general case, additional variables were considered.

By adding (W_{fuse}) as the weight of the fuselage, as well as (b) for wingspan and (I_0) as the moment of inertia at the wing's root, the following equation can be used for the wingtip deflection of a wing with or without taper ratio (λ):

$$\delta = \left(\frac{PW_{fuse}}{EI_0} \right) \left(\frac{b^3}{96} \right) \left(\frac{1 + 2\lambda}{1 + \lambda} \right) \tag{26}$$

This equation requires the use of the moment of inertia of the airfoil in order to be correctly utilized.

5.3   Computer Aided Design Modeling and Structural Analysis

There are many Computer Aided Design (CAD) softwares and programs that are capable of performing the modeling and structural analysis tasks needed for this project. Examples of these types of software include Autodesk, Ansys, CREO, SOLIDWORKS, and many more. Each program has a unique interface and different capabilities. For example, Ansys is able to perform advanced flow simulations that the other CAD softwares cannot. However, the structures team decided that flow simulation was not a necessity for the chosen modeling and structural analysis program, as the software and simulation team would be selecting an analysis program designed specifically for this purpose. This, combined with the structures team's prior experience with various CAD softwares and familiarity with SOLIDWORKS, the structures team selected SOLIDWORKS as the team's primary CAD modeling and structural analysis program.

SOLIDWORKS has a built-in analysis tool and corresponding toolbar which the structures team used to run stress analysis tests. Through this analysis tool, the team could manipulate material properties, component interfaces, and applied loads in the model and observe the resulting deflections and stresses. Realistic environments and loading conditions could be replicated, which was particularly useful in evaluating the structural integrity of designs.

6   Software and Simulation

Computer software played a significant role in the design of the plane. There are two main categories of software that are used in aerodynamic design. The first type of software uses a numerical analysis to simulate flow around a body by solving the Navier-Stokes equations. The second type of software uses theoretical equations to estimate various parameters about the body. The main goal of the software team was to analyze aircraft configurations and wing shapes in coordination with the aerodynamics team. In the first term, the software team provided the aerodynamics team with comparisons between airfoil shape, wing tips, and tail configurations. Later in the design process, the team also ran stability analysis as well as stall and ground conditions in the XLFR5 software. These helped more accurately predict plane behavior and lead to better construction and performance of the final plane.

6.1   Choosing Software

After some initial research, two main software programs were identified to meet team needs, SOLID-WORKS Flow Simulation and XFLR5. Initially one team member worked with each of the programs to

simulate various wing shapes and compare results, however due to the complexity of SOLIDWORKS Flow Simulation and the inaccuracy of initial results, the team moved forward with learning XFLR5. Testing of the Horizon Hobby Plane, discussed in later sections, verified the effectiveness of XFLR5 as an aerodynamic analysis tool.

6.2 XFLR5 Review

The primary set of 2D equations XFLR5 uses are based off of the Lifting Line Theory (LLT), the Vortex Panel Method (VPM), and for 3D bodies XFLR5 uses the Vortex Lattice Method (VLM)[20]. Because XFLR5 is based on these equations, it also carries the assumptions and simplifications made in those equations. The main simplifications made in these equations are that the fluid is incompressible, the aircraft is operating at a low Reynolds number, and the angle of attack and angle of sideslip are small. Although XFLR5 uses theoretical calculations, it is still quite accurate within small angles of attack or sideslip.

6.2.1 Viscous Flow

Viscous flow theory involves the integration of friction, thermal conductivity, and mass diffusion to a fluid passing by a body surface. Without these factors, drag on a body can be calculated as zero. In reality, inviscid assumptions can be made for high Reynolds numbers, but are not practical for a low Reynolds number scenario [5]. Using viscous fluid assumptions, XFLR5 can more accurately predict the real properties of plane surfaces.
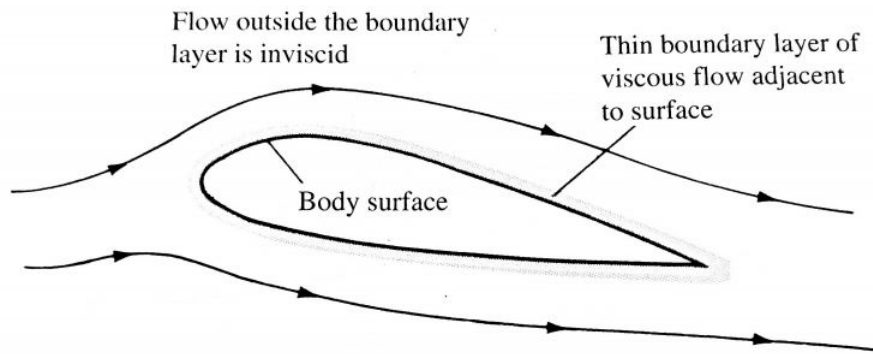
Figure 13: Viscous flow theory. Copyright: John D. Anderson, 2016 [5]

6.2.2 Lifting Line Theory

Lifting line theory was developed during World War I to predict the properties of a finite wing. This theory uses vortex filament strengths to estimate the downwash distribution across a wing section. For a single line, the bound vortex induced by trailing vortices (w) can be expressed as:

$$w(y) = -\frac{\Gamma}{4\pi} \frac{b}{(b/2)^2 - y^2} \tag{27}$$

where (Γ) is the strength of the vortex, b is the total wing span, and y is the position along the wing span. When infinite lines are superimposed along a wing span, the downwash velocity can be expressed as a function of an arbitrary location (y_0) along the lifting line[5]:

$$w(y_0) = -\frac{1}{4\pi} \int_{-b/2}^{b/2} \frac{(d\Gamma/dy)dy}{y_0 - y} \tag{28}$$

and the equation for the induced angle of attack (α_i) is:

$$\alpha(y_0) = \frac{1}{4\pi V_\infty} \int_{-b/2}^{b/2} \frac{(d\Gamma/dy)dy}{y_0 - y} \qquad (29)$$
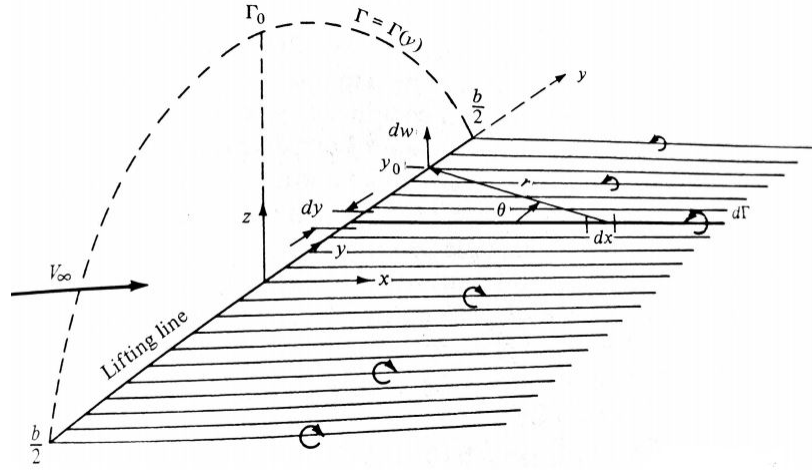
Figure 14: Lifting line theory across wingspan (b). Copyright: John D. Anderson, 2016 [5]

6.2.3 Vortex Lattice Theory

One final major calculation performed by XFLR5 is the vortex lattice method. The lifting line theory is still accurate at performing preliminary lift and drag calculations, however the vortex panel method is more suited for low-aspect-ratio wings and complex shapes. This model applies the vortex line distribution in both the x and y directions, forming infinitesimally small areas on a wing surface. Here, vortices cause two strength distributions, (γ) as the spanwise strength and (δ) as the chordwise strength. Wake vortex strength (δ_w) factors in the vortices produced by the wake of the airfoil, which remains constant with x.
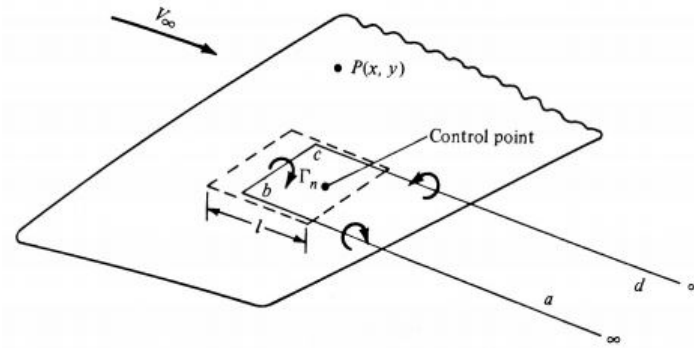
Figure 15: Single vortex line. Copyright: John D. Anderson, 2016 [5]

Considering a point (ξ, η) the normal velocity induced at point P can be estimated as [5]:

$$w(x,y) = -\frac{1}{4\pi} \int \int_S \frac{(x-\xi)\gamma(\xi,\eta) + (y-\eta)\delta(\xi,\eta)}{[(x-\xi)^2 + (y-\eta)^2]^{3/2}} d\xi d\eta - \frac{1}{4\pi} \int \int_W \frac{(y-\eta)\delta_w(\eta)}{[(x-\xi)^2 + (y-\eta)^2]^{3/2}} d\xi d\eta \qquad (30)$$

32
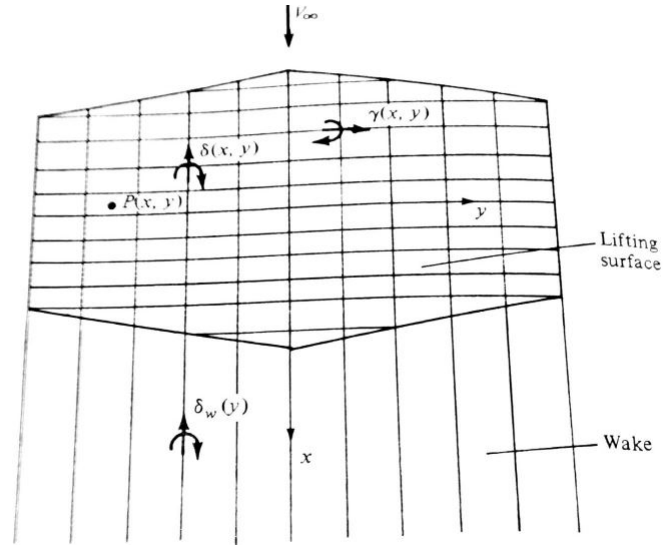
Figure 16: Total vortex panel method. Copyright: John D. Anderson, 2016 [5]

With such complex computations to evaluate for all plane surfaces, the software is a more efficient and accurate option than calculating the values by hand.

6.2.4 XFLR5 Aircraft Modeling and Aerodynamic Analysis

The above theories are applied to 3D bodies in order to calculate the aerodynamic properties of lifting surfaces and aircraft bodies. In order to define the lifting surfaces, the aerodynamics properties of the 2D airfoil were run through the XFLR5 simulation software. The team ran the airfoil over a range of Reynold's Numbers from 500,000 to 1,200,000 in order to simulate all conditions of the aircraft in flight. After importing the airfoils into the 3D plane modeler, the dimensions of the wing were given to create the 3D model.

This series of events was completed for the wing airfoil as well as the airfoils used in the tail. The horizontal and vertical tails were also created in the same model as the final chosen wing. The lifting surfaces were simulated at velocities from 8 to 15 meters per second in order to recreate expected flight conditions. With the analyses defined, results from XFLR5 such as drag, moments, lift, downwash, and surface area were incorporated into later aerodynamic and stability analyses.

Part III
System Design

1   Development and Verification of Design Tools

Background research led to the development of a library of analyses tools consisting of equation lists, software, and spreadsheets that would be used to develop and evaluate potential aircraft designs. In order to validate the accuracy of these tools, team members used the tools to evaluate an existing remote-controlled aircraft and compare them to the actual values reported in the manufacturer's instruction manual. Project advisor Professor Cowlagi provided a Horizon Hobby Timber aircraft, pictured in Figure 17, for this purpose. This hobby plane is 1.040 meters in length, has a wingspan of 1.555 meters, and weighs 1.4 kilograms. The center of gravity is located .06 meters behind the leading edge of the wings, with a tolerance of +/- .005 meters [21].

Figure 17: Drawing of the Horizon Hobby Timber model aircraft from the instruction. Copyright: Horizon Hobby [21]

Team members carefully measured the Horizon Hobby Timber and obtained the following additional measurements:

- Wing

  - Airfoil - NACA 3313
  - Chord - 0.24m
  - Dihedral Angle - 2 degrees

- Tail

  - Airfoil - NACA 0009, 0011
  - Span - 0.56m
  - Root Chord - 0.16m
  - Tip Chord - 0.10m
  - Sweep Angle - 12 degrees

- Vertical Distance between Wing and Horizontal Tail - 0.03 m

The following sections detail the tools that each of the sub-teams developed in A Term, and how the hobby plane evaluations validated these tools.

1.1 Aerodynamics Tools

The aerodynamics team began by compiling a detailed list of equations, shown in Appendix B, relating to aerodynamic forces and moments, wing and tail properties, flight performance, and more. The team then developed calculations spreadsheets from these equations to be used later in the design process. Some of the spreadsheets calculated the aircraft properties (including lift coefficient and wing geometry) required to produce desired flight parameters and aerodynamic properties. Other spreadsheets did the opposite, returning flight parameters and aerodynamic properties based on aircraft properties inputs. Each spreadsheet incorporated redundancies so that multiple equation forms were used to calculate the same parameter. In all of these cases, the different methods returned nearly identical values, within small error margins, indicating the accuracy of the theoretical equations and assumptions.

The aerodynamics team members tested some of these spreadsheets using measurements taken from the Horizon Hobby Timber. By inputting the wing dimensions, tail dimensions, and plane weight, the team obtained values for the lift force and lift coefficient for both level flight and steady climb at various flight speeds. For these steady flight analyses, the following assumptions were made:

$$L = W \tag{31}$$

$$T = D \tag{32}$$

The team also incorporated drag force data of the Horizon Hobby Timber obtained from wind tunnel tests. With these additional inputs, the spreadsheets also computed the induced drag, induced angle of attack, drag coefficients, lift-to-drag ratio, required thrust, and other parameters. Table 1 summarizes some of these results, and Appendix C includes the full spreadsheet with complete results. The team verified the validity of these results by comparing to the XFLR5 aerodynamic analysis results produced by the software team.

Horizon Hobby Timber Aerodynamic Properties at Level or Steady Climb Flight					
Flight Speed (m/s)	Lift Coefficient	Induced Angle of Attack (deg)	Lift-to-Drag Ratio	Drag Coefficient	Induced Drag Coefficient
10	0.47616	1.34758	17.78612	0.02677	0.01309
15	0.21163	0.59893	10.98528	0.01926	0.00258
20	0.11904	0.33689	7.68516	0.01549	0.00082

Table 1: Summary of Horizon Hobby Timber calculations.

Another tool the aerodynamics team found to help with aircraft design is an online database of airfoils called "Airfoil Tools" (airfoiltools.com). This website contains data on 1636 different airfoils, including their geometry and aerodynamic data. For each airfoil, the website displays plots of lift coefficient versus drag coefficient, lift coefficient versus angle of attack, lift-to-drag ratio versus angle of attack, drag coefficient versus angle of attack, and pitch moment versus angle of attack for a variety of Reynold's Number or velocity ranges. The database includes search and comparison features to help find airfoils that meet desired criteria or that are similar to other airfoils. The aerodynamics team and software team together verified a sampling of data from this website against XFLR5 analyses of the same airfoils, and found Airfoil Tools to be a reliable database to find and compare airfoils.

1.2 Propulsion Tools

The propulsion team consulted Hacker Motor and AXI manufacturer catalogues of brushless motors with accompanying propeller, battery, and Electronic Speed Control (ESC) specifications. Using Equation 19, which estimates thrust with 90 to 95% accuracy from motor speed, propeller dimensions, and flight velocity, the propulsion team developed a MATLAB script to graph propeller maximum thrust profiles

with battery voltage decay. This complete MATLAB script is included in Appendix D. To confirm these calculated thrust values, the team utilized an online RC plane calculator (eCalc) to analyze the performance of various motor, propeller, battery, and ESC combinations.

eCalc is a paid membership calculator uses standard electric motor and propeller theory and equations to return theoretical outputs and performance parameters for a specific propulsion system (motor, battery, controller, and propeller) input by the user. eCalc has become a standard in the RC Aviation community because it incorporates detailed product specifications and data provided directly by manufacturers, so it produces the most accurate predictions available, short of actual static and dynamic test data. The Hacker Motor website includes direct links to prefilled eCalc simulations to provide customers with performance estimates for each of their motor products. Appendix G lists the key equations and theory that online "eCalc" simulators use to predict various performance parameters for a particular propeller and motor combination. This calculator also evaluated motor RPM, the thrust-to-weight ratio for given aircraft parameters, motor operating temperature, and sustainable flight time for the motor and propeller combinations the team investigated. The theoretical results from the eCalc and MATLAB script provided initial estimates that could be compared to static and dynamic propulsion tests in the wind tunnel to validate test data and aid in the selection of a propulsion system.

1.3   Stability and Controls Tools

The controls team developed MATLAB codes to calculate tail dimensions, control surface dimensions, and trim condition controls in order to achieve static and dynamic stability. A list of the equations used is provided in Appendix E. The static stability MATLAB code, which is included in Appendix F, was tested using measurements from the Horizon Hobby Timber to confirm its accuracy. Assuming a flight velocity of 10 meters per second, the MATLAB code computed a neutral point location of 11 centimeters behind the wing's leading edge and a static margin of 20%. Maneuverable acrobatic aircraft such as this acrobatic hobby plane typically have high static margins. The calculated static margin for the Horizon Hobby Timber falls within the expected range, validating the tool.

1.4   Structures Tools

The combined CAD and hardware structures team studied videos of aircraft failures and crashes from previous SAE Aero Design competition flights, which helped determine the most common points of structural weakness in aircraft for this application. These videos indicated that wing tip deflection has been a serious problem for many teams in the past. Excessive wing tip deflection caused the wing spars to fail, leading to the separation of the wings from the fuselage. The team also identified the landing gear as a common failure due to lack of structural integrity. The third most common point of failure indicated by these videos was the connection of the rudder to the fuselage was a weak point. The failure of this connection led to many aircrafts losing control and crashing. These videos provide strong evidence of where the weak points on this type of aircraft are, confirming intuition and information gathered through background research regarding aircraft structures.

The CAD structures team created 3D models of the Horizon Hobby Timber in SOLIDWORKS using the previously listed measurements as well as accurate material properties data from CES EduPak. They then used the built-in software to perform structural evaluations including stress tests and wing deflection, as shown in Figure 18. The wing deflection simulation represented the wing spar with a model of an aluminum rod. A distributed force was applied over the length of the spar. The results of these tests aligned with the aircraft specifications and expected values, providing validation for both the SOLIDWORKS structural analysis software as well as for the accuracy of the information in the CES EduPak database. Additionally, the team verified the SOLIDWORKS results with hand calculations using standard structural analysis equations, which are listed in Appendix H.
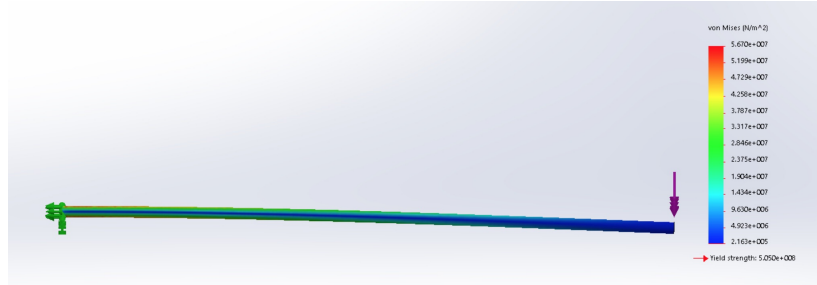
Figure 18: Wing deflection test simulation on the Horizon Hobby Timber in SOLIDWORKS.

1.5 Software Tools

From chord length, maximum thickness, and location of the maximum thickness on the Horizon Hobby Timber airfoil, the airfoil shape of both the wing and tail sections of the aircraft were determined. Both airfoils were assumed to be standard (National Advisory Committee for Aeronautics) NACA airfoil shapes. The main wing consisted of a NACA 3313, and the tail of a NACA 0009. From these airfoils and the dimensions previously listed, the software team modeled the the wing and tail lifting surfaces in XFLR5. After adding the body drag data from the wind tunnel tests of the hobby plane to the model, the team ran a full-body analysis of the plane. A fixed-weight analysis was performed for angles of attack ranging from -5 to 13 degrees.

According to the XFLR5 results, the theoretical cruising speed at a 0 degree angle of attack was approximately 20 m/s for this aircraft. At a higher angle of attack of 5 degrees, the required cruising velocity was 12 m/s. Through comparison to the aircraft manual and videos of the Horizon Hobby Timber in flight, the software team determined the analysis results to be accurate within a reasonable error margin, thus validating the XFLR5 analysis software. Below are the results from the XFLR5 simulation both with and without the plane winglets:
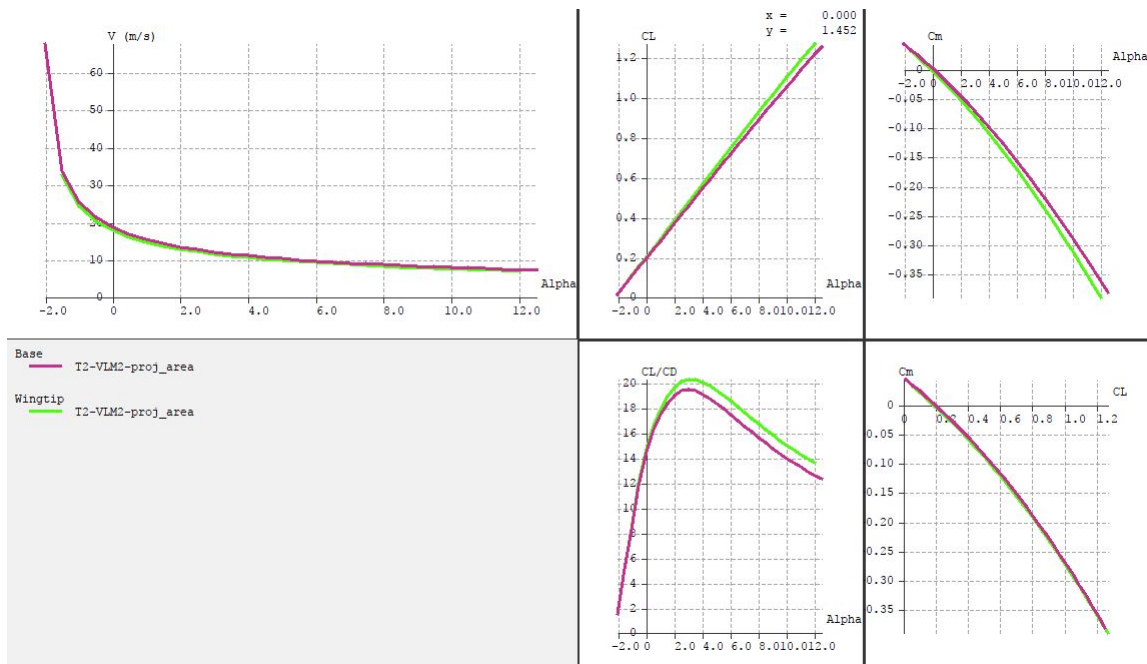
Figure 19: Results from XFLR5 analysis of hobby plane.

37

2   Design Goals and Objectives

With the ultimate goal of achieving a high FFS, the team aimed to maximize the number of "passenger" tennis balls the aircraft would be able to carry. To obtain this goal and stay within the design constraints listed in the official 2018 competition rules, the project team identified the following primary design objectives:

1. Maximize available volume in the passenger cabin and luggage bay to accommodate the largest number of passengers and associated luggage as allowed by the total takeoff weight restriction of 55 pounds;

2. Minimize the weight of the aircraft structure to accommodate the largest number of passengers and associated luggage as allowed by the total takeoff weight restriction of 55 pounds.

Throughout the design process, the team developed additional design objectives specific to each system of the aircraft.

2.1   Initial Design Assumptions

Before starting to develop initial designs, the project team considered the primary objectives and established initial assumptions and constraints for the aircraft regarding the estimated shape, weight, and size. The team decided to pursue a conventional fixed-wing aircraft with a single fuselage and aft-mounted tail. The official 2018 competition rules specifically require fixed-wing aircraft, and there is abundant literature to guide the design and analysis process for a conventional aircraft configuration. Prior MQP reports and SAE Aero Design reports recommended using conventional aircraft models rather than non-conventional aircraft such as flying wings due to simplicity of design and ease of manufacturing.

Next, the team considered the weight and size of the aircraft. To ensure that the final aircraft would be able to accommodate the largest payload possible, the initial sizing of the aircraft used the maximum takeoff weight of 55 pounds (246 N) as the design weight. The team worked to provide the lift, thrust, and structure necessary to support the maximum allowable weight. The 2018 competition rules limit the aircraft to a wingspan of no more than twelve feet (3.65 m), and the team took full advantage of this in order to maximize wing surface area for increased lift force.

3   Propulsion Design

Preliminary design analysis began by studying previous reports' propulsion analysis and design; broader analysis was achieved by simulating various motor and propeller combinations as well as conducting static and dynamic thrust tests. This data was used to understand the propulsion system and how it influences the overall performance of the airplane.

3.1   Motor and Propeller Selection

From previous designs, the the two most common motors used were the Hacker Motor A40-12L 14 pole outrunner, with a peak power consumption of 1100 Watts, and the AXI 60 4130/20 outrunner, with a peak power consumption of 1950 Watts. Although the aircraft is restricted to 1000 Watts, a motor rated for higher wattage can theoretically run more efficiently at lower power inputs. To gain a general idea of the capabilities of these two motors, a variety of simulations were run using a motor and propeller e-calculator. The results of these simulations are summarized in Table 2. In addition to evaluating the thrust output of each motor in combination with different propeller sizes, the simulations evaluated the operating temperature and flight time that could be sustained. Safe motor operating temperature was an important factor when selecting a motor-propeller combination, as high operating temperatures can cause the motor to overheat, run less efficiently, and potentially damage itself. A maximum flight time of two minutes was determined based on the expected flight velocity range and the flight path description in the competition rules.

Motor	Prop (inches)	RPM	Power (Watts)	Flight Time (min)	Temperature (C)	Thrust (N)	T/W
Hacker	16x8	7400	1070	3.3	70	47.5	0.24
	16x10	**~6750**	**~1000**	**2.8**	**85**	**49.2**	**0.28**
	17x8	~6500	~1000	2.6	91	48	0.27
AXI	16x8	5639	490	7.4	49	27.5	0.14
	17x8	5466	580	6.3	55	31	0.15
	18x8	5284	672	5.4	63	35.3	0.17
	19x8	5094	767	4.7	73	37.5	0.19
	20x8	4900	863	4.1	84	40.5	0.2
	21x8	4700	958	3.7	97	43.3	0.22
All measurements taken at a simulated flight speed of 12m/s and a wing area of 2.3 m^2							

Table 2: Simulated Results for Propeller and Motor Combinations.

These simulations indicated that the most effective motor and propeller combination is the Hacker A40-12L motor driving a 16x10 inch propeller, yielding 49.2 Newtons of thrust. In addition, this combination would allow the motor to run within the manufacturer's recommended operating temperature.

3.1.1 Static and Dynamic Thrust Testing

These theoretical results were then confirmed by conducting practical static and dynamic thrust tests in the wind tunnel. To measure the thrust generated, a force balance composed of two perpendicular aluminum bars joined at a pivot was used. The motor was mounted in the test section of the wind tunnel horizontally, as it would be on the actual aircraft. A scale was placed underneath the long lever arm, and weights which countered the mass of the long lever arm were attached to the short arm. The team measured and recorded the scale's reading for a specific amount of weight, which then would be used to correlate the scale's reading to thrust generated by the motor. Figure 20 depicts the wind tunnel and force balance experimental setup for propulsion testing, and Figure 21 illustrates the calculations performed to convert the scale reading to the actual thrust magnitude.
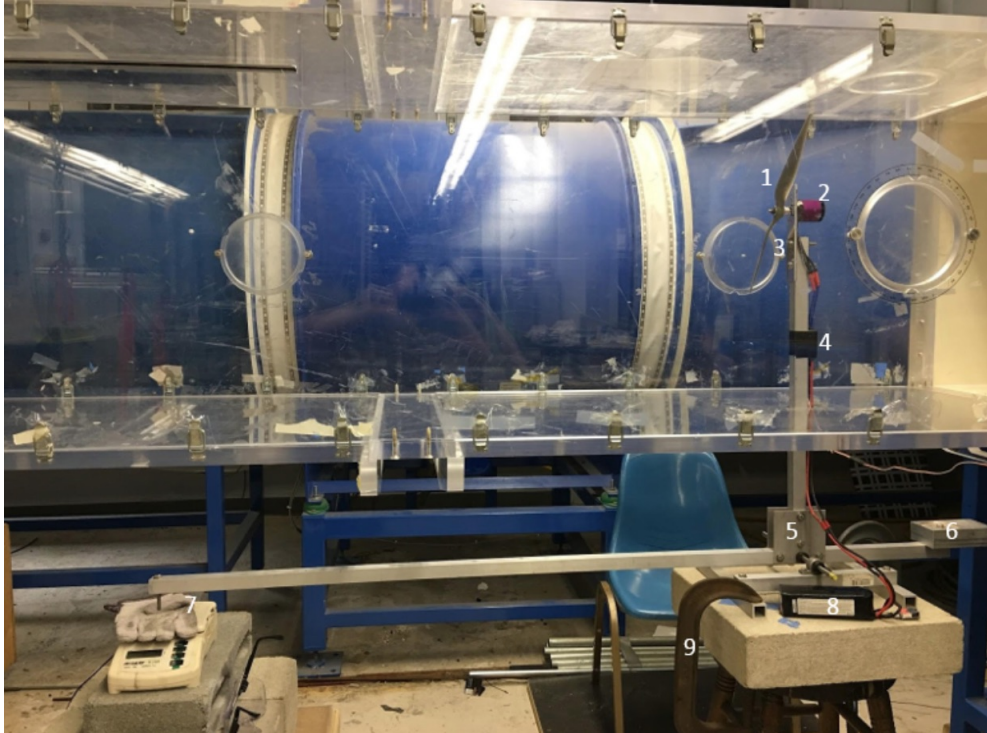
Figure 20: Wind tunnel test section and force balance to measure thrust generated by a motor and propeller. (1) Test propeller; (2) Test motor; (3) Custom-made aluminum motor mount; (4) Motor Electronic Speed Controller, taped to vertical aluminum bar for safety; (5) Force balance; (6) Force balance counter weight; (7) Digital scale to measure force; (8) Battery; (9) C-Clamp to hold force balance in place.
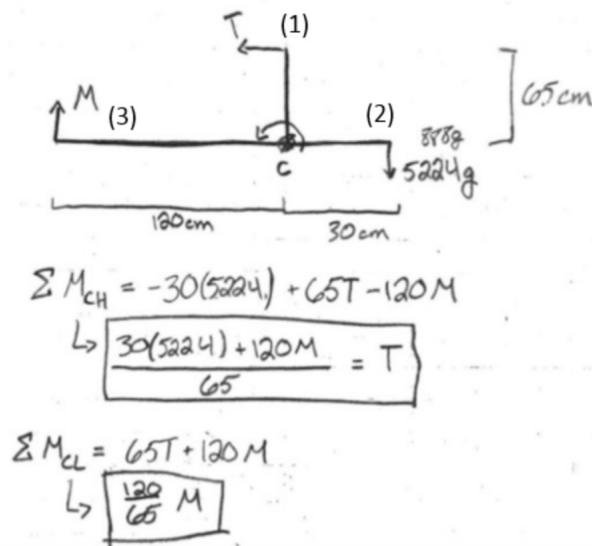
Figure 21: Force balance diagram and calculations. (1) Location of the motor and propeller; (2) Location of the counter weight; (3) Location of the scale to measure the force.

During testing, a 6 cell Li-Poly battery pack with 3300mAh and 45C powered the motor, and a 60 Amp ESC and power meter were used to limit the power to 1000 Watts. These parameters were chosen to align with the manufacturer recommendations for the Hacker A40-12L. These parameters were also used for the AXI 4130/20, since the manufacturer recommendations for the AXI 4130/20 do not comply with the competition's 1000 Watt power limit. Each test was conducted by a team of at least two people, and pre-test checklists, shown in Appendix L, ensured consistency and safety.

For both static and testing, the motor was secured to the force balance, and the ports of the wind tunnel were closed. The three wires of the motor were connected to a 60 amp brushless speed controller, and the control input was provided by a servo tester rather than a wireless receiver in order to reduce the number of points of possible failure. The 6 cell Li-Po battery, with cell "low voltage" alarm connected to the balance lead, was then plugged in and the servo tester was set to various levels in order to obtain valuable thrust data.

Several static and dynamic trials of each motor and propeller combination were tested to verify the simulation predictions. Through these tests, the most effective motor and propeller combination was confirmed to be the Hacker A40-12L running a 16x10 inch propeller, which at max throttle averaged 48 Newtons of static thrust, close to predictions. After dynamic testing, the team was able to develop an experimental equation relating the maximum thrust values against the relative airspeed, shown in figure 22. This maximum thrust equation was important for takeoff and flight analysis during the aerodynamic design of the aircraft.
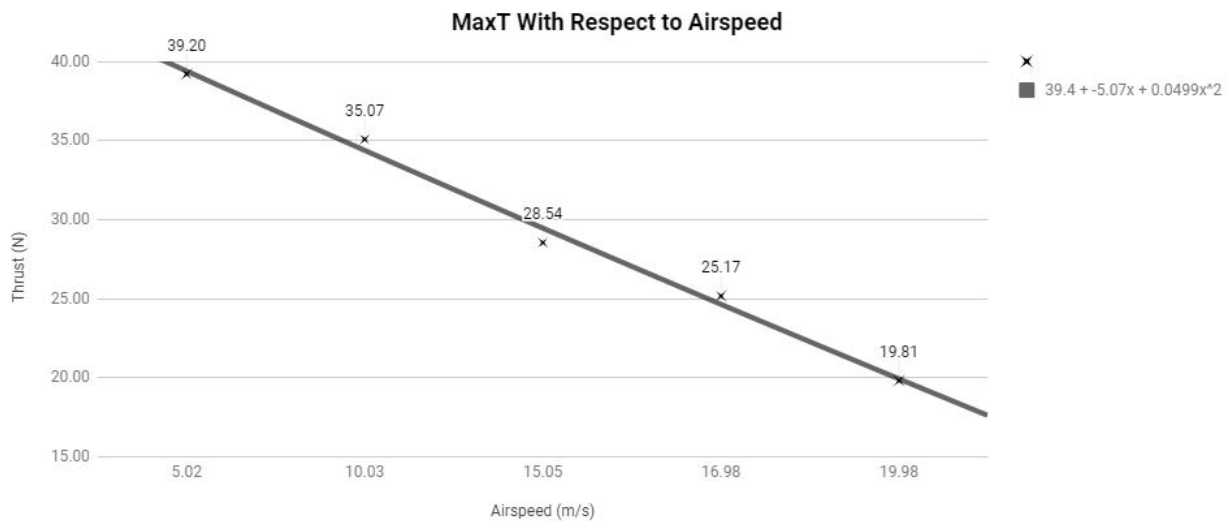
Figure 22: Maximum thrust versus airspeed curve developed from propulsion tests.

4 Aerodynamic Design

4.1 Airfoil Selection

Previous MQP and SAE Aero Design reports revealed that the Selig S1223 high lift low Reynolds number airfoil, referred to as the S1223, is a commonly used standard airfoil shape for heavy-lifting model aircraft. The S1223, pictured in Figure 23, is designed to generate large amounts of lift during low Reynolds number flight. It has its max thickness of 12.1% of the chord length at 19.8% of the chord behind the leading edge, and its max camber of 8.1% of the chord length at 49% of the chord behind the leading edge [22].
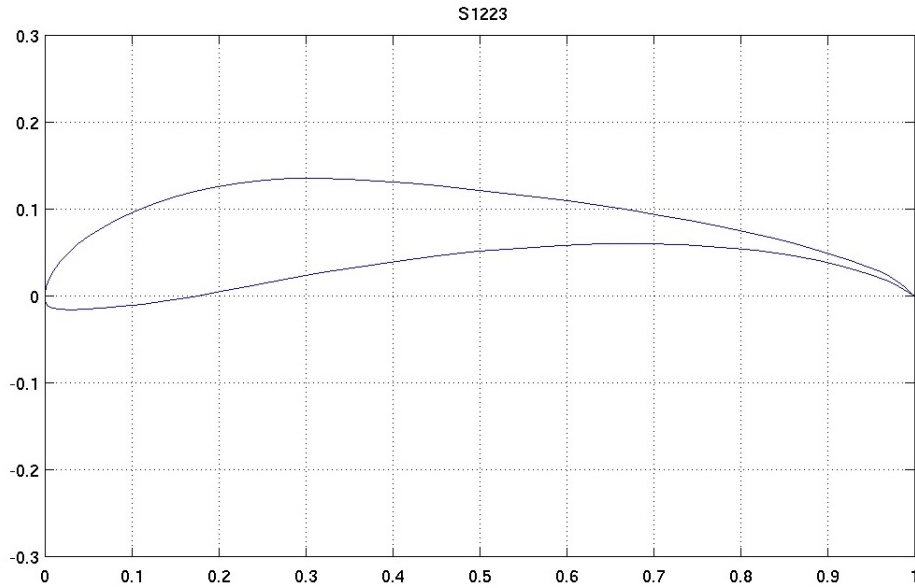
Figure 23: Profile of the Selig S1223 high lift airfoil. Copyright: UIUC Airfoil Coordinates Database [23]

The aerodynamics group used Airfoil Tools to search for standard airfoil shapes with high-lift, low-speed aerodynamic properties similar to those of the S1223, using the "similar airfoils" feature. This yielded three more airfoils for the team to consider: the Richard T. LaSalle modification of the S1223, called the S1223-RTL; the Eppler E423 high lift airfoil, or E423, and Gottingen 233 (MVA CA4) airfoil, or GOE233. The S1223-RTL, shown in Figure 24, varies only slightly from the S1223. It has a max thickness of 13.5% of the chord length at 19.9% of the chord behind the leading edge, and a max camber of 8.3% of the chord length at 55.2% of the chord behind the leading edge [22]. Figure 25 shows the E423, with a max thickness of 12.5% of the chord length at 23.7% of the chord behind the leading edge, and a max camber of 9.5% of the chord length at 41.4% of the chord behind the leading edge [22]. Figure 26 shows the GOE233, with a max thickness of 11.6% of the chord length at 19.8% of the chord behind the leading edge, and a max camber of 8.2% of the chord length at 49.8% of the chord behind the leading edge [22].
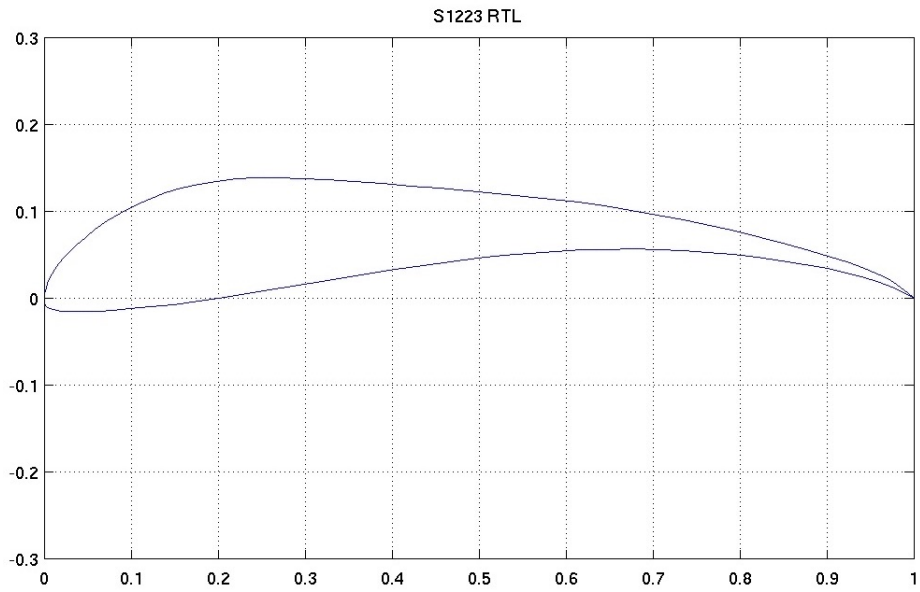
Figure 24: Profile of the Richard T. LaSalle S1223-RTL airfoil. Copyright: UIUC Airfoil Coordinates Database [23]
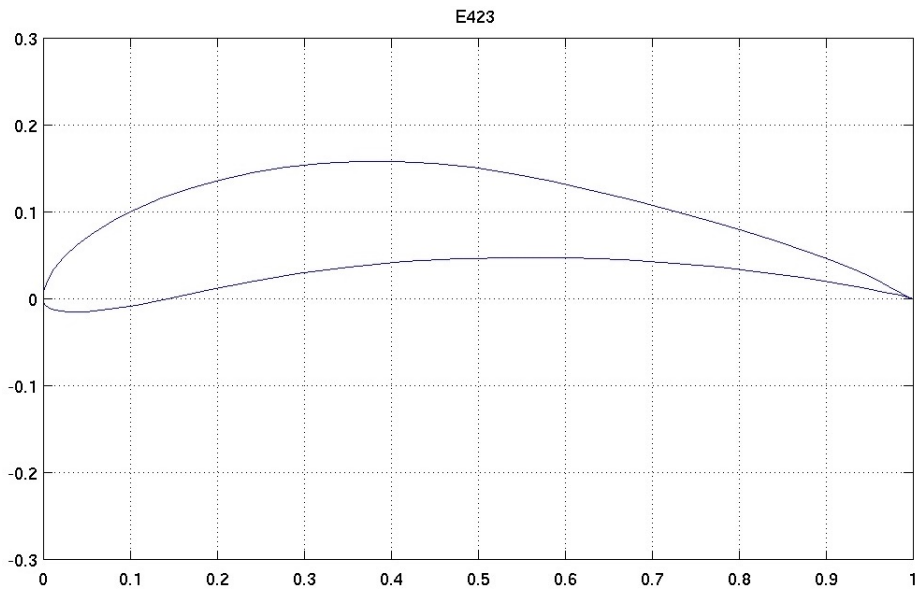
Figure 25: Profile of the Eppler E423 high lift airfoil. Copyright: UIUC Airfoil Coordinates Database [23]

43
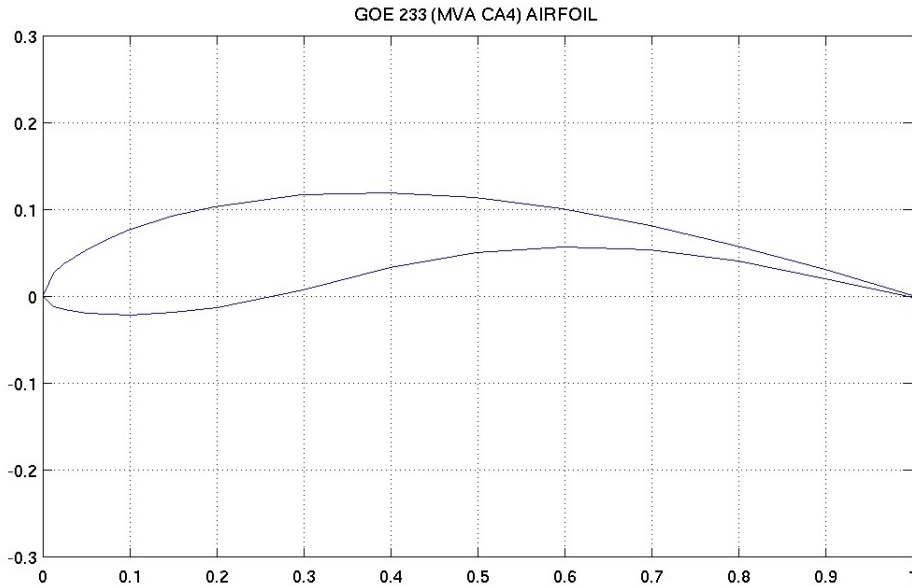
Figure 26: Profile of the Gottingen GOE233 airfoil. Copyright: UIUC Airfoil Coordinates Database [23]

The software and simulations team obtained for each of the four airfoils a .dat file describing the airfoil shape from Airfoil Tools. They imported these files into XFLR5 to generate simulated airfoils for aerodynamic analysis. By examining previous reports, the aerodynamics team estimated the wing mean chord length to be between 0.75 and 1.0 meters and the cruise flight speed to be approximately 15 meters per second, which yielded an estimated Reynolds number range of approximately 800,000 to 1,000,000. For a consistent comparison, the software and simulations team evaluated all four airfoils at a 1,000,000 Reynolds number using the XFLR5 XFoil Direct Analysis tool. In this analysis, XFLR5 simulated a viscous flow across the airfoil and the resultant pressures, forces, and moments as the airfoil angle of attack varied.

To narrow down the options from the four initial airfoils, the team first looked at the coefficient of lift results from the XFoil Direct Analysis. Figure 27 shows a graph of the dimensionless lift coefficient (Cl) as a function of angle of attack in degrees (Alpha). In this graph generated by XFLR5, the green line represents the S1223, brown represents the S1223-RTL, purple is the E423, and blue is the GOE233. This data shows that for a given speed, the S1223 generates the greatest amount of lift, which validates why this airfoil is commonly used in SAE Aero Design and similar competitions. As expected, the S1223-RTL modification to the S1223 performs similarly to the S1223. These two airfoils have approximately the same lift slope, but the S1223 has a slightly higher lift coefficient for most angles of attack. The S1223-RTL performs better than the S1223 at high angles of attack above 14 degrees. The E423 has a slightly lower lift slope than both the S1223 and S1223-RTL, while the GOE233's lift slope is comparable to the two Selig airfoils. The E423 generates significantly more lift than the other three airfoils at negative angles of attack of -3 degrees and lower, however it underperforms the Selig airfoils at positive angles of attack. The GOE233 lift coefficient is significantly lower than the three other airfoils at all angles of attack, maxing out with 1.82 at 16.9 degrees, compared to the other three maximum lift coefficients: 2.40 at 14.0 degrees (S1223), 2.5 at 17.0 degrees (S1223-RTL), and 2.03 at 12.3 degrees (E423). Since a high lift coefficient is crucial to successfully carry a large payload, the GOE233 airfoil was eliminated from further investigation.
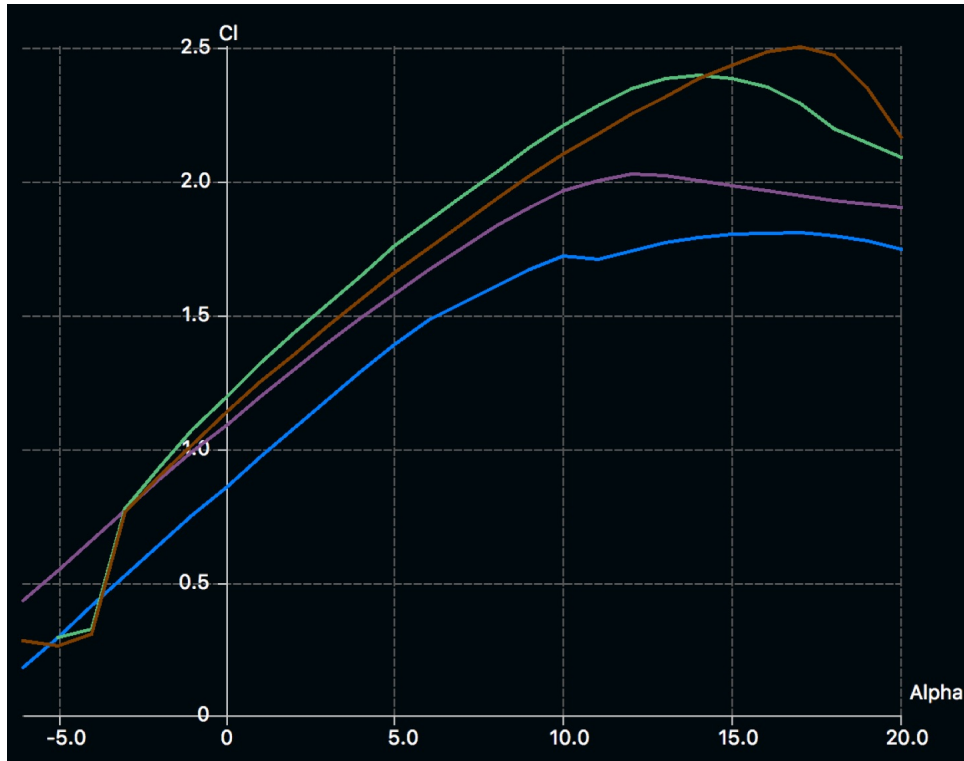
Figure 27: Coefficients of lift for the S1223 (green), S1223-RTL (brown), E423 (purple), and GOE233 (blue) at a constant Reynolds number of 1,000,000.

Next the team looked at the lift-to-drag ratios of the three airfoils. In addition to maximizing lift, the chosen airfoil should minimize its generated drag for more efficient flight. This is especially important due to the aircraft's limited thrust supply. Figure 28 shows the lift-to-drag ratio (equivalent to Cl/Cd) as a function of angle of attack for the S1223 (green), S1223-RTL (brown), and E423 (purple) airfoils, as generated by the XFLR5 XFoil Direct Analysis tool at a 1,000,000 Reynolds number. For angles of attack below 11 degrees, the E423 has a substantially higher lift-to-drag ratio than either of the Selig airfoils. Since the S1223-RTL has a lower lift coefficient and lower lift-to-drag ratio than the S1223 at most low angles of attack, it does not provide an advantage over the S1223 and thus was not considered further for the aircraft.
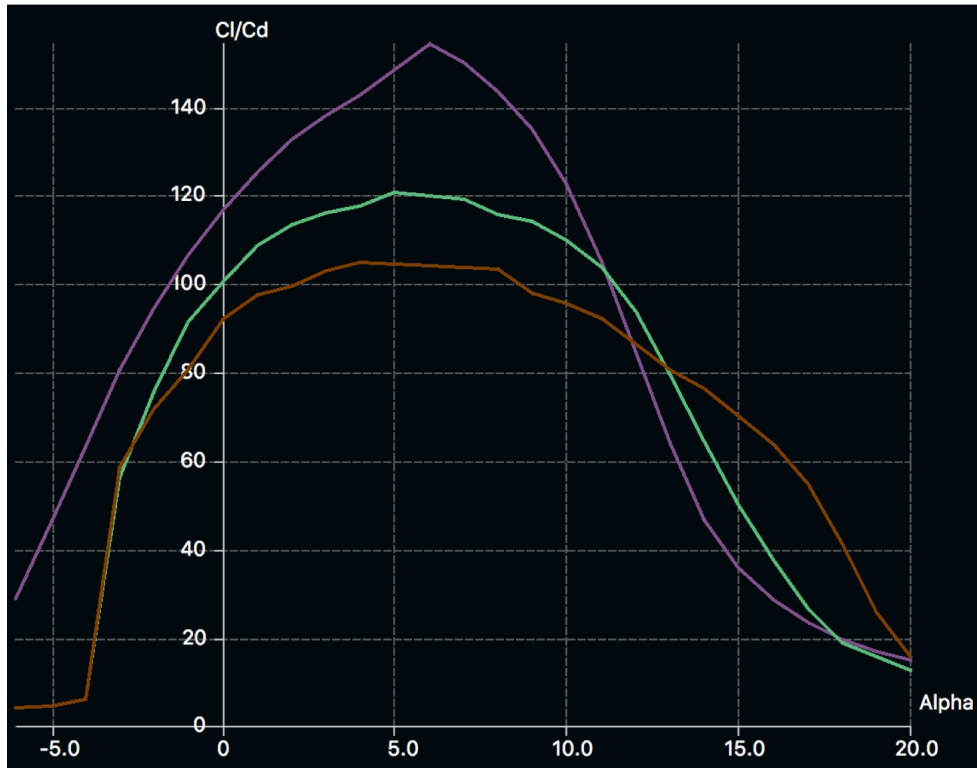
Figure 28: Lift-to-drag ratios for the S1223 (green), S1223-RTL (brown), and E423 (purple) at a constant Reynolds number of 1,000,000.

Although the E423 has a maximum lift-to-drag ratio 27% higher than that of the S1223, the team decided to evaluate the moment coefficients of the two airfoils before making a final selection. A smaller pitching moment generated by the airfoil is desirable because it requires a smaller horizontal stabilizer to achieve longitudinal stability, which would help reduce aircraft structure weight and thus accommodate a greater payload capacity. As Figure 29 shows, the E423 (purple) produces a smaller moment coefficient than the S1223 (green) for all angles of attack above -3 degrees. Although the E423 generates less lift than the S1223 for most angles of attack, the E423 has more a desirable lift-to-drag ratio and pitch moment coefficient than the S1223, giving it an aerodynamic advantage for this type of aircraft.
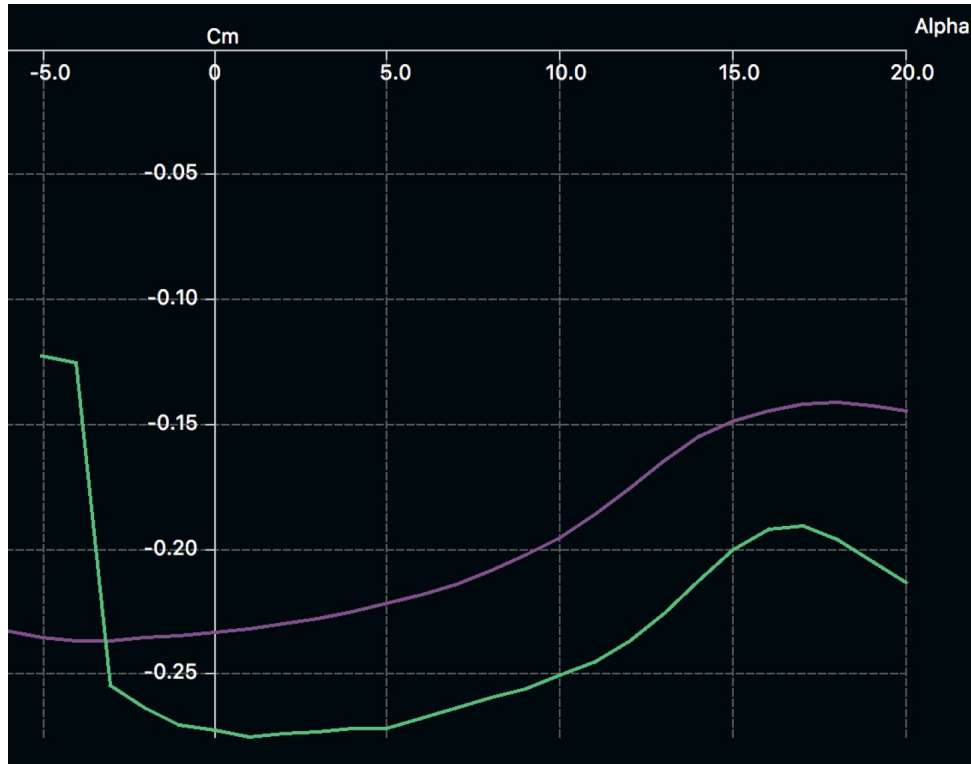
Figure 29: Moment coefficients for the S1223 (green) and E423 (purple) at a constant Reynolds number of 1,000,000.

Before making a final selection between the S1223 and E423 airfoils based on airfoil performance results from XFLR5, the team manufactured models of both airfoils to test in the wind tunnel. The first models were constructed from standard pink insulating foam. Laser-cut forms made of medium-density wood served as guides for hot wire cutting the foam. These guides were ultimately made from medium-density woods, as the hot wire cutter was able to slice and deform templates made from balsa and other low-density woods. With the use of the guides, the aerodynamics team cut a foam model of the E423 airfoil and the S1223 airfoil, each approximately 0.175 meters in chord, and 0.19 meters in span. Holes were drilled into the foam models to match the mounting bracket for the wind tunnel force measuring apparatus.

To gain accurate aerodynamic measurements from the models in the wind tunnel, Reynolds number equivalency is desired. With the scale of the models approximately one-sixth of the anticipated wing chord length, the airstream velocity would need to be increased from the expected cruise velocity by nearly six times to achieve Reynolds number equivalency. These high speeds could not be reached with the small wind tunnel, so the team decided to run the wind tunnel near maximum speed and assume Reynolds independence for the aerodynamic performance. However, the foam was not strong enough to withstand such high airstream velocities, even with a thin sheet of reinforcing aluminum along the trailing edge. Therefore, these tests did not produce any conclusive data.

The team recreated both E423 and S1223 models out of sheets of one-eighth inch thick laser-cut balsa wood connected with two wooden dowels and glued together. As with the foam models, these were mounted into the wind tunnel and run at maximum speeds. The S1223 broke in the wind tunnel, however the E423 was able to withstand the high velocities. Although these tests did not result in any aerodynamic data that could be used to compare the two airfoils, it provided valuable information on the structural stability of each airfoil shape. The balsa wood S1223 broke due to its very thin trailing edge. The E423 trailing edge is significantly thicker, which made it stronger and easier to fabricate. Based on this information regarding structural integrity, combined with the aerodynamic performance evaluations from XFLR5, the

team selected the E423 for the aircraft's main wing airfoil shape.

4.2 Wing Design

4.2.1 Initial Wing Sizing and Shape Design

To obtain an initial size estimate for the wing, the aerodynamics team evaluated the steady-level cruise trim condition, where the lift force is exactly equal to the aircraft weight. This calculation used the maximum allowed weight limit of 240 Newtons, the estimated cruise velocity of 15 meters per second, and the lift coefficient of the E423 airfoil at a zero angle of attack, which is 1.08. This yielded a minimum required wing area of approximately 1.61 square meters, which was rounded up to 1.7 square meters as a safety factor. Using the maximum allowed wingspan of 3.6 meters, this produced a required mean geometric chord of 0.47 meters.

Using these estimated dimensions, the aerodynamics and software/simulation team used XFLR5 to model and evaluate the aerodynamic performance of several different wing shapes. Among the wing shapes tested were rectangular, rectangular bi-wing, elliptical, 1:2 trailing edge taper, 1:2 leading edge taper, and 1:2 symmetric taper, shown below in Figure 30. Each wing shape was evaluated at a constant speed of 15 meters per second using the E423 airfoil profile.
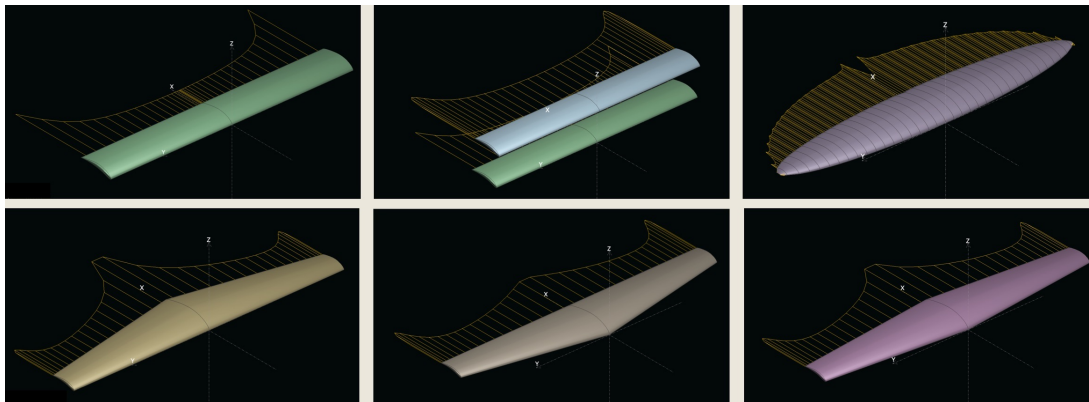
Figure 30: Six possible wing shapes modeled in XFLR5.

Figure 31 shows the lift, drag, and pitch moment properties of the six evaluated wing designs, as generated by XFLR5. As expected, the biplane model produces nearly twice as much lift as the simple rectangular wing, due to its doubled surface area, however it also produces more than twice the drag and would weigh twice as much as a simple rectangular wing. Therefore, the team determined this would not be an appropriate design for the aircraft. The elliptical and three tapered versions all generated higher lift coefficients and lift-to-drag ratios than the rectangular wing. Of these wing shapes, the elliptical wing had the highest lift and lift-to-drag ratios. However, its continuously curved planform presents significant fabrication challenges, so the team decided to pursue options that have easily manufactured straight-edge planforms.
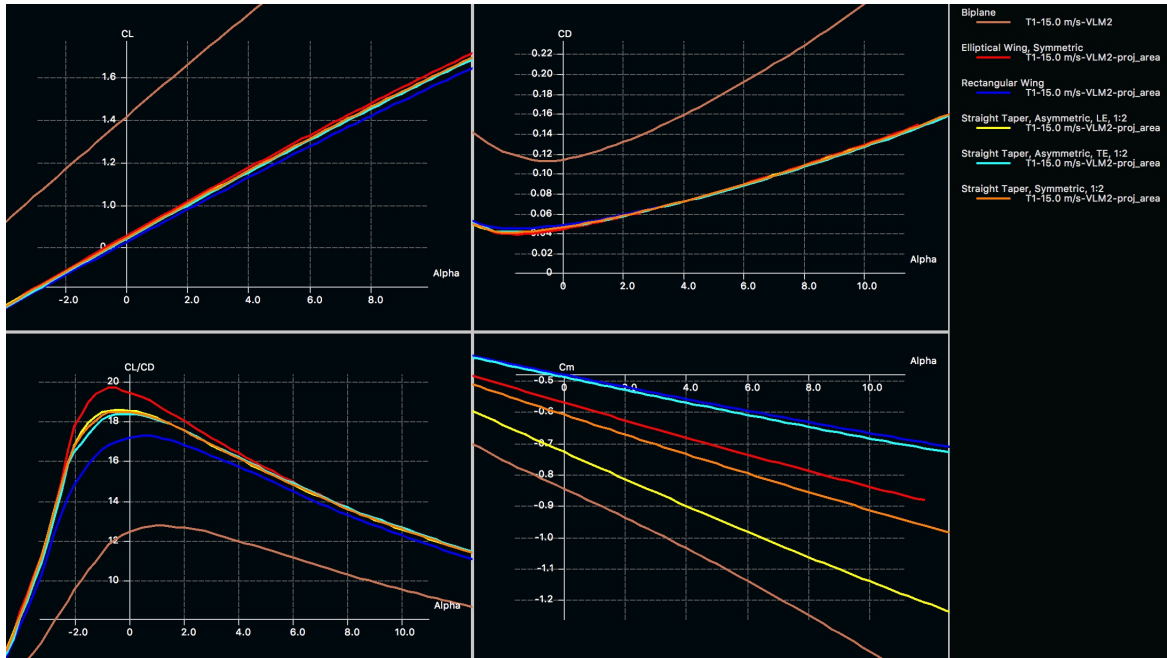
Figure 31: The coefficients of lift, coefficients of drag, lift-to-drag ratios, and coefficients of moments for the rectangular (dark blue), biplane (brown), elliptical (red), straight trailing edge taper (light blue), straight leading edge taper (yellow), and straight symmetric taper (orange) wing shapes, evaluated in XFLR5 at a constant velocity of 15 m/s.

The three straight tapered options all produced very similar coefficients of lift and drag curves. However, at small angles of attack, the leading edge taper produced slightly more lift and had a slightly higher lift-to-drag ratio than both the trailing edge and symmetric tapers. However, the leading edge taper generated a much larger pitching moment. The trailing edge taper produced the least amount of lift as well as the least amount of drag, and had the trailing edge taper had the greatest lift-to-drag ratio for all angles of attack greater than 1.5 degrees. Additionally, the trailing edge taper had the smallest pitching moment, one that was only slightly larger than the moment produced by a simple rectangular wing. Due to its favorable aerodynamic properties and ease of manufacture, the aerodynamics and software/simulation team determined the trailing edge straight taper to be the most ideal shape for the aircraft wing.

4.2.2 Refined Wing Sizing

The previously calculated wing size of 1.7 square meters only accounted for the wing area required to maintain steady level cruise flight, it did not account for flight conditions in which the wing needs to generate a lift force greater than the aircraft weight, such as takeoff and climb. To refine the required wing size, the team evaluated the aircraft's takeoff. The competition rules limit the takeoff distance to 200 feet, however the team chose a goal takeoff distance of 160 feet in case of takeoff complications. The team developed a MATLAB script to analyze the rolling distance, takeoff distance, takeoff speed, and climb rate of the aircraft based on various aircraft parameter inputs. The MATLAB script was developed using the derivation and assumptions in Anderson's *Aircraft Performance and Design*. Since the thrust of the propeller and motor decreases with increasing speed, as described by the experimental thrust curve provided by the propulsion team, Anderson's book approximated the thrust throughout takeoff as a constant at 70% of the static value [16]. The text also used the velocity at takeoff as 1.1 times the velocity of stall, which is calculated with the following equation [16]:

$$V_{stall} = \sqrt{\frac{2}{\rho} \frac{W}{S} \frac{1}{C_{Lmax}}} \tag{33}$$

where rho is the air density, W is the aircraft takeoff weight, S is the wing area, and C_{Lmax} is the maximum coefficient of lift of the aircraft. The lift, drag, weight, thrust, rolling resistance, and ground effect were all taken into account in order to create an accurate model of takeoff conditions. The aircraft parameter inputs included the angle of wing incidence, wing area, landing gear configuration, chord length, aspect ratio, tire material, wing mounting, and flaps. The complete MATLAB script for computing takeoff distance is included in Appendix I.

Using this MATLAB script, the team manipulated various inputs and observed their effects on the calculated takeoff distance. Through trial and error, the team determined that the landing gear configuration must be designed to keep the propeller perpendicular to the runway during roll. This maximizes the horizontal thrust and acceleration of the aircraft, resulting in a shorter takeoff distance. The team also experimented incorporating flaps or a wing incidence angle, however both of these diminished takeoff performance. With flaps, the moment created a large moment the tail would not be able to counteract. A wing incidence angle also created more drag for the aircraft, resulting in a longer takeoff.

Even with these improvements, the aircraft design still failed to produce satisfactory takeoff results. Using the estimated wing area of 1.7 meters and maximum takeoff weight of 240 Newtons, the takeoff calculation MATLAB script returned a distance of 386.6 feet, which is more than 150% the allowable distance. Thus, the team determined that the wing area would need to be increased. Running several iterations of the takeoff script with varying wing areas yielded a plot of takeoff distance as a function of wing area for a 240 Newtons (55 pound) aircraft, represented by the red line in Figure 32. The plot shows that a wing area of nearly three square meters, almost double the original estimate, would be required to achieve the maximum 200-foot takeoff distance (represented by a black line in Figure 32). Since this would result in an extremely heavy wing and ultimately reduce the aircraft's payload capacity, the team determined that for the available thrust and takeoff limitation, the initial goal takeoff weight of 55 pounds was unrealistic. Therefore, the team settled on a lower goal takeoff weight of 45 pounds, or 200 Newtons. Again using the MATLAB script to evaluate takeoff distances for various wing areas, a second plot was generated. This is represented by the blue line in Figure 32. According to the calculation, takeoff could be achieved within the maximum allowable distance for the lower weight with a wing area of just 1.82 square meters, only slightly larger than the original wing size estimate. To achieve the goal takeoff distance of 160 feet (represented by a blue dot in Figure 32), the minimum required wing area would be 2.3 square meters, a 35% increase from the original wing size estimate. Therefore, the design wing area was increased from 1.7 square meters to 2.3 square meters.
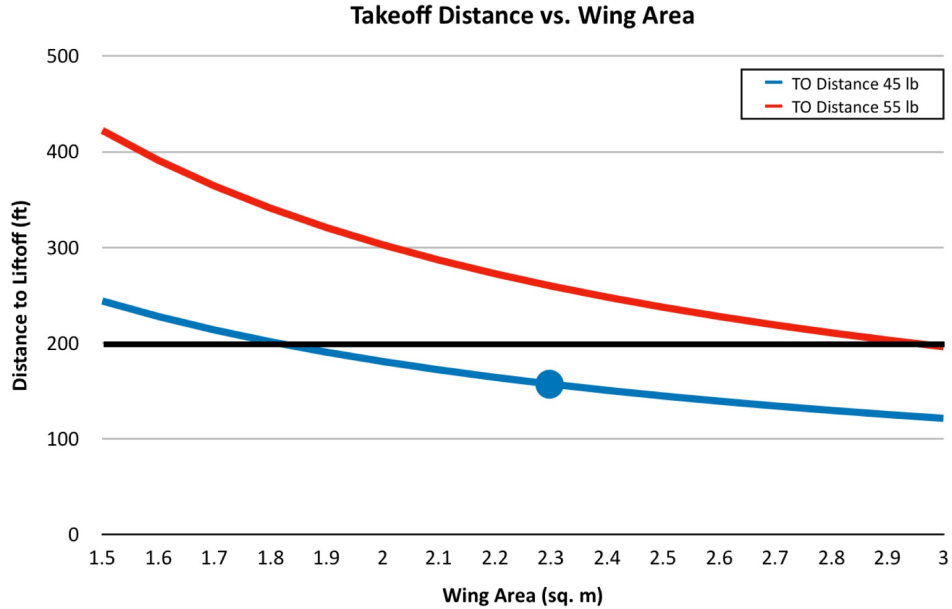
Figure 32: Takeoff distance in feet as a function of wing area for a 240 Newton/55 pound aircraft (red line) and for a 200 Newton/45 pound aircraft (blue line).

4.2.3 Final Wing Design

Enlarging the initial wing design to an area of 2.3 square meters resulted in a MAC of .88 meters, nearly double that of the original 1.7 square meter design. Since a longer chord length increases induced drag and pitching moment, the team investigated modifications to the wing shape that would reduce drag and increase lift. First, the software and simulation team evaluated the aerodynamic performance of the original straight taper wing shape using taper ratios of 1:4, 1:2, and 3:4. These evaluations showed that smaller taper ratios reduce the drag due to the smaller wing tips, and thus improve the lift-to-drag ratio, however they also produce larger pitching moments. Conversely, the larger taper ratios have shorter MACs and thus have reduced pitching moments, but at the expense of increased induced drag. Therefore, the team decided to keep the initial taper ratio of 1:2 because of its favorable balance aerodynamic properties.

Next the team evaluated a blended-shape design for the wing that would retain the aerodynamic properties of the 1:2 trailing edge straight taper while also shrinking the MAC to help reduce induced drag. This resulted in a wing that was rectangular in the center with a straight taper on the outside portion of the span. Figure 33 shows an example of this blended shape design. The software and simulation team evaluated this design with both leading and trailing edge tapers, as well as configurations in which the rectangular portion occupied 25%, 50%, and 75% of the wingspan. The most favorable design with the best lift, drag, and moment properties was the leading edge taper across 50% of the wingspan. The analysis of this wing design is shown in yellow in Figure 34 along with the analysis results of the simple rectangular wing (tan) and 1:2 leading edge straight taper design (blue) for comparison.
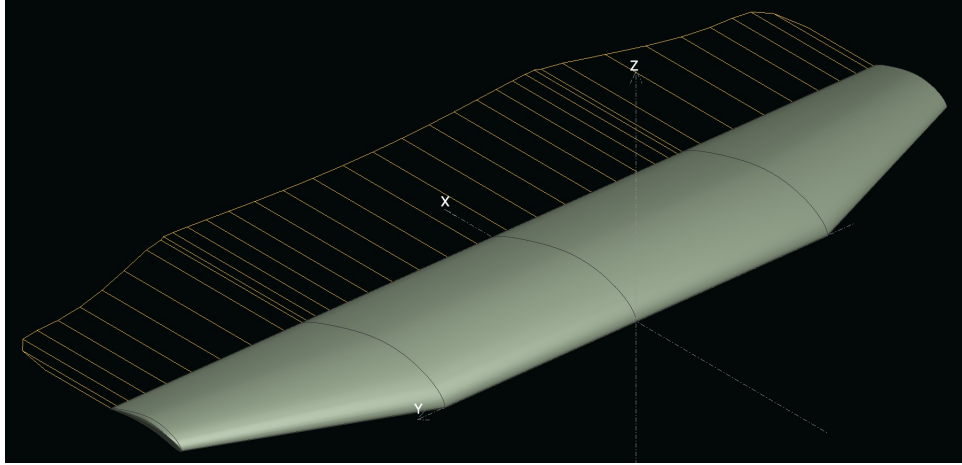
Figure 33: Example of a blended-shape wing design, modeled in XFLR5.
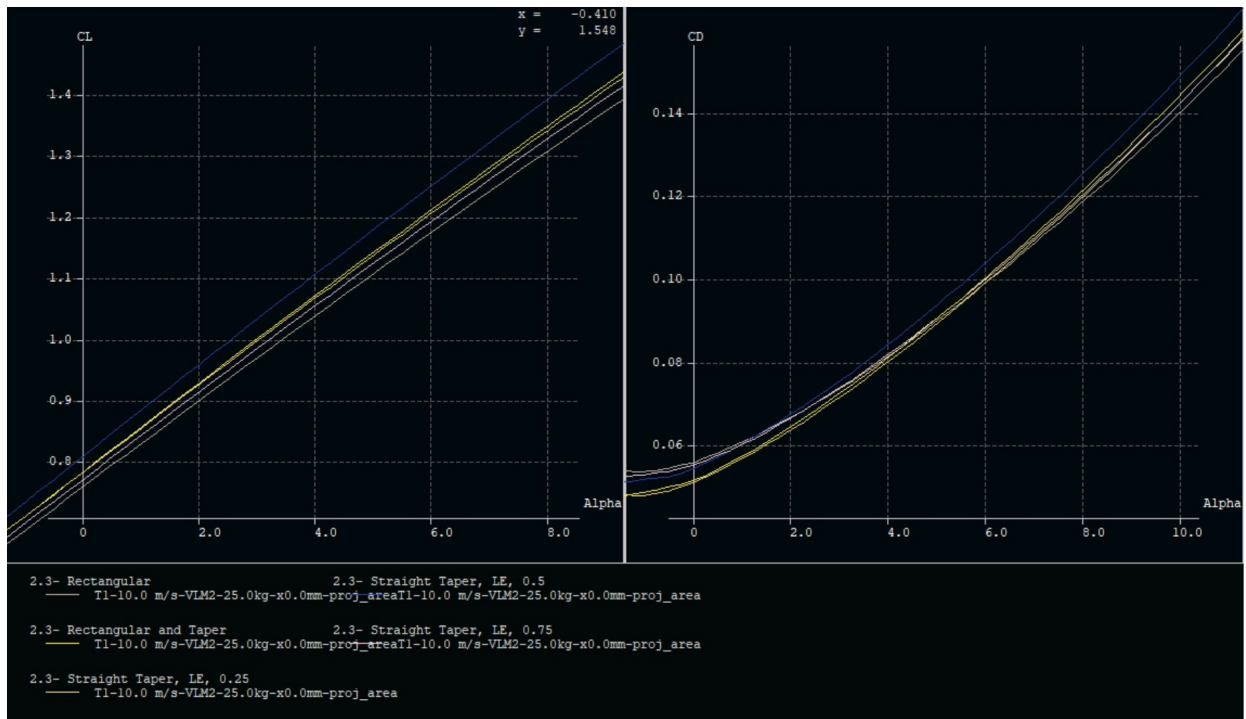
Figure 34: Lift and drag coefficient plots for rectangular (blue), blended-shape (yellow), 1:4 leading-edge straight taper (mustard), 1:2 leading-edge straight taper (blue), and 3:4 leading-edge straight taper (pink) wings at a constant Reynold's number of 100,000.

To further reduce drag and improve the lift-to-drag ratio, the team added winglets to the blended-shape wing model. The winglets dimensions were scaled down from a Boeing design. As Figure 35 shows, the addition of the winglets resulted in a significantly improved lift-to-drag ratio profile (shown in pink) for the chosen wing design. However, the winglets also added a small amount of pitching moment, but the team determined this would not have a significant impact on the required horizontal stabilizer size and therefore would not be a disadvantage.
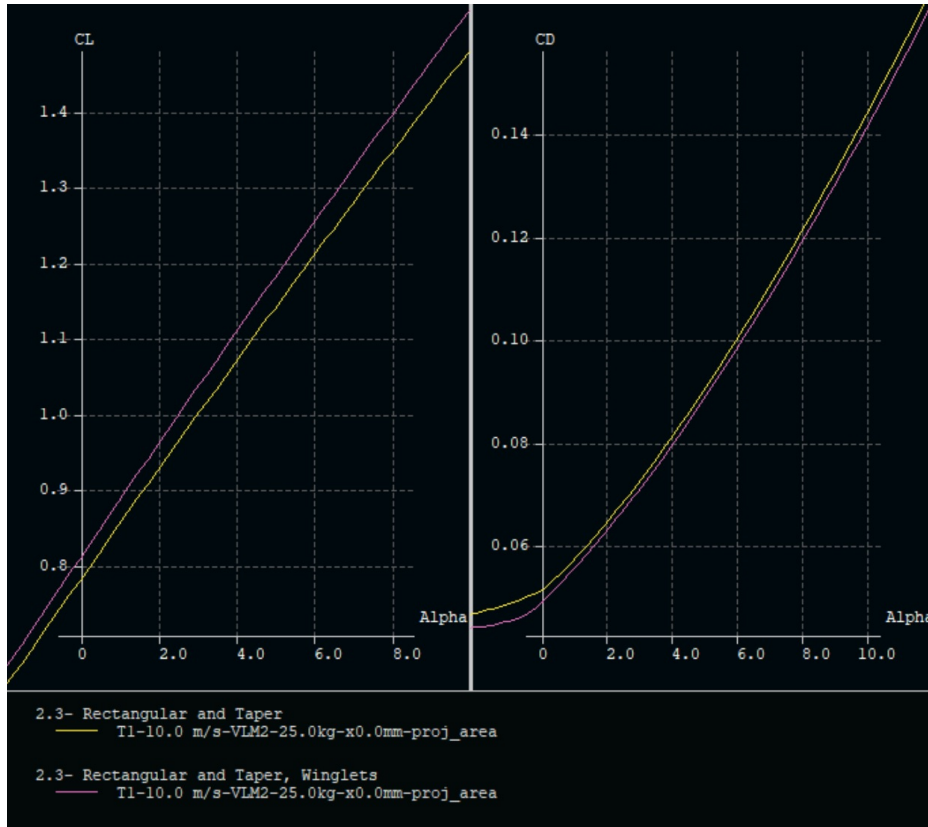
Figure 35: Lift and drag coefficient plots for the chosen blended wing design with winglets (pink) and without winglets (yellow) at a constant Reynold's number of 100,000.

The XLFR5 model of the final wing design is shown below in Figure 36. The wing has an area of 2.3 square meters and a MAC of 0.68 meters. The root chord is 0.75 meters, and tapers along the leading edge to 0.375 meters at the base of the winglets. The wingspan was reduced to 3.5 meters to accommodate the wingtips, and the rectangular section spans 50% of this, or 1.75 meters. The aspect ratio of the wing is 5.32. This wing produces a maximum lift coefficient of 1.95, and results in a takeoff distance of 161.8 feet, which is very close to the goal takeoff distance of 160 feet.
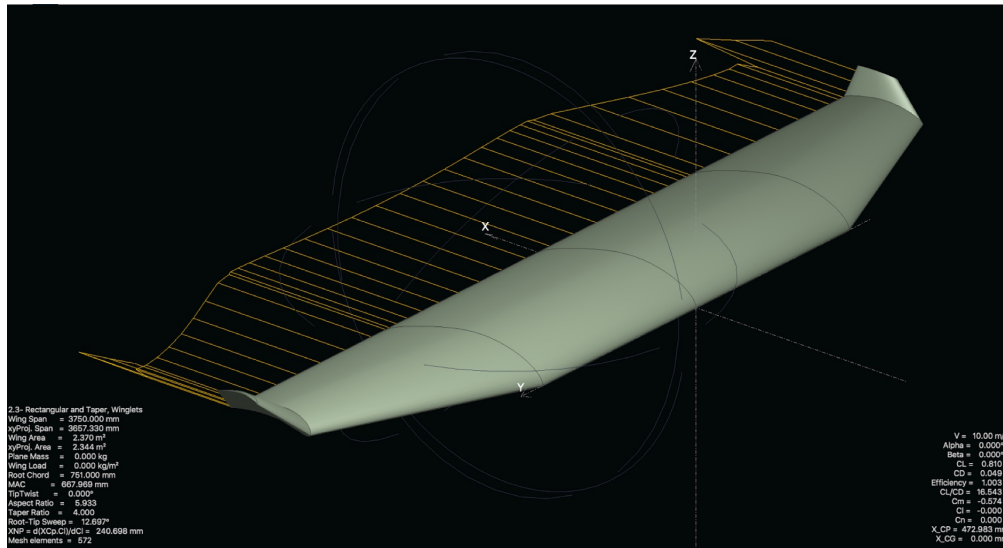
Figure 36: XFLR5 model of the final wing design, displaying the induced drag profile in yellow.

4.3   Tail Design

4.3.1   Tail Configuration

Finding the optimal size for the tail was crucial for static stability. Horizontal and vertical stabilizer dimensions were designed to achieve longitudinal and lateral stability, respectively. For an aircraft with the propeller at the front of the fuselage, an aft horizontal and tail is most effective [7]. The team considered both the conventional aft tail and t-tail designs for the aircraft, both of which are pictured in Figure 37. The conventional tail is the most commonly used tail design, as it is simple, efficient at achieving stability, and easy to analyze for aerodynamic and control properties [7]. The T-tail is also lightweight and efficient, and due to the horizontal tail being located above the main wing, it has a larger moment arm and experiences reduced airflow disturbance effects from the main wing [7]. However, aircraft with T-tails are at risk of entering a "deep stall," which can occur when the aircraft pitches to an angle of attack where the horizontal stabilizer is in the wake of the main wing [7]. The airflow over the horizontal stabilizer is turbulent and reduces the effectiveness of the horizontal stabilizer and control surfaces, so any small disturbance can cause the aircraft to suddenly pitch to an angle of attack well above the stall angle of attack, leading to a potentially irreversible stall condition [7]. Figure 38 depicts an example of an aircraft entering a deep stall. Due to this instability of the T-tail, the aerodynamics and stability and controls teams chose the conventional aft tail configuration for the aircraft design.
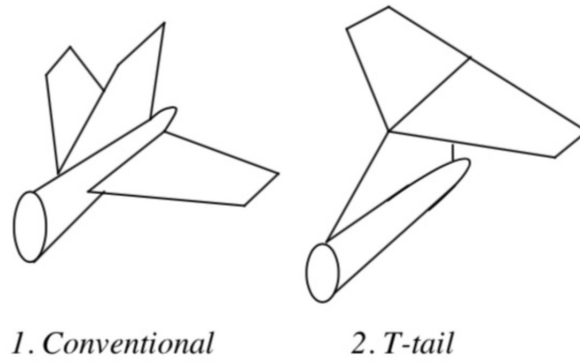
Figure 37: The conventional and T-tail aft tail designs. Copyright: Mohammad H. Sadraey, 2013 [7]
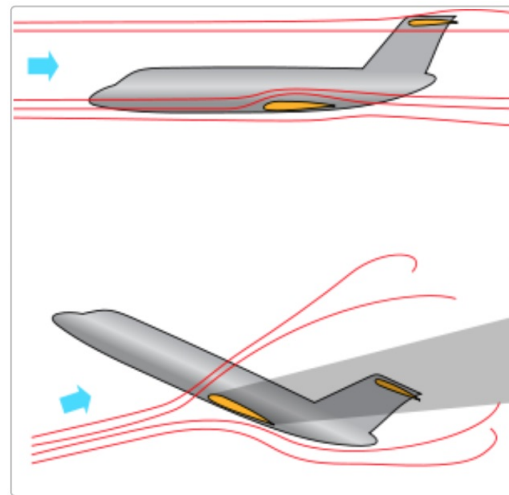
Figure 38: A T-tail aircraft entering a deep stall condition. Copyright: SKYbrary, 2015 [25]

4.3.2 Tail Sizing

For initial tail sizing, the team referred to examples of horizontal and vertical tail volume coefficients typically used for different aircraft applications, summarized in Table 3. The design team determined that the bomber/military transport was the most appropriate comparison to the project aircraft, as they both must generate high lift and maintain stable flight at low speeds, and do not require significant maneuverability. Therefore, the team chose to design for an approximate horizontal tail volume coefficient between 0.7 and 1.1, and a vertical tail volume coefficient between 0.08 and 0.10.

No	Aircraft	Horizontal tail volume coefficient $(\overline{V}_H)$	Vertical tail volume coefficient $(\overline{V}_V)$
1	Glider and motor glider	0.6	0.03
2	Home-built	0.5	0.04
3	GA-single prop-driven engine	0.7	0.04
4	GA-twin prop-driven engine	0.8	0.07
5	GA with canard	0.6	0.05
6	Agricultural	0.5	0.04
7	Twin turboprop	0.9	0.08
8	Jet trainer	0.7	0.06
9	Fighter aircraft	0.4	0.07
10	Fighter (with canard)	0.1	0.06
11	Bomber/military transport	1	0.08
12	Jet Transport	1.1	0.09

Table 3: Horizontal and vertical tail volume coefficients for various aircraft. Copyright: Mohammad H. Sadraey, 2013 [7]

The horizontal tail volume coefficient equation (Equation 16) allowed the team to calculate the required surface area of the horizontal tail. An initial aspect ratio for the horizontal tail was determined using the following estimate [7]:

$$AR_{Htail} = \frac{2}{3} AR_{wing} \tag{34}$$

A 1:2 taper ratio was added to the horizontal tail to reduce drag and weight. XFLR5 analyses and the MATLAB stability scripts developed by the stability and controls team were used to manipulate the horizontal tail dimensions, incidence angle, and moment arm to achieve proper stability. After evaluating various configurations, the team decided upon a horizontal tail volume coefficient of 0.70 and moment arm of 1.89 meters (measured from the wing leading edge to the horizontal tail leading edge), which produced favorable lift-to-drag and moment coefficient versus angle of attack curves. Table 4 summarizes the final horizontal tail dimensions and parameters.

Horizontal Stabilizer Parameters

Parameter	Dimension	Unit
Span	1.6	m
Root Chord	0.5	m
Tip Chord	0.25	m
Mean Aerodynamic Chord	0.389	m
Straight Leading Edge Taper Ratio	0.5	
Aspect Ratio	4.27	
Surface Area	0.6	m²
Moment Arm	1.89	m
Horizontal Tail Volume Coefficient	0.7	
Inclination Angle	-3	deg

Table 4: Summary of final horizontal tail dimensions.

By using the chosen vertical tail volume coefficient range of around 0.08 to 1.1 and the horizontal stabilizer moment arm of 1.9 meters, the team solved the vertical tail volume coefficient equation (Equation 16) to find the required vertical tail surface area. Based on typical transport aircraft characteristics, the vertical tail aspect ratio was estimated at 0.95 [7]. From these initial estimates, the MATLAB stability scripts were used to adjust the vertical tail aspect ratio for refined lateral stability. Table 5 shows the final vertical stabilizer parameters.

Vertical Stabilizer Parameters

Parameter	Dimension	Unit
Span	0.6	m
Root Chord	0.6	m
Tip Chord	0.3	m
Mean Aerodynamic Chord	0.47	m
Straight Leading Edge Taper Ratio	0.5	
Surface Area	0.27	m²
Moment Arm	1.81	m
Vertical Tail Volume Coefficient	0.06	

Table 5: Summary of final vertical tail dimensions.

In the case of a spin, a large enough yawing moment is needed for the aircraft to recover [7]. The vertical tail must be in a wake free region to effectively generate a yawing moment. The vertical stabilizer has a longer root chord length and shorter moment arm than those of the horizontal stabilizer. To minimize airflow disturbance from the horizontal stabilizer and elevator from reducing the rudder effectiveness, the trailing edges of the two stabilizers were aligned [7]. This allows for a large area of the vertical tail to fall outside of the horizontal tail wake region without shortening the moment arm of the vertical tail.

4.3.3 Tail Airfoil

The horizontal and vertical tail airfoils should be symmetrical and non-lifting. The team wanted the airfoil to be thin and lightweight, but thick enough so that it could be easily manufactured and would maintain structural integrity. The team used Airfoil Tools and identified the NACA-0009 9.0% smoothed, or n0009sm-il, standard airfoil as an appropriate airfoil for both the horizontal and vertical stabilizers. The profile of this airfoil is shown in Figure 39.
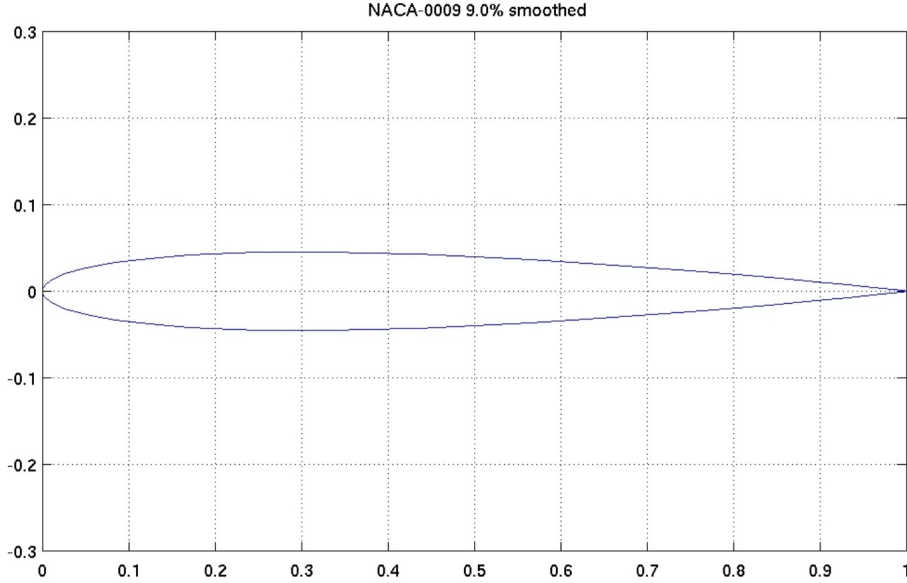
Figure 39: Profile of the NACA-0009 9.0% smoothed airfoil. Copyright: UIUC Airfoil Coordinates Database [23]

5   Controls Design and Initial Stability Analysis

To size the control surfaces, the controls team gathered typical surface area percentages of similar transport aircrafts. The chord length of each rectangular elevator is 0.15 meters. Their span each is 0.8 meters with surface area of 0.12 meters squared which covers 40% of the total horizontal tail area. The rudders surface area is 0.11 squared meters which is 33% of the vertical tail surface. The rudders are rectangular with a chord length of 0.33 meters. The span of each aileron is 0.655 meters which covers is 40% of the exposed half-span of the wing. The chord length of the rectangular ailerons are 0.17 meters.

The controls team found the maximum torque required for each servo by calculating the torque for each control surface using the below equation:

$$\tau = \rho c_{cs}^2 V^2 L sin(and) \frac{tan(\theta_{cs})}{tan(\theta_{servo})} \tag{35}$$

in which τ is the torque, ρ is the sea level air density, c_{cs} is the control surface chord length, V is the aircraft velocity, and L is the control surface span. θ_{cs} and θ_{servo} are the maximum deflection angles of the control surface and the servo, estimated to be 25 degrees and 45 degrees, respectively. By substituting a speed of 15 meters per second, the maximum required torque for both of the elevators and the rudder were 66 ounce-inches each, and 68 ounce-inches for both the ailerons. The team selected the Hitec HS-645MG servo with 107 to 133 ounce-inches torque at 4.8 and 6 Volts respectively, which provides the required torque with a 1.36 factor of safety.

A trim analysis of the control surfaces was conducted to obtain the necessary elevator deflection at cruise. This was done by capturing the moment coefficient versus angle of attack plot at various elevator deflection angles, which is plotted on the right in Figure 40. With a desired cruise angle of attack of 1 degree, the elevator deflection was determined to be approximately 4 degrees.
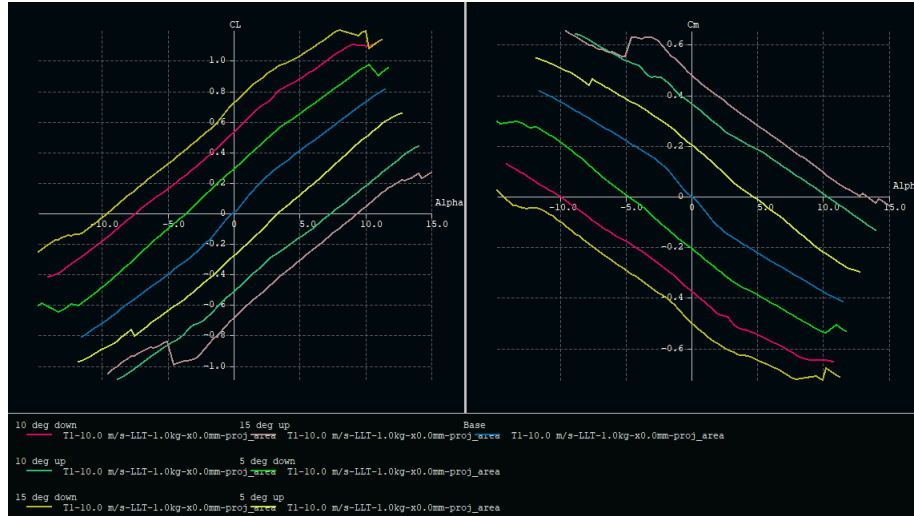
Figure 40: Lift and moment coefficients of the horizontal tail with elevator deflection varying from -15 degrees (yellow) to +15 degrees (pink).

To ensure static stability, the team located the neutral point and the most forward point for longitudinal stability on the aircraft. The neutral point was calculated based on the aerodynamic design of the wing and horizontal tail. Using equations (21) through (23), the location of the neutral point was determined to be 45.1 centimeters aft of the leading edge of the wing and 55.9% of the wing mean chord. The aerodynamic center was approximated to be at the quarter chord point, which was the most forward point based on the moment balance of the aircraft. To achieve a static margin of 10% to 15%, the center of gravity was expected to be placed at approximately 38.3 to 34.9 centimeters behind the leading edge of the wing.

6   Fuselage and Structural Design

The team designed the fuselage based on the size of the payload, the electronics, and the installation of wing, tail, and the landing gear. With durability as a primary focus for the design of the fuselage and structure, the team chose to use a solid construction method as opposed to using a lighter balsa wood frame and thin skin. To obtain a shorter and lighter weight fuselage, the team decided on a two-row seat configuration for 36 passengers. A 20-centimeter usable space was designed for the luggage bay in front of the passenger bay to bring forward the CG. A maximum height of 22.5 centimeters was required to set the electronics board under the payload as to keep the fuselage as short as possible. The final length of the fuselage was 1.758 meters with a width of 20.32 centimeters.

For landing gear, the design team chose a tricycle configuration. For a stable landing, two larger wheels were set aft of a steerable, spring loaded front wheel, which provided control during taxi, takeoff, and landing. The front landing gear was designed to sustain a 200-pound load, which significantly exceeded the maximum loads expected upon landing. A small, free-spinning tail dragger wheel was added to the underside of the tail to avoid any damage to the tail during takeoff rotation.

Part IV
Aircraft Fabrication

1 One-Tenth Scale Wing Model

To verify the XFLR5 model analysis and to further evaluate the aerodynamic performance of the wing design, the team tested a scale wing model in the wind tunnel. To fit inside the wind tunnel test section, a 10% scale model was selected. Based on the failure of both foam and wood airfoil models during previous wind tunnel tests, the team decided to 3D print the scale wing to achieve a model with enough structural integrity to withstand the high airstream velocities. A Dimension SST 1200ES Rapid Prototyping machine, owned by the WPI Mechanical Engineering Department, was used to print the model. This machine prints with ABS thermoplastic in layers 0.01 inches thick [24].

Team member Blake Rice developed the SOLIDWORKS models to print. To ensure the wing had the proper airfoil profile, he used a converter script to generate a SOLIDWORKS sketch from the E423 .dat file. From this airfoil profile, he modeled the blended wing design using the dimensions the design team provided, and scaled the model down to one-tenth the original size. To accommodate the 10-inch square printing platform and 12-inch height limitation of the Dimension SST 1200ES, Blake divided the model into three sections: the rectangular center portion and two tapered end sections (including the fixed winglets). He added holes to the rectangular section to fit the wind tunnel force balance mounting plate, and holes in each of the three parts so they could be attached using two 0.25-inch diameter wooden dowels at each interface. Figure 41 shows the three completed SOLIDWORKS CAD models. The three parts were printed vertically on the printing platform, with the airfoil profile in the horizontal plane for the best resolution. After printing, the four wooden dowels were glued in and the parts were clamped together until dry. The finished 3D-printed 10% scale wing model is shown in Figure 42. Part IV Section 1 details the wind tunnel test procedure and results for the wing model.
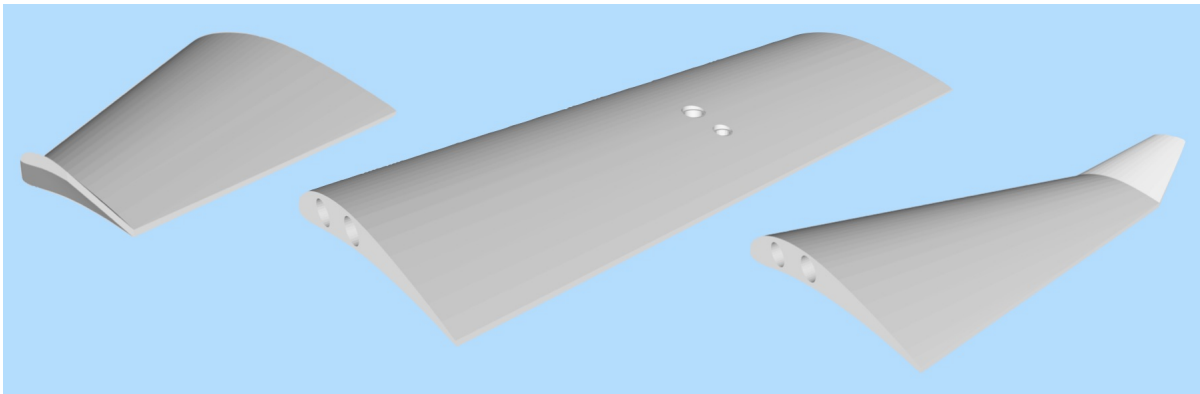
Figure 41: Three parts of the 10% scale wing modeled in SOLIDWORKS for 3D printing.
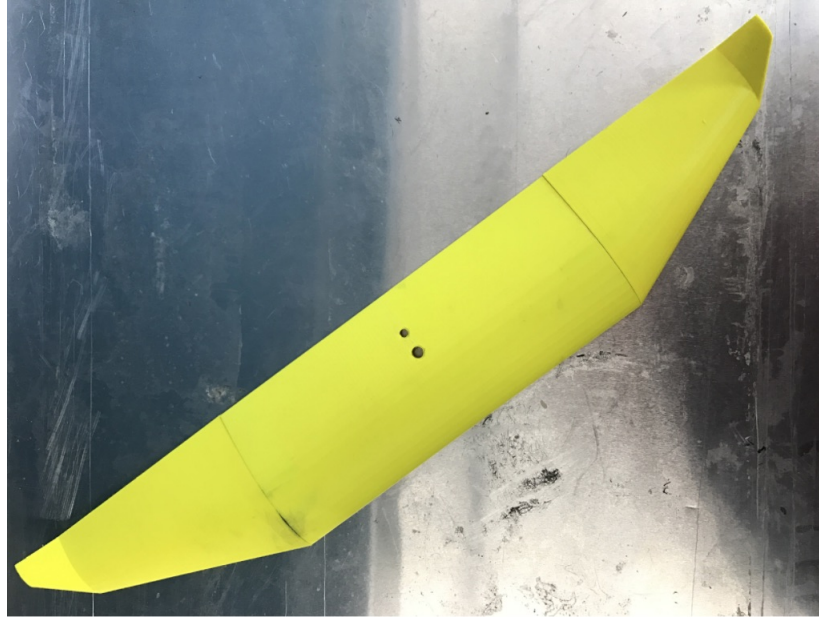
Figure 42: 3D-printed 10% scale wing model.

2   One-Third Scale Glider Model

The glider was created as a proof of concept for both the proposed manufacturing methods and the aerodynamic design. The glider consisted of a one-third scale wing made of foam ribs and balsa wood skin, and a one-third scale tail cut from insulation foam, connected together with a wooden dowel for the proper moment arm. The wing was constructed in three separate pieces (left and right tapered sections, and center rectangular section), and the tail was constructed in four pieces (vertical tail, left and right horizontal sections, and a central foam piece that connected the tail sections to the wooden dowel).

To create the foam ribs of the wing, sections were sketched in SOLIDWORKS and laser-cut into plywood to create templates. These laser-cut sections were used as templates for hot wire cutting one-inch-thick sheets of EPS insulation foam to create the ribs. This process is pictured in Figure 43 Two wooden templates of the same size were used to cut three equal foam ribs for the middle rectangular section, while four templates of different sizes were used to cut two ribs with the appropriate taper for the left and right tapered portions. Figure 44 shows an example of a completed foam rib.

Figure 43: Hot wire cutting foam ribs using laser-cut wooden templates.

Figure 44: Completed foam rib fabricated by hot wire cutting.

For each rib cut using the appropriate templates, both a top and bottom inverse shape, or blank, was also formed in the foam. Once all seven sets of ribs and blanks were formed, they were joined together into the three sections (rectangular center and outer tapers) using wooden dowels as spars. Next, each section was layered with a 1/16 inch-thick balsa wood skin. A sheet of balsa wood was laid across the lower blanks, then glued to the foam ribs using Gorilla Glue. Next, another sheet of balsa wood was glued to the top surfaces of the foam rib, and the top blanks were placed on top. A weight applied over the top of the blanks held the balsa wood skin in place as the glue set. Once all three sections were constructed, they were glued together at the wooden spars to form the complete wing.

For the tail, wooden templates were laser-cut to create guides for hot wire cutting. Two identical horizontal stabilizer sections and a single vertical stabilizer were cut from EPS insulation foam. The three tail sections and the wing were glued to foam blocks that were then mounted to a one-inch diameter wooden dowel, which represented the fuselage. The wing has a zero-degree incidence angle, and the horizontal tail has a -3 degree incidence angle. Rubber bands secured the wing to the dowel and prevented it from slipping. The completed one-third scale glider is pictured in Figure 45. This glider model did not include wingtips or control surfaces, since the team wanted to observe the inherent stability of the aerodynamic design without control inputs.

Figure 45: One-third scale glider model.

3 Full-Size Wing and Tail Construction

To construct the wing and horizontal and vertical stabilizers, the same foam rib method from the glider construction was used. The main wing was again produced in 3 segments, the horizontal tail was constructed in two halves, and the vertical tail was made in one piece. Due to the inability to find large enough sheets of balsa wood and to minimize the cost, the full-size models were skinned using rolls of one-quarter-inch thick flexible insulation foam cut to the proper size and shape.

3.1 Main Wing Frame

The frame, which makes up the primary structural body of the main wing, consists of hotwire-cut foam ribs and aluminum square tubing spars. The wing was originally modelled in SOLIDWORKS to determine the locations of the ribs based on structural needs and the need to disassemble the aircraft wing into three parts. It was determined two supporting spars would be required to support the full wing. The leading edge spar is constructed of 1-inch aluminum square tubing ($\frac{1}{8}$ inch wall thickness). In the tapered sections this spar was angled to match the leading edge of the tapers. The rear spar is $\frac{3}{4}$ inch aluminum tubing ($\frac{3}{8}$ inch wall thickness) and extends from wingtip to wingtip, passing through all the ribs. The leading edge spar passes through all ribs, with the exception of the two wingtips, due to the small profile resultant from the taper. Instead, they were riveted to the rear spar on the inside of the ribs, so as not to extend into the rib. The frame disassembles into three parts: the 6-foot main wing section and the two tapered wing tips. Mounting brackets on each side of the four spar connection points attach the three segments together, and two bolts with wing nuts secure each connection. Figure 46 depicts a SOLIDWORKS model of the full rib-and-spar frame.
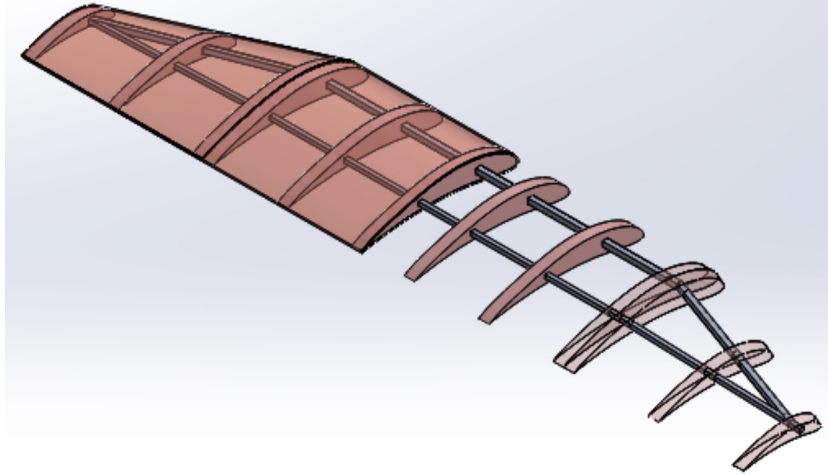
Figure 46: Main wing rib and spar frame assembly modeled in SOLIDWORKS.

3.1.1 Ailerons Formation

Ailerons were cut from the main wing using the hot wire cutting method and laser-cut guides. The trailing edge portion of the main wing tapered sections were separated from the rest of the frame to act as ribs for each aileron. The front of each aileron rib was trimmed so each control surface can rotate freely about the rotation axle, which was $\frac{5}{8}$ aluminum rod inserted through each control surface foam rib. Shaft collars were attached at the ends to hold the control surfaces in place, and laser-cut wooden end brackets were also used to fix the rods to the wing and tail in the correct location.

3.2 Main Wing Skinning

Following the construction of the three wing frame segments, made up of ribs and adhered spars, the main wing progressed into the sealing stage of fabrication. This consisted of preparing pre-cut sections of the flexible insulation foam, which was used to seal the top and bottom of the frames in a procedure identical to that used for the glider wing. The three sections were sealed with these foam sheets through the use of Gorilla Glue as an adhesive component. Foam sheets were used to seal the aileron segments which were cut away from the main wing ribs, allowing for control surfaces consisting of foam ribs with hollow foam skin, similar to the wing.

The sheets were cut in such a way that left a small gap at the leading edge of the wing which would span roughly two inches. In order to close this gap and prevent airflow inside of the wing itself, an additional strip of insulation foam was cut to cover this two inch gap. The foam was lined with several cuts along the entire length in order to allow for an effective bending about the curve desired for the leading edge. These strips were placed into the gap, and fixed in place with standard packing tape in order to manually ensure the continuity of foam skin from the top wing planform through to the bottom along the leading edge on all wing segments.

The wing sealing was completed with the addition of Monokote on all surfaces. An additional strip of Monokote was heat-adhered to the static sections of the wing segments to span over the first few inches of the ailerons, as the leading edges of these control surfaces consisted of open skins, and there was a priority established for freedom of deflection while minimizing the introduction of internal airflow via these open gaps. This process is pictured in Figure 47. These strips of Monokote would allow for deflections of the ailerons while keeping these gaps covered.

Figure 47: Heat sealing the Monokote skin to the wing.

3.3   Tail Frame and Control Surfaces Formation

The airfoil shape of the horizontal and vertical tails was cut into 2-inch foam ribs, just as with the main wing. There are six ribs for the horizontal tail and three ribs for the vertical tail. $\frac{5}{16}$ inch round aluminum rods serve as tail spars to promote ideal strength and weight, while allowing for plausible spar sizing at the tail tips. Similarly to the main wing, the trailing edge sections of all ribs were cut away from the static ribs to form the control surfaces, pictured in Figure 48. The horizontal tail was constructed as a single piece that attaches directly to the tail boom, while the vertical tail is detachable for ease of transportation.
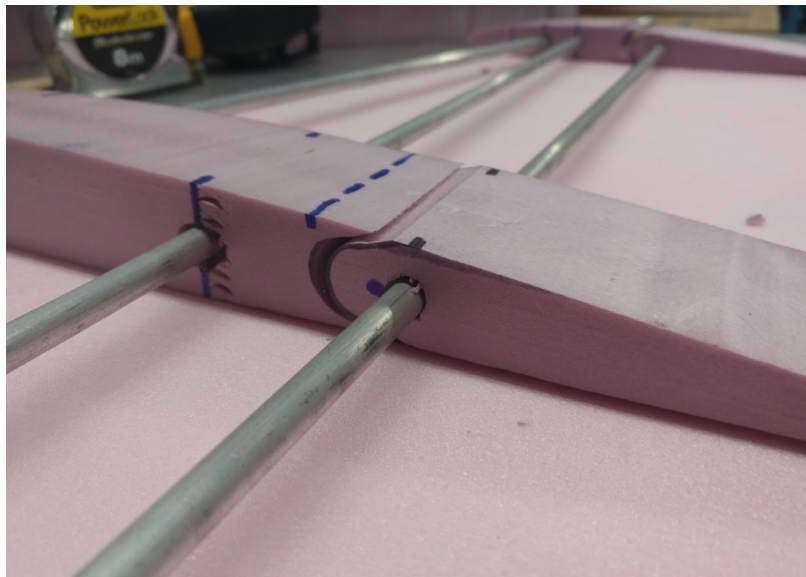
Figure 48: Control surface rib cut away from horizontal tail rib.

The rear spar of the horizontal tail, which also serves as the rotation axle for the elevator (also shown in Figure 48), runs through a 1-inch aluminum square tube, which telescopes onto the $\frac{3}{4}$ inch aluminum

square tube tail boom. To achieve the proper incidence angle for the horizontal tail, the front angled spars run through a second piece of 1-inch aluminum square tubing, which is affixed directly below the primary tube. The ends of the front angled spars were threaded and the holes in the walls of the aluminum tube were tapped to allow a secure fit at the convergence point.

The end of the rear vertical tail spar (which serves as the rotation axle for the rudder) is also threaded. Both vertical tail spars are inserted into holes in the 1-inch aluminum square tubing to which the horizontal tail is mounted. The vertical tail is secured to the tail boom using a wing nut on the threaded end of the rear spar. Figure 49 pictures the horizontal and vertical tail rib-and-spar frames in their assembled configuration.
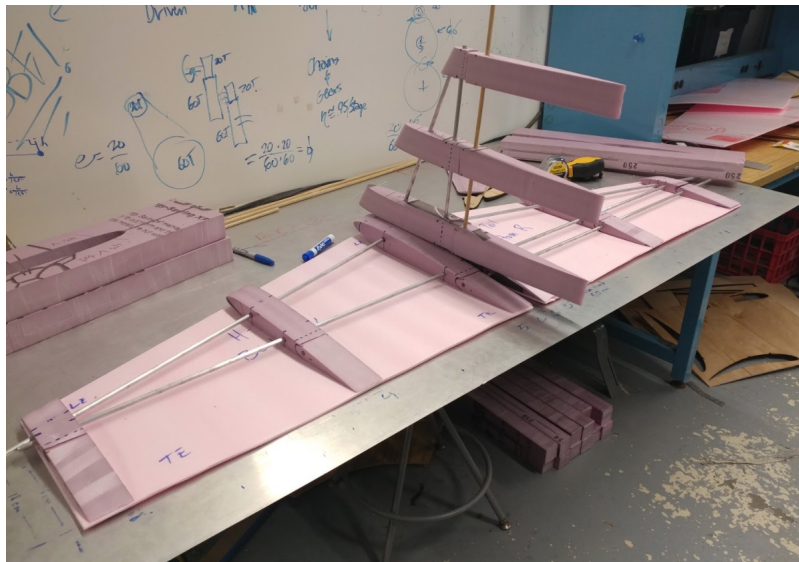
Figure 49: Horizontal and vertical tail frame assembly.

3.4   Tail Skinning and Control Surface Mounting

Once the frames for the horizontal and vertical tails were set, the static sections were sealed using pre-cut sheets of insulation foam, identically to the method used for the main wing. As opposed to the bending strip of foam used for the leading edge of the main wing, dowels were secured with packing tape to fill the gaps where the upper and lower foam skins converge. The elevators and rudder were also sealed and had control horns secured to the mid-tail control ribs to allow deflection via a control arm. Once sealing was completed with the use of Gorilla Glue, the servos were slotted into the respective bays which had been cut out.

The tails and controls were skinned with Monokote and allowed to set. Once this was completed, the vertical tail and rudder were arranged onto the tail mount to allow disconnection. A small portion at the bottom of the rudder was cut away to allow full elevator deflection and full rudder deflection to occur simultaneously without interference. Once controls were properly trimmed and tested, they were secured to the mount. This was done with the use three end caps laser-cut from wood and glued flush to the outer ribs of both the horizontal and vertical tail. The control surface rotation axles pass through holes in each end cap and are secured with shaft collars.

4   Fuselage Construction

The two construction techniques examined for a lightweight and sturdy fuselage were a foam construction method and a balsa frame design. The team decided to move forward with foam construction due

to its superior ability to survive crashes compared to a balsa frame design. For this method, the CAD team using SOLIDWORKS to divide the fuselage model longitudinally into five cross-section slices. Then pink insulation foam board panels were hot-wire cut into these cross-section shapes and adhered together using foam board adhesive to make up the full width of the fuselage. An opening was left in the three inner foam board sections for the passenger bay. The cargo hold and electronics hold were cut out from the full fuselage after the inner panels were adhered together, also using a hot wire cutter. These can be seen in a side view of the fuselage before the outer wall panels were affixed, pictured in Figure 50.
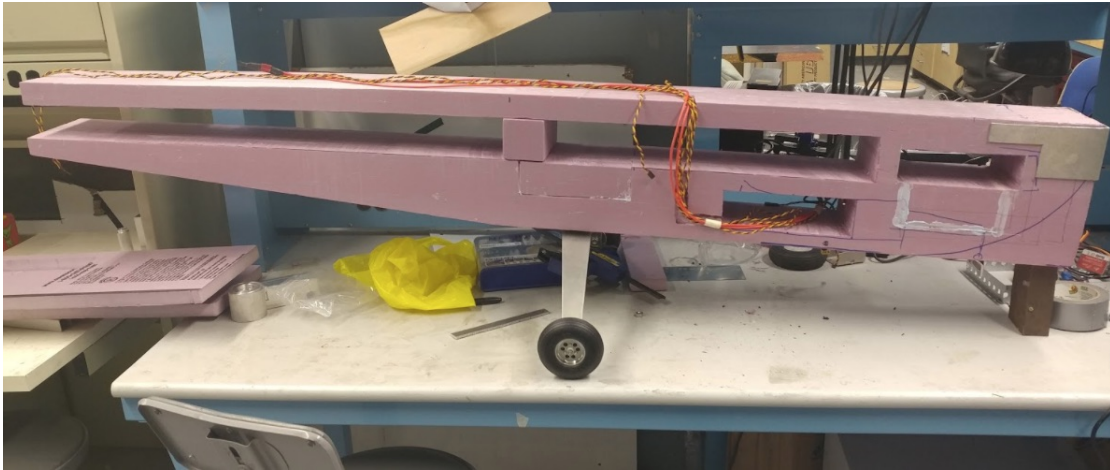
Figure 50: Side view of the fuselage without external panels.

For the landing gear, parts of the foam were cut out to allow for a flat aluminum mounting plate to be inserted into the foam. The landing gear was bolted to this plate as well as a second plate adhered to the underside of the fuselage that compressed the foam. The removed foam was readhered to the inside of the fuselage fill in the void above the mounting plate, shown in Figure 51. All the wiring was placed on the inside of the outer fuselage panels before it was adhered to the main fuselage, with disconnects on either end so that the wiring is fixed in place, but components are accessible and replaceable. Additionally, the motor mount was adhered using a compression fit, adhesion and being bolted to the frame. The nose and front edges of the fuselage were sanded into smooth curves to improve aerodynamics. The fuselage was finally covered in monokote to smooth out the finish and perform as aerodynamically as possible. The completed motor mount, rounded nose, and monokoted fuselage is shown in Figure 52.
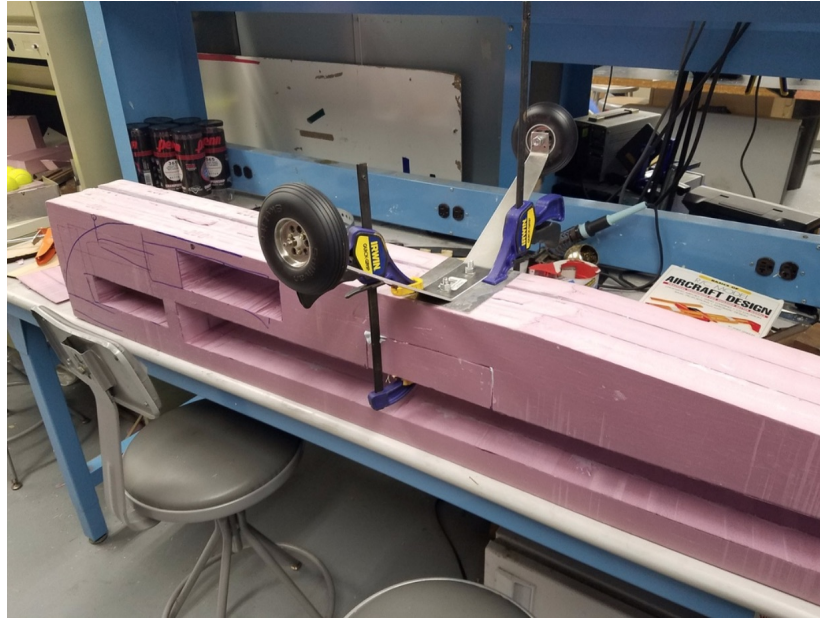
Figure 51: Landing gear and mounting plate installed into the fuselage.

Figure 52: Completed nose with propulsion equipment installed.

4.1 Passenger Bay Construction

The removable passenger bay was constructed from a one-inch insulation foam board, with holes slightly smaller than the maximum diameter of a tennis ball drilled so that each tennis ball fits comfortably in its own "seat." The bottom of the bay was reinforced with a sheet of corrugated cardboard. String handles were attached so the passenger bay can be easily loaded and unloaded from the fuselage. The maximum capacity of the passenger bay is 36.

4.2 Landing Gear Construction

The main landing gear is a commercial off-the-shelf hobby gear that was attached to the fuselage. It is reinforced with aircraft lock wire so as to not buckle or spread under the load of the aircraft upon landing. The front landing gear is a custom-built steerable gear with a suspension that can support 100 pounds of force. This gear absorbs the shock from landing or bumps to avoid damaging the airplane. The front gear has 4-inch diameter wheels, and the rear gear has 6-inch diameter wheels. This arrangement provides the 0 degree angle of attack required for takeoff. The rear and front landing gear can be seen in Figures 51 and 52 respectively, both included previously in this section.

5 Central Spine and Component Attachment

A central spine runs the length of the fuselage to provide structural integrity and attachment points for components. This spine, made from 1-inch aluminum square tubing, was glued to the top of the fuselage, and secured with supporting brackets strapped around the fuselage. Under the main wing, the central spine is reinforced with two parallel beams on the outer edges of the fuselage. The main wing is bolted to all three beams using a total of 6 threaded rods. The three beams were milled with 25-centimeter long channels so that the location of the wing is adjustable and can be manipulated to achieve optimal stability during testing.

A telescoping tail boom, made from $\frac{3}{4}$ inch aluminum square tubing, runs from the tail to the fuselage, attaching the two together. This spine is bolted into the main spine in 4 places to ensure that tail motion is minimized relative to the fuselage and main wing.

Part V
Aircraft Testing and Modifications

1 One-Third Scale Glider Tests

The one-third scale glider model was tested for inherent longitudinal stability. A team member threw the glider at various initial speeds, pitch angles, and altitudes, while two team members recorded the flight and made visual observations regarding the pitch moment and oscillatory patterns. Test flights were performed with the CG located at several different points along the centerline of the wing. A metal weight attached to the nose of the glider was used to shift the center of gravity to one-third of the root chord length. With this CG location, when thrown with a small initial pitch angle, the model was observed to glide smoothly with minimal longitudinal oscillation, indicating a stable configuration. The observations of this test verified the longitudinal stability of the aerodynamic design, as well as proved the strength and durability of the wing fabrication method.

2 Ground Roll Tests and Resultant Modifications

A critical step in verifying the performance of the aircraft was conducting mock takeoff runs. The team conducted a series of taxi and mock takeoff runs for different plane configurations during different stages of manufacturing to verify propulsion and power sufficiency, ground steerability, control surface response, and overall stability during ground roll. All tests were performed on a rubberized athletic track and repeated on an astroturf field.

The first attempt at a mock takeoff was done midway through the manufacturing process and did not include the main wing or tail. In order to simulate the additional weights of these missing components, the aircraft was loaded with 36 tennis balls and 20 pounds of cargo, bringing the total aircraft weight up to

46 pounds. At full power in this test configuration and using the 16x10 propeller, the team found that the aircraft was unable to overcome static friction.

The initial tests indicated that the selected motor and propeller combination was unable to produce enough thrust at rest to overcome the static friction between the plane's landing gear and runway. Prior propulsion testing indicated that the 16x8 propeller with the Hacker motor was more effective than the 16x10 propeller at rest and low speeds due to its lower pitch angle. After determining that the 16x10's reduced performance at the desired cruise velocity should not prohibit the aircraft's ability to sustain level flight, the team installed the 16x10 propeller onto the aircraft and repeated the taxi and power tests with more success. This new propeller was able to generate enough thrust at rest to overcome the static friction, therefore the team decided to use the 16x10 propeller for future tests and in our final design.

With this issue resolved, the team conducted a second mock takeoff run, with the objective of testing the stability of the landing gear and aircraft maneuverability using the steerable front wheel. Again, this test was done without a main wing or a tail. However, to improve handling for testing purposes, the test was completed at a lower weight of 24 pounds. Pilot John Russell conducted the test by trimming out the front wheel so that the aircraft would roll in a straight path with minimal pilot correction. He drove the aircraft a distance of 200 feet under full power. He reported that at low speeds, the aircraft handled quite well and was very easy to maneuver, however the aircraft became increasingly unstable at higher ground speeds. The team was unable to measure a top speed for the aircraft in this configuration due to the instability of the aircraft under full power at high speed.

For the third set of mock takeoffs, the team installed the tail of the aircraft but did not install the main wing, to prevent the aircraft from generating enough lift to lift off the ground. In order to simulate the total intended takeoff weight of 45 pounds, the team added a mass equal to the mass of the main wing located at the wing's center of mass position on the fuselage. The aircraft was powered up to full throttle and released, again driving in a straight line. At a distance of 200 feet (the specified takeoff distance), the aircraft was able to reach a speed of 6.2 meters per second on the track, and 5 meters per second on the astroturf. With the tail installed on the aircraft, high speed taxing became significantly more stable. The team also observed that near the middle of the 200-foot distance, the lift generated by the horizontal tail was significant enough to slightly lift the front landing gear off the ground. Although the pilot maintained full control throughout the third set of mock takeoffs, the aircraft was not able to reach the required design takeoff speed of 10 meters per second within the competition-specified distance.

3   Taxi and Ground-Roll Testing Conclusions

The taxi tests successfully verified that the electronics and controls were fully functional, and that the front landing gear provided good steerability and ground handling. The pilot was able to maintain stability and control at high speeds and full power throughout the ground roll, which the team expected to improve further with the installation of the main wing in future tests. However, on both the rubberized track and astroturf, the aircraft failed to reach the design required takeoff speed within the 200-foot distance, as restricted by competition rules. Although the competition runway surface should have a lower coefficient of friction and allow for increased acceleration, the installation of the main wing will significantly increase drag and thus reduce acceleration. Considering that the aircraft reached a maximum of 6.2 meters per second in 200 feet during the test, the team determined that the aircraft was under powered for takeoff and would be unsuccessful in takeoff and flight tests with the current configuration. Since the takeoff weight could not be decreased (it was tested using the minimum allowable competition payload), the team decided that the thrust needed to be increased.

Considering the fast-approaching deadline for the official design reports and drawings to the SAE competition, as well as the strict 1000-watt propulsion limitation, the team members and project advisors elected to withdraw from the SAE Aero Design West competition in April. The team was then free to increase the wattage in order to increase propulsion output, however the project advisors constrained the team to only abandon this rule; the aircraft was the adhere to all other SAE Aero Design Competition rules and restrictions.

4 Pre-Flight Propulsion, Stability, Dynamics Assessment, and Resulting Modifications

The primary issue with initial testing was lack of adequate propulsion for takeoff conditions, however the dynamic stability of the aircraft in flight was also a concern brought to the team's attention following completion of the manufacturing phase. The team decided to re-evaluate the static and dynamic stability by locating the aerodynamic center, center of gravity, and neutral point of the constructed aircraft. The horizontal stabilizer incidence angle, elevator trim position, takeoff velocity, cruise speed, rate of climb, and other parameters were also re-assessed before the team selected a final propulsion system for the aircraft.

4.1 Static Stability Analysis

Both the empty and the loaded center of gravity locations were determined through a weight balance test. The team attached a fish scale to the metal spine of the fuselage, and adjusted its location to find the point where the aircraft maintained a near perfect balance along its length. Without the passengers or luggage, the location of the empty-weight center of gravity was 62 centimeters behind the leading edge of the wing, which was was aft of the neutral point (45.1 centimeters behind the leading edge) and indicates a statically unstable configuration. Competition rules require that the aircraft must be flyable in both empty and loaded configurations. In order to comply with this rule, a ballast of approximately 14 pounds was added to the front of the plane, inside the luggage compartment. This shifted the empty-weight center of gravity in front of the neutral point from 62 to 39 centimeters behind the leading edge of the wing, achieving static stability. This corresponds to a static margin of 14.91%. When the aircraft was loaded with the intended payload, the center of gravity moved forward to 35 centimeters behind the leading edge of the wing, which yields a 9.03% static margin. Both the empty-weight (with ballast) and loaded static margins were within the desired range of 10% to 15% for longitudinal static stability. Figure 53 depicts the locations of the aerodynamic center, neutral point, and centers of gravity on the aircraft.
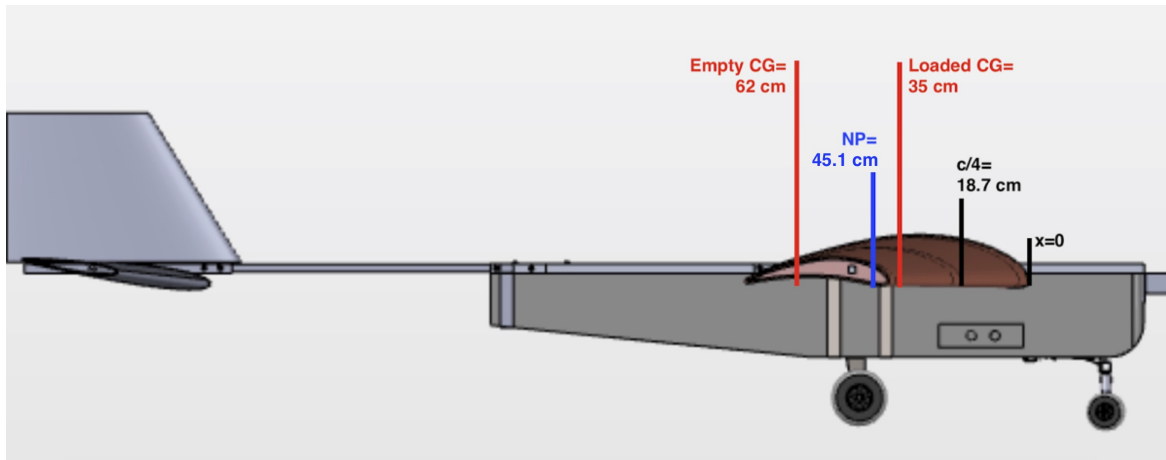
Figure 53: Stability envelope for longitudinal static stability.

4.2 Trim Analysis

To verify the correct horizontal stabilizer incidence angle for trim stability, the team aimed to achieve balanced pitching moments about the wing's aerodynamic center, assuming no elevator deflection or pilot input. The team calculated a simple force balance including the pitching moment of the wing, the lifting force of the horizontal stabilizer, and the weight force of the entire aircraft. Since the wing's lifting force acts at the aerodynamic center, the moment of this force about the aerodynamic center (approximated

71

at the wing's quarter-chord location) is zero. Additionally, the pitching moment of the horizontal tail is negligible due to the tail's symmetric airfoil and small incidence angle.

According to the XFLR5 simulation, the wing produces a moment of 173 Newton-meters about its aerodynamic center at 18 meters per section and a zero angle of attack. Using a total aircraft weight of 45 pounds or 245 Newtons acting at the previously located center of gravity, the force balance could be solved to find the required lifting force from the horizontal tail to achieve a net moment of zero about the quarter-chord. The team using both the empty weight without ballast center of gravity (62 centimeters behind the wing's leading edge) and fully loaded with ballast (35 centimeters behind the wing's leading edge) to find the two extreme values for the tail lifting force. With the "worst case" scenario using the furthest back center of gravity, the required tail lifting force was -36.6 Newtons (downward force), and at the most forward center of gravity location, the required tail lift was -72.79 Newtons. Using moment data from XLFR5 from a simulation of the horizontal tail at 18 meters per second, shown below in Figure 54, the team found these two lifting forces to correspond to tail incidence angles of -4 and -8 degrees, respectively. The actual incidence angle of the constructed tail was -6.5 degrees, which falls within the calculated range. This indicated that the constructed tail configuration would be sufficient to achieve steady, level flight using minimal elevator deflection, so long as the actual center of gravity remains between 69 and 35 centimeters behind the wing's leading edge.
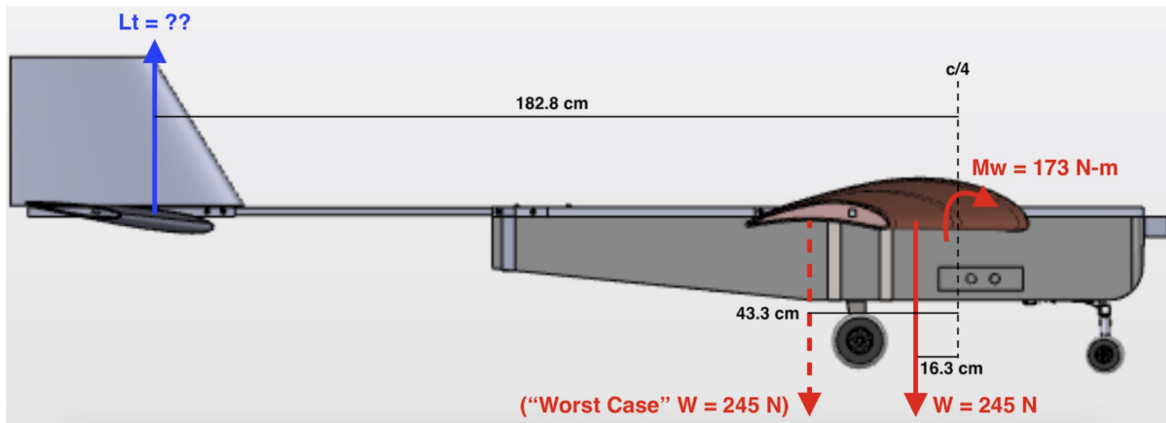
Figure 54: Longitudinal moment balance about the quarter-chord.

In order to verify the moment balance computations, the team used XFLR5. Two analyses were performed to ensure the stability of the plane in flight using the moment coefficient of the plane with the horizontal tail mounted at 0 degrees and -6.5 degrees. The moment coefficients for both tail incidence angles as a function of angle of attack are plotted in Figure 55.
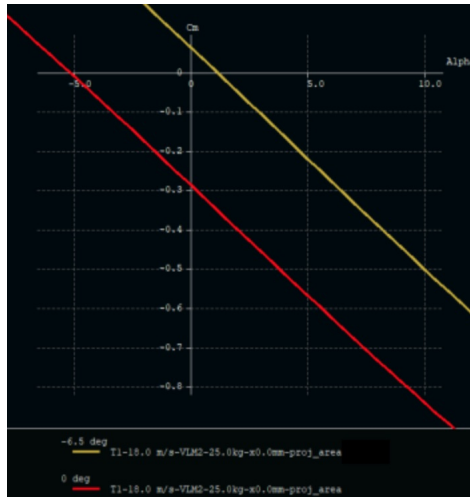
Figure 55: Moment coefficient vs. angle of attack for plane with horizontal tail incidence angle of 0 and -6.5 degrees. Both analyses were run at the estimated cruise speed of 18 m/s.

As indicated from the plot, the mounted incidence angle of -6.5 trims the plane to 1.2 degrees. The design of the plane aimed to have an angle of attack at trim of 1 degree to 1.5 degrees to gain the necessary lift for flight. This analysis confirms that the current configuration is acceptable. Additionally, Figure 56 shows that at the estimated flight speed of 18 meters per second and trim of 1.2 degrees, the lift generated by the aircraft approximates 312 Newtons, greater than the maximum weight of the aircraft, 245 Newtons.
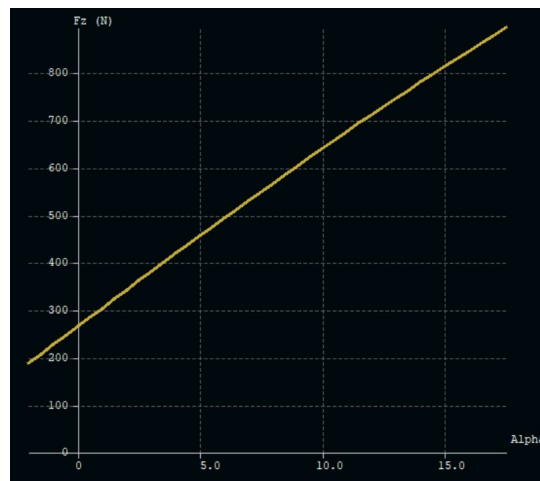
Figure 56: Total lift versus angle of attack at 18m/s.

4.3   Required Thrust for Cruise and Takeoff Conditions

The team estimated the required thrust to maintain steady, level flight at various flight velocities using a simple MATLAB script, included in Appendix M. This MATLAB script performed basic aerodynamic calculations to find the stall velocity and takeoff velocity, as well as lift and drag coefficients as a function of velocity. The stall velocity was calculated using an assumed aircraft weight of 50 pounds and a maximum lift coefficient of 1.2, which was obtained from XLFR5, and the takeoff velocity was set at 1.2 times the stall velocity. This yielded a stall velocity of 10.9 meters per second and a takeoff velocity of 13.1 meters per

second, which is a slight increase from the original estimated takeoff velocity. This increase was primarily due to the increased drag of the actual aircraft compared to the theoretical design, and was not expected to pose any significant challenges to taking off within the 200-foot limit since the motor power would also be increased.

The script computed the lift coefficient as a function of velocity by evaluating steady cruise flight in which the lift force is equal to the aircraft weight. To determine the drag coefficient as a function of velocity, the simple drag polar equation was used:

$$C_D = C_{D_0} + K C_L^2 \tag{36}$$

C_{D_0} and K were obtained from the XFLR5 full-plane simulation, and were found to be 0.044 and 0.8, respectively. The C_{D_0} value is higher than expected because the team assumed a "worst-case" drag profile in the XFLR5 simulation, in which a 1.2 drag coefficient was applied to the entire frontal area of the fuselage to overestimate the miscellaneous drag effects of blunt faces, rear upsweep, landing gear, and manufacturing defects. The team expected the true drag value to be lower than this (the ideal theoretical case typically estimates this value at 0.02 or 0.03 for low-efficiency propeller aircraft), but wanted to account for the largest possible drag conditions to ensure the chosen motor would have sufficient power. From the calculated drag coefficient, the MATLAB script plotted the drag force as a function of velocity, which is assumed to be equivalent to the thrust force during unaccelerated cruise flight. Therefore, this function, which is plotted in Figure 57, served as the minimum thrust the motor must be capable of providing at each flight speed in order to maintain cruise flight. The plot also includes the required thrust curves if the aircraft weight were instead 45 pounds or 55 pounds, in order to illustrate how altering the aircraft weight would impact the propulsion requirements.
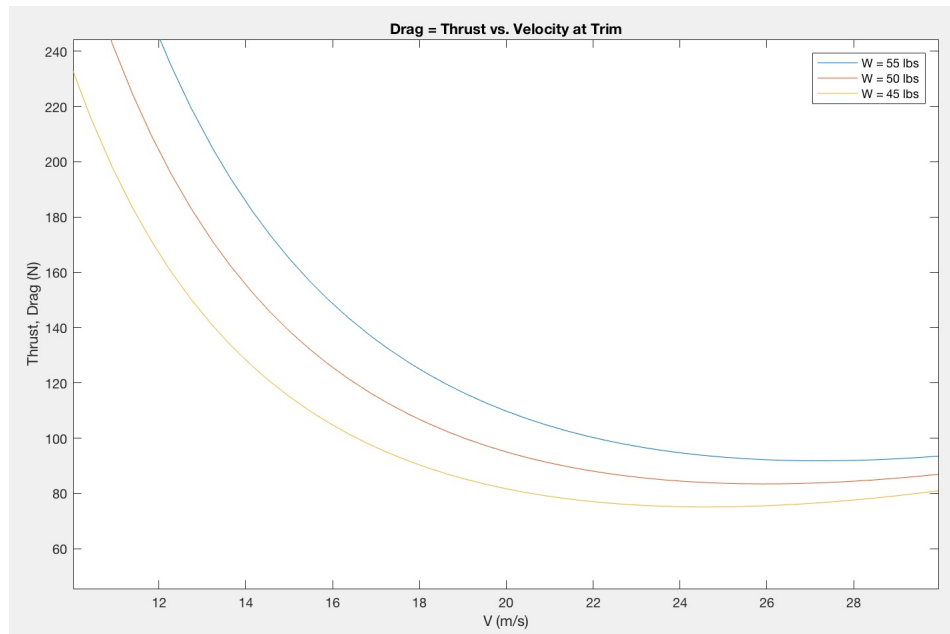
Figure 57: Required thrust as a function of velocity for aircraft weights of 45, 50, and 55 pounds.

Additionally, the team evaluated the more ideal case in which 0.03 was used for the C_{D_0} input value. This required thrust curve is plotted in Figure 58 along with the worst-case $C_{D_0} = 0.044$ curve, both using 50 pounds for the aircraft weight. Based on these results, the team decided to increase the design flight speed from 15 meters per second to approximately 20 meters per second for improved drag efficiency. At this flight speed, the team determined that the upgraded propulsion system should be capable of supplying at least 85 Newtons during cruise flight.
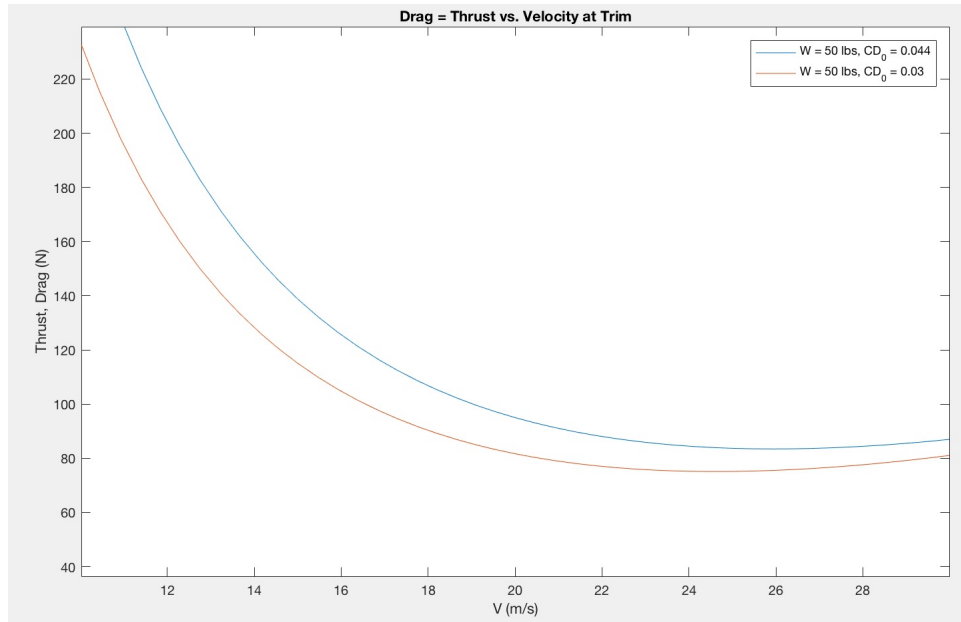
Figure 58: Required thrust as a function of velocity for aircraft with C_{D_0} of 0.044 and 0.03.

4.4 Propulsion System Upgrade

No longer restricted to the SAE competition limit of 1000 Watts, the team investigated the A-60 family of Hacker motors rated up to 3000 Watts. Universally, this family of motor would need to increase battery voltage to 10-12 cells and capacity to at least 4500mAh. Due to financial constraints, the team determined the best course of action was to wire four "3300mAh, 6 cell" batteries in series and parallel to construct a "6600mAh, 12 cell" battery.

Using this battery, simulations were then conducted in eCalc using a 22"x12"E propeller and the A60-14L, A60-16L, and A60-18L motor variants. These calculations utilized an aircraft mass of 45 pounds, a wing area of 2.4 square meters, and the "worst case scenario" drag coefficient of 0.044 (generated by XLFR5) over a frontal cross-sectional area of 0.125 square meters. From these tests, the results of which are tabulated in Appendix N, the team determined that the motor and prop combination that could produce the most thrust efficiently for the longest operating time was the A60-16L with a 22"x12"E propeller. At peak efficiency, this motor and propeller system had a calculated flight time of 4.9 minutes and a static thrust of 124.2 Newtons.

The team constructed a new, larger motor mount by bending $\frac{1}{4}$-inch aluminum plate, and installed the upgraded motor to the nose of the fuselage. The team then moved the fuselage (wing and tail detached) to the loading dock area outside Higgins Labs to conduct a static power-up test of the new propulsion system. A rope was used to tie down the back of the aircraft, and weights were placed in front of the rear landing gear to act as chocks to reduce chance of the plane moving. For the first test, the motor was slowly spun up from zero power to about 25% power and back down to zero. The team did not observe any vibrations or excessive motion during this test, and the motor appeared to be functioning as expected. On the second test, the motor was slowly spun up beyond 25% power. At approximately half power, the motor shaft and propeller sheared off from the motor. After further inspection, the team observed that the motor mount was still strongly secured to the front of the aircraft, however the screws holding the motor to the mount were very loose. The team concluded that the failure was due to excessive vibration. The team believes that the thinness of the motor mount transmitted and amplified vibrations from the motor, which loosened the motor screws and caused the propeller to oscillate out-of-plane. When the oscillations became large enough, the propeller struck the motor mount, and the sudden torque sheared the shaft.

From this test and observations, the team concluded that the failure was due to the inadequate motor mount, and not due any of the propulsion equipment. The team decided to continue to use the A60-16L Hacker motor and 22"x12"E propeller, and investigate new options for sturdier motor mounts that would dampen vibration from the motor. The team found a commercially available motor mount designed specifically for the A60 family of Hacker motors. This mount minimized vibrations and prevented resonance in all three directions by supporting the motor at both the front mounting bracket and at the rear of the can. Through the use of a bearing, the mount allowed the motor to rotate while being supported in two directions. The team purchased this motor mount, a replacement A60-16L motor, and a new 22"x12"E propeller. After assembling the new system, the team conducted a static bench test to verify that the mount adequately dampened vibrations throughout the motor's full throttle range. These tests were successful and did not yield excessive vibration of the motor or mount. Once the new propulsion system and mount was installed on the front of the aircraft, the team conducted a static thrust test of the motor and fuselage. For this test, the wing of the aircraft was removed and the fuselage was tied down to prevent the fuselage from rolling away. The motor and propeller were tested and spun up to full power. These tests were also successful. The team did not observe any out-of-plane motion of the propeller or any large vibrations in the motor, motor mount, or fuselage. All rivets, screws, and other fasteners were still tightly secured at the conclusion of the test, indicating that vibrations were dampened to safe levels. With several successful propulsion tests, the team was able to schedule a maiden flight for the aircraft.

4.5 Leading Edge Modifications

Due to the foam and Monokote manufacturing processes the team used to fabricate the wings and vertical tail, there were significant imperfections in the shape of their respective leading edges. In order to create a more ideal shape and curve fit for the leading edge of the wings and vertical tail for improved aerodynamics, the team added moldable plastic sheets wrapped around the leading edges, as shown in Figure 59. These high-density polyethylene sheets are 0.003 inches thick. The pieces were cut to approximately 1 foot wide and spanned the length of each section of the wing, including both tapered sections. The same was done for the horizontal tail. This material created a smooth and more aerodynamic leading edge for the wings and tail, reducing drag significantly and yielding much more desirable and accurate calculations and aircraft characteristics. Additionally, a strip of this same material was used to bridge the gap between the left and right sides of the main wing where the spars are bolted to the fuselage. This improved airflow over the top of the wing and reduced drag.

Figure 59: Wing leading edge smoothed using Polyethylene sheet.

5 Flight Testing

On Saturday, April 21, the team travelled to the Millis Model Aircraft Club in Medfield, Massachusetts to test fly the completed aircraft. Upon arrival, the team observed fair weather with a 10 to 15 mile-per-hour winds, with gusts of up to 20 miles per hour. The team assembled the aircraft and calibrated the control surface neutral position, where each control surface was aligned with the full airfoil. The aircraft was then placed on the runway facing into the wind to begin the flight test. One team member held the plane in place while the RC pilot Mickey Callahan brought the aircraft up to full throttle, at which point the aircraft was released and began the ground roll acceleration. The aircraft initially veered towards the port side, which was corrected with rudder and the steerable landing gear. The plane reached takeoff speed after about 140 feet of ground roll and pitched up into a stall (pictured in Figure 60) despite the pilot's best effort to keep it on the ground and maximize ground speed. The pilot attempted to correct this by pitching the elevator down to level the plane, however, there was not enough airspeed to level the plane out to regain speed. The pilot was able to level the plane as it came down and landed on its gear. The impact from the landing had bent the mounting bracket for the front landing gear, pictured in Figure 61. and deformed the rear landing gear mount. Additionally, the team found that the propeller and motor shaft had sheared off. After speaking with the pilot, the team believes this is an instance of a tail-heavy aircraft, the unstable pitching effects of which may have been magnified by the negative incidence angle of the tail.

Figure 60: The aircraft in flight entering a stall condition.

Figure 61: Damaged front landing gear after flight test.

Part VI
Results and Conclusions

The final aircraft, shown in Figure 62, performed some aspects of its design well. All of the mechanical and electrical components performed as designed and expected. The most significant flaw the team identified in the performance of the aircraft was the inability to level out the plane after takeoff, resulting in a stall. This is likely due to the aircraft being tail-heavy. The team believes that a positive tail incidence angle may have helped alleviate this issue.
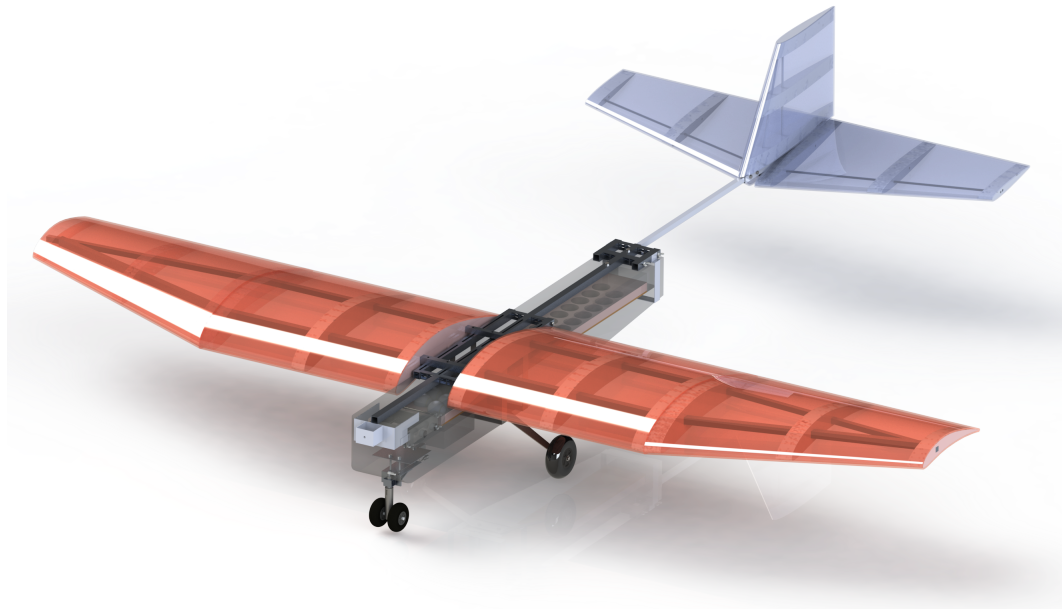
Figure 62: The completed aircraft, photographed and fully modeled in SOLIDWORKS.

The aircraft was fabricated using methods that were effective in producing a high-durability aircraft, however often at the cost of increased weight. Structural integrity was preserved through aluminum frames in the wings and a solid foam fuselage. This durable design added significant structural weight, resulting in the need to reduce the payload to a minimum and significantly upgrade the propulsion system. The foam skin performed well, but resulted in difficulties with adhering the monokote. Additionally, the control surfaces were loosely held in place, which could lead to flutter at higher speeds.

In its flight test, the aircraft successfully took off within the prescribed distance and withstood the impact of the stalled landing with minimal damage. With some minor adjustments, the plane could be returned to an airworthy and more stable state.

1 Future Recommendations

Through the process of designing, fabricating, and testing the aircraft, the team gathered some recommendations for teams designing aircraft for similar competitions or MQPs in the future. First, it is important to avoid underestimating structure weight when designing the aircraft. In attempting to design a durable aircraft, the team manufactured a plane that was much heavier than originally intended. The team found that the final plane exceeded the takeoff weight limit to carry the intended 36 tennis balls and respective cargo, so the payload had to be reduced to the minimum of 10 passengers and 5 pounds of luggage. This would have resulted in a lower FFS at the SAE competition. Additionally, the team found that with the heavier structure weight and reduced cargo, it was difficult to adjust the center of gravity to a desirable location for longitudinal stability. Minimizing the structure weight is essential to maximizing the capabilities of the aircraft.

Another flaw with the team's process was failing to consider manufacturing techniques and resources during design. Part of this is due to inexperience in the design process, but most of the cause of this was the inexperience of the team as it pertains to many of the manufacturing techniques required to fully construct the aircraft. Not considering the manufacturing methods and materials during design also led to some components being designed in shapes that optimized performance, but were later discovered to be complex to execute during the manufacturing phase. While it is difficult to fully understand a manufacturing process or the advantages and disadvantages of a process unless a team has tried it, more research into the specific resources and techniques to be used for manufacturing before finalizing a design is imperative to ensure that the design is feasible. Knowledge of some of these processes beforehand would have saved the team much time and effort in redesigning and constructing.

The team also struggled to develop a manufacturing plan before beginning the manufacturing phase of the project. As a result, construction was overseen by only a couple of team members. This first meant that if there were any time conflicts and those individuals could not be present, many of the other team members were uninformed and unable to continue construction without guidance. Establishing a very detailed manufacturing plan is essential to ensuring that all components of the aircraft are completed on time and in an appropriate fashion. This manufacturing plan should clearly state the materials and resources needed, instructions for completing the process, the name of a team member who is knowledgeable about the task, and an assignment to a team member who is responsible for completing the component construction.

Another important aspect the team overlooked during the manufacturing process was to update analyses and models with each new modification. Constantly adjusting models as changes were made and issues arose would allow the team to attain a more accurate result when it came to testing. With the models not updated, the team attempted to manufacture to the specifications of the original design, however it was found that imperfections did occur. Had these imperfections been accounted for in the models, they likely could have been corrected or offset in other aspects and could have resulted in a more successful test flight.

The team found that one of the most important, and most challenging, aspects of this project was the logistical component. Especially with 12 students on one team, it was difficult to keep track of individual responsibilities and expectations. The team should have done more to hold each other accountable for individual tasks, such as using Gantt charts and checklists to plan and document all tasks, logging work, and taking the time to review completed work and ensure its accuracy. Overall, the project management component of this project was lacking and it would have served the team better to create one or several team manager positions. This would encourage accountability for adherence to the schedule, allow for more effective delegation of tasks, and streamline communication between subgroups and individuals.

2 Final Conclusions

Overall, the team recognized significant value in a project of this scale. This project exposed team members to all aspects of the aerospace engineering curriculum, including controls, structures, and aerodynamics, as well as hands-on manufacturing. While not every team member was involved in all of these aspects, weekly team meetings allowed each member to experience and observe the many different

stages and components of designing, constructing, and fabricating a complete aircraft. Each team member was in some way involved in both the design and manufacturing of the aircraft. Aside from the aerospace-specific principles the team learned, the design process as a whole was also reinforced through the execution of this project. Finally, a notable lesson for the team was to not underestimate the importance of project management. Initially, this was overlooked and eventually cost the team valuable time. In a project with a tight deadline such as this, organization and time management was imperative. Better team structure and communication could have resulted in an earlier flight test, with further potential to result in successful flights. Although the team was not able to compete in the SAE Aero Design West 2018 Competition, this MQP provided each student with valuable skills and lessons applicable to future careers in aerospace engineering or broader technical fields.

References

[1] Olinger, D. (2017). *MQP 2017-18 Introduction and Guidelines* [Powerpoint Presentation].

[2] CHRobotics LLC. (2013, March 25). *AN-1005 Understanding Euler Angles* [PDF Document]. Retrieved October 15, 2017, from http://www.chrobotics.com/docs/AN-1005-UnderstandingEulerAngles.pdf

[3] Lutze, F. H. (2003). *AOE 3104 Vehicle Performance - Supplemental Notes* [PDF Document]. Retrieved from http://www.dept.aoe.vt.edu/ lutze/AOE3104/

[4] TLG Aerodpace, LLC. (n.d.). Aircraft Loads. Retrieved October 23, 2017, from http://tlgaerospace.com/index.php/services/aircraft-loads/

[5] Anderson, J. D. (2016). *Fundamentals of Aerodynamics* (6th ed.). New York, New York: McGraw-Hill.

[6] Hoerner, S. F. (1965). *Fluid-Dynamic Drag* (2nd ed.). New York, NY: Author.

[7] Sadraey, M. H. (2013). Tail Design. In *Aircraft Design: A Systems Engineering Approach* (Chapter 6). John Wiley Sons, Ltd.

[8] Carpenter. (2015).

[9] MIT Electric Vehicle Team. (2008). *A Guide to Understanding Battery Specifications.* Retrieved October 18, 2017, from http://web.mit.edu/evt/summary_battery_specifications.pdf

[10] Calculate Flight Time of LiPo Battery. (2011, July 30). Retrieved October 18, 2017, from http://www.scoutuav.com/2011/05/12/calculate-flight-time/

[11] What is Thrust? (n.d.). Retrieved October 12, 2017, from https://www.grc.nasa.gov/WWW/k-12/airplane/thrust1.html

[12] Scythian, M. D. (2017, April 15). Accurate Two-Blade Propeller Thrust Calculation [Online Video Lecture]. Retrieved from https://www.youtube.com/watch?v=BfDP1ytkUlst=319s

[13] Wolfe, J. (2011). *Electric Motors and Generators.* Retrieved October 1, 2017, from http://www.animations.physics.unsw.edu.au/jw/electricmotors.html

[14] Etkin, B. (2005). *Dynamics of Atmospheric Flight.* Mineola, NY: Dover Publications.

[15] Etkin, B. Reid, L. D. (1996). *Dynamics of Flight Stability and Control.* New York, NY: John Wiley & Sons.

[16] Anderson, J. D. (1999). *Aircraft Performance and Design.* New York, NA: WCB/McGraw-Hill

[17] Lennon, A. (2005). Basics of R/C model aircraft design: practical techniques for building better models. Wilton (Connecticut): Air Age.

[18] Megson, T.H.G. (2014). *Introduction to Aircraft Structural Analysis* (2nd ed.). Elsevier Ltd.

[19] Megson, T. H. G. (2007). *Aircraft Structures for Engineering Students* (4th ed.). Elsevier Ltd.

[20] Deperrois, A. (n.d.). XFLR5 [Computer software]. Retrieved October 21, 2017, from http://www.xflr5.com/xflr5.htm

[21] Horizon Hobby. (2017). *Timber: Instruction Manual* [PDF Document]. Champaign, IL: Horizon Hobby.

[22] Airfoil Tools. (2018). Retrieved from airfoiltools.com

[23] University of Illinois Urbana-Champaign, Department of Aerospace Engineering. (2018). *UIUC Airfoil Coordinates Database.* Retrieved from http://m-selig.ae.illinois.edu/ads/coord_database.html

[24] Stratasys Inc. (2015). Dimension 1200es. Retrieved from http://usglobalimages.stratasys.com/Main/Files/Machine_Spec_

[25] Deep Stall. (21 September 2015). Retrieved from SKYbrary Aviation Safety: https://www.skybrary.aero/index.php/Deep_Stall

Part VII
Appendix

A   SAE Aero Design Rules

2018 Collegiate Design Series
SAE Aero Design Rules

Version 2018.1

FOREWORD

Welcome to SAE Aero Design 2018. Our goal each year is to create and refine a set of competition events with relevant real-world challenges that students of all engineering disciplines and levels of experience can enjoy as you apply your engineering knowledge in a design team environment to create an original aircraft design. After designing your aircraft, your team then must build what you have designed and then compete head to head with other teams to see which team is the best in several different areas: a design report, an oral presentation and the flight performance of your aircraft. SAE Aero Design consists of three competition classes: Regular Class, Micro Class and Advanced Class. Regular Class traces its lineage back to the very beginning of SAE Aero Design, when the event was created as a heavy lift competition for model aircraft. Regular Class continues as our entry level class. In 2017, SAE Aero Design introduced a new "passengers and their luggage" theme to Regular Class and that theme continues this year. We have introduced one notable change: Regular Class aircraft now have a wingspan limit of 144". Advanced Class is the most challenging class, due to its complexity. Not only does your team have to design and build an aircraft, but you must also design and create a number of reliable systems for your aircraft including downlinked FPV video, downlinked telemetry, a reliable ground station and a payload delivery system. Each system must work in concert with all others in your aircraft for your team to have a reliable and competitive aircraft. The rules also require team members to work in concert during flight operations in order to accomplish the complete Advanced Class mission.

For the 2018 SAE Aero Design competition, we are proud to present a new set of rules for Micro Class that we hope you will find interesting and challenging. The aircraft container has a new form factor. The physical payload now required for Micro Class is a common low density industrial material that should challenge teams when they are integrating this new payload to their aircraft and when teams are designing the aircraft to fit the new aircraft storage requirement. All of this new low density payload that the team ever plans to carry must fit in their aircraft storage container with their aircraft. One final change is the Assembly Demo for Micro Class. It is no longer an optional demo; it is now required for all teams in Micro Class. Teams can gain points for a fast assembly and lose points if their assembly takes too long.

Everyone on the SAE Aero Design Rules Committee is excited as we prepare for the 2018 competition season and we hope you will enjoy the challenge of the new Micro Class rules. We have made a number of small changes and refinements in all sections of the rules. As always, please do read the rules closely. Based on past history, we expect both East and West events to sell out quickly, so be sure to sign up early. As Rules Chair Brian Czapor explained in last year's forward: If you are unfortunate enough to be a waitlisted team, we encourage you to move forward with your design and plan to attend. In 2016 and 2017, all waitlisted teams were contacted and invited to attend after other teams dropped out.

We at SAE Aero Design wish all teams the best of luck as they prepare for the 2018 events!

Tom Blakeney, SAE Aero Design Rules Committee

TABLE OF CONTENTS

1 COMPETITION REQUIREMENTS

1.1 INTRODUCTION

Official Announcements and Competition Information

The SAE Aero Design competition is intended to provide undergraduate and graduate engineering students with a real-world design challenge. These rules were developed and designed by industry professionals with the focus on educational value and hands-on experience through exposure to today's technical and technology advancement. These rules were designed to compress a typical aircraft development program into one calendar year, taking participants through the system engineering process of breaking down requirements. It will expose participants to the nuances of conceptual design, manufacturing, system integration/test, and sell-off through demonstration.

SAE Aero Design features three classes of competition—Regular, Advanced, and Micro.

- **The Regular Class** is an all-electric class intended to develop a fundamental understanding of aircraft design.

- **The Advanced Class** continues to use internal combustion engines. It exposes students to system integration with the focus on data acquisition and aircraft performance of complex and multi-faceted missions.

- **The Micro Class** is an all-electric class designed to help students engage in trades between two potentially conflicting requirements, carrying the highest payload fraction possible, while simultaneously pursuing the lowest empty weight possible.

Other SAE Aero Design Competitions: SAE Aero Design Brazil:

SAE BRASIL http://www.saebrasil.org.br

1.2 SAE AERO DESIGN RULES AND ORGANIZER AUTHORITY

General Authority

SAE International and the competition organizing bodies reserve the rights to revise the schedule of any competition and/or interpret or modify the competition rules at any time and in any manner, that is, in their sole judgment, required for the efficient and safe operation of the event or the SAE Aero Design series as a whole.

1. **Penalties**
   SAE International and the competition organizing bodies reserve rights to modify the points and/or penalties listed in the various event descriptions; to accurately reflect the operations execution of the events, or any special conditions unique to the site.

2. **Rules Authority**
   The SAE Aero Design Rules are the responsibility of the SAE Aero Design Rules Committee and are issued under the authority of the SAE International University Programs Committee. Official announcements from the SAE Aero Design Rules Committee, SAE International or the other SAE International Organizers shall be

considered part of and have the same validity as these rules. Ambiguities or questions concerning the meaning or intent of these rules will be resolved by the officials, SAE International Rules Committee or SAE International Staff.

3. **Rules Validity**

   The SAE Aero Design Rules posted at www.saeaerodesign.com/go/downloads and dated for the calendar year of the competition are the rules in effect for the competition. Rule sets dated for other years are invalid.

4. **Rules Compliance**

   By entering an SAE Aero Design competition, the team members, faculty advisors and other personnel of the entering university agree to comply with, and be bound by, the rules and all rules interpretations or procedures issued or announced by SAE International, the SAE Aero Design Rules Committee and other organizing bodies. All team members, faculty advisors and other university representatives are required to cooperate with, and follow all instructions from competition organizers, officials and judges.

5. **Understanding the Rules**

   Teams are responsible for reading and understanding the rules in their entirety for the competition in which they are participating. The section and paragraph headings in these rules are provided to facilitate reading: they do not affect the paragraph contents.

6. **Loopholes**

   It is virtually impossible for a set of rules to be so comprehensive that it covers all possible questions about the aircraft's design parameters or the conduct of the competition. Please keep in mind that safety remains paramount during any SAE International competition, so any perceived loopholes should be resolved in the direction of increased safety/concept of the competition.

7. **Participating in the Competition**

   Teams, team members as individuals, faculty advisors and other representatives of a registered university who are present on-site at a competition are considered to be "participating in the competition" from the time they arrive at the event site until they depart the site at the conclusion of the competition or earlier by withdrawing.

8. **Visa--United States Visas**

   Teams requiring visas to enter to the United States are advised to apply at least sixty (60) days prior to the competition. Although most visa applications seem to go through without an unreasonable delay, occasionally teams have had difficulties and in several instances visas were not issued before the competition.

   AFFILIATED CDS STUDENT TEAM MEMBERS WILL HAVE THE ABILITY TO PRINT OUT A REGISTRATION CONFIRMATION LETTER FOR THE INDIVIDUAL EVENT(S) THAT THEY ARE ATTENDING. ONCE A STUDENT TEAM MEMBER AFFILIATES THEMSELVES TO THEIR TEAM PROFILE PAGE UNDER THEIR INDIVIDUAL EDIT SECTION, THEY WILL HAVE THE OPPORTUNITY TO PRINT OUT THEIR PERSONALIZED LETTER WITH THE FOLLOWING INFORMATION: STUDENT'S NAME, SCHOOL'S NAME, THE CDS EVENT NAME, OFFICIAL DATES AND LOCATION(S).

9. **Letters of Invitation**
Neither SAE International staff nor any competition organizers are permitted to give advice on visas, customs regulations or vehicle shipping regulations concerning the United States or any other country.

10. **Certificates of Participation**
SAE International and competition organizers do not create any Participation Certificates outside of the auto-generated certificate obtained using the directions available at http://students.sae.org/cds/aerodesign/faq/.

Certificates are available as soon as students are affiliated to the current competition's team. Certificates will not be available once that competition year closes.

11. **Violations of Intent**
The violation of the intent of a rule will be considered a violation of the rule itself. Questions about the intent or meaning of a rule may be addressed to the SAE International Officials, Competition Organizers or SAE International Staff.

12. **Right to Impound**
SAE International and the other competition organizing bodies reserve the right to impound any on-site vehicle/aircraft at any time during a competition for inspection and examination by the organizers, officials and technical inspectors.

1.3 SOCIETY MEMBERSHIP AND ELIGIBILITY

1. **Society Membership**
Individual team members must be members of one of the following societies: (1) SAE International or an SAE International affiliate society, (2) ATA, or (3) IMechE or (4) VDI. Proof of membership, such as a membership card, is required at the event. Students who are members of one of the societies listed above are not required to join any of the other societies in order to participate in any SAE competition. Students may join online at: http://www.sae.org/students.

Teams are also required to read the articles posted on the SAE Aero Design News Feed (www.saeaerodesign.com/go/news) published by SAE International and the other organizing bodies. Teams must also be familiar with all official announcements concerning the competitions and rule interpretations released by the SAE Aero Design Rules Committee.

2. **Team Pilots**
Team pilots are not required to be students or SAE International members, but all pilots must be current members of the Academy of Model Aeronautics or the Model Aircraft Association of Canada (AMA has an agreement with MAAC). Valid AMA membership cards must be presented at the flying field prior to flying any team's aircraft. Non-US pilots can obtain a discounted AMA Affiliate membership that covers flying activities while in the US by going to the AMA web site and submitting the following form: https://www.modelaircraft.org/files/902.pdf.

1.4 LIABILITY WAIVER AND INSURANCE REQUIREMENTS

All on-site participants and faculty advisors are required to sign a liability waiver. Individual medical and accident insurance coverage is the sole responsibility of the participant.

1.5 RINGERS PROHIBITED

In order to maintain the integrity of a fair competition, the faculty advisor must prohibit ringers. A ringer is someone that has exceptional skills related to the competition (e.g., a professional model builder) that cannot be a legal member of the team but helps the team win points.

1.6 DESIGN AND FABRICATION

The aircraft must be designed and built by the SAE International student members without direct involvement from professional engineers, radio control model experts, pilots, machinists, or related professionals. The students may use any literature or knowledge related to R/C aircraft design and construction and information from professionals or from professors as long as the information is given as discussion of alternatives with their pros and cons and is acknowledged in the references in the design report. Professionals may not make design decisions, nor contribute to the drawings, the report, or the construction of the aircraft. The faculty advisor must sign the Statement of Compliance given in the Appendix.

1.7 ORIGINAL DESIGN

Any aircraft presented for competition must be an original design whose configuration is conceived by the student team members. Photographic scaling of an existing model aircraft design is not allowed. Use of major components such as wings, fuselage, or empennage of existing model aircraft kits is prohibited. Use of standard model aircraft hardware such as engine mounts, control horns, and landing gear is allowed.

1.8 OFFICIAL LANGUAGES

The official language of the SAE Aero Design series is English. Document submissions, presentations and discussions in English are acceptable at all competitions in the series.

Team members, judges and officials at Non-U.S. competition events may use their respective national languages for document submissions, presentations and discussions if all the parties involved agree to the use of that language.

SAE Aero Design East	English
SAE Aero Design West	English
SAE Aero Design Brazil	Portuguese and English

1.9   UNIQUE DESIGNS

Universities may enter more than one team in each SAE Aero Design competition, but each entry must be a unique design, significantly different from each other. If the aircraft are not significantly different in the opinion of the rules committee and organizer, then the university will be considered to have only a single entry and only one of the teams and its aircraft will be allowed to participate in the competition. For example, two aircraft with identical wings and fuselages but different empennage would likely not be considered significantly different. For guidance regarding this topic, please submit a rules question at www.saeaerodesign.com.

1.10   AIRCRAFT CLASSIFICATION/DUPLICATE AIRCRAFT

1. **One Aircraft per class**
    A university or college can only have one aircraft registered for one class. A university cannot register more than one team per class.

2. **Backup Aircraft**
    When a team has an identical aircraft as a back-up, the back-up aircraft must go through inspection with the primary aircraft.

3. **Scoring with Backup Aircraft**
    Team will forfeit all flight points earned with the original aircraft if the team decides to fly with an entirely new aircraft.

    If a team decides to replace more than 50% of the original aircraft with spare parts, the team will forfeit all flight points earned with the original aircraft.

    If a team decides to replace less than 50% of the original aircraft with spare parts, the team will retain all flight points earned with the original aircraft.

    Once the spare parts have successfully flown with original parts of the aircraft, the spare part will no longer be classified as spare.

1.11   AIRCRAFT ELIGIBILITY

Aircraft will only be allowed to compete during a _single academic year_. Aircraft may be entered in both SAE Aero Design East and SAE Aero Design West during the same _calendar year_, but that same aircraft may not be used in either competition during the following year. Entering the same aircraft in SAE Aero Design West one year and SAE Aero Design East the next year is not allowed.

1.12 REGISTRATION INFORMATION, DEADLINES AND WAITLIST (NEW)

Teams intending to participate in the 2018 SAE Aero Design competitions must register their teams online per the open registration schedule.

Table 1.1 Open Registration Schedule

Event	Team Limit	Start (Open)	End (Closed)
SAE Aero Design East	75 Teams	October 2nd, 2018 10:00 am EST	November 13th, 2018 11:59 PM
SAE Aero Design West	75 Teams	October 2nd, 2018 10:00 am EST	November 13th, 2018 11:59 PM

The registration fee is non-refundable and failure to meet these deadlines will be considered a failure to qualify for the competition. Separate entry fees are required for the East and West events.

1. **Team/Class/University Policy**
   A university or college can only have one aircraft registered for one class. A university cannot register more than one team per class. The registration fees indicated on the website ($1000) must be paid within 48 hours of registration.

2. **Individual Registration Requirements – ACTION REQUIRED**
   All participating team members and faculty advisors must be sure that they are individually affiliated to their respective school / university on the SAE International website (www.sae.org) Team Profile page.

   If you are not an SAE International member, go to www.sae.org and select the "Membership" link. Students will need to select the "Student Membership" link and then follow the series of questions that are asked Please note all student participants must be SAE International members to participate in the events.

   Faculty members who wish to become SAE International members should choose the "Professional Membership" link. Please note: this is not mandatory for faculty advisors.

   All student participants and faculty advisors must affiliate themselves to the appropriate team(s) online. To affiliate, refer to the SAE Aero Design FAQ page (http://students.sae.org/cds/aerodesign/faq/).

   The "Add New Member" button will allow individuals to access this page and include the necessary credentials. If the individual is already affiliated to the team, simply select the Edit button next to the name. Please be sure this is done separately for each of the events your team has entered.

   All students, both domestic and international, must affiliate themselves online prior to the competition.

   **NOTE: When your team is registering for a competition, only the student or faculty advisor completing the registration needs to be linked to the school. All other students and faculty can affiliate themselves after registration has been completed; however this must be done prior to two weeks before the competition start date.

1.13 WAITLIST

Once an event reaches the 75 team capacity, all remaining registered team will be asked to be placed on a waitlist. The waitlist is capped at 40 available spaces per event and will close on the same day as registration closes. Once a team withdraws from an event, an SAE International Staff member will inform your team by email (the individual who registered the team to the waitlist) that a spot on the registered teams list has opened. You will have 24 hours to accept or reject the position and an additional 24 hours to have the registration payment completed or process for payment begun. Waitlisted teams are required to submit all documents by the deadlines in order to be considered serious participants and any team that does not submit all documents will be removed from the waitlist.

1.14 POLICY DEADLINE

1. **Failure to meet deadlines**

   Teams registering for SAE Aero Design competitions are required to submit a number of documents prior to the competition including a Design Report and Technical Data Sheet that the event judges use to evaluate the team during the competition. When these documents are not submitted our judges cannot properly assess the team. Additionally, teams that do not submit required documents typically do not come to the competition. Teams that do not notify us that they are withdrawing create the following problems:

   1. They are included in the static event schedules and judging time is wasted.
   2. Their unused registration slot cannot be offered to a team on the waitlist. Additionally, failure to submit the required documents is a clear violation of the rules.

2. **Late Submission Penalty**

   Late submission or failure to submit the Design Report will be penalized five (5) points per day. If your required documents are received more than five (5) days late it will be classified as "Not Submitted" and your team will not participate and the automatic withdrawal policy will be in effect (see section 3).

3. **Automatic Withdrawal Policy**

   Failure to submit the required Design Report, Technical Data Sheet, and Drawings within 5 days of the deadline will constitute an automatic withdrawal of your team. Your team will be notified before or on the 4th day of no submission that we have not received your documents and after the 5 days your team's registration will be cancelled and no refund will be given.

1.15   FACULTY ADVISOR

Each team is expected to have a Faculty Advisor appointed by the university.   The Faculty Advisor is expected to accompany the team to the competition and will be considered by competition officials to be the official university representative. Faculty Advisors may advise their teams on general engineering and engineering project management theory, but may not design any part of the vehicle nor directly participate in the development of any documentation or presentation.   Additionally Faculty Advisors may neither fabricate nor assemble any components nor assist in the preparation, maintenance, or testing of the vehicle. In Brief - Faculty Advisors may not design, build or repair any part of the aircraft. Faculty Advisors that are not eligible student team members may not participate in flight operations during competition weekend except as noted.

1.16   QUESTIONS, COMPLAINTS AND APPEALS

1.   **Questions**
     Any questions or comments about the rules should be brought to the attention of the Rules Committee by submitting a rules question at https://www.saeaerodesign.com.

     General information about hotels and other attractions in the area as well as a schedule of events will be posted on the SAE International website according to the competition in which you are competing: students.sae.org/cds/aerodesign/

2.   **Complaints**
     Competition officials will be available to listen to complaints regarding errors in scoring, interpretation, or application of the rules during the competition. Competition officials will not be available to listen to complaints regarding the nature, validity, or efficacy of the rules themselves at the competition. In other words, the Organizer will not change the rulebook at the field.

3.   **Appeal / Preliminary Review**
     A team can only appeal issues related to own-team scoring, judging, venue policies, and/or any official actions. Team Captain(s) and/or faculty advisor must bring the issue to the Organizer's or SAE International staff's attention for an informal preliminary review before filing an official appeal.

     A team cannot file an appeal to cause harm to another team's standing and/or score.

4.   **Cause for Appeal**
     A team may appeal any rule interpretation, own-team scoring or official actions which the team feel has caused some actual, non-trivial, harm to own-team, or has had a substantive effect on their score.

     Teams may not appeal rule interpretations or actions that have not caused them any substantive damage.

5. **Appeal Format**
If a faculty advisor or team captain(s) feel that their issue regarding an official action or rules interpretation was not properly addressed by the **event officials**, the team may file a formal appeal to the action or rules interpretation with the Appeals Committee.

All appeals must be filed in writing (see Appendix F) to the Organizer by the faculty advisor or team captain only.

All appeals will require the team to post twenty five (25) points as collateral. If the appeal is successful and the action is reversed, the team *will not* forfeit the twenty five (25) collateral points. If the appeal is overruled, the team will forfeit the twenty five (25) collateral points.

All rulings issued by the Appeals Committee are final.

6. **Appeals Period**
All appeals must be submitted within thirty (30) minutes of the end of the flight round or other competition event to which the appeal relates.

7. **Appeals Committee**
When a timely appeal is received, the committee will review in detail the claims. All contentions or issues raised in the formal appeal will be addressed in a timely manner. The consideration in each review is whether the actions in dispute were just and in-line with the intent of the rules. Once the review is completed, a new order will be issued affirming, reversing or modifying the original determination.

All rulings issued by the Appeals Committee are final.

The Appeals Committee must consist of a minimum of three members: the Organizer or delegate, SAE International representative, and either the Chief Steward, the Chief Judge, the Air Boss and/or rule committee member.

1.17 PROFESSIONAL CONDUCT

1. **Unsportsmanlike Conduct**
In the event of unsportsmanlike conduct by team members or that team's faculty advisor, the team will receive a warning from a Competition Official. A second violation will result in expulsion of the team from the competition and loss of any points earned in all aspects of the competition.

2. **Arguments with Officials**
Arguments with or disobedience toward any competition official may result in the team being eliminated from the competition. All members of the team may be immediately escorted from the grounds.

3. **Alcohol and Illegal Material**
   Alcoholic beverages, illegal drugs, firearms, weapons, or illegal material of any type are not permitted on the event sites at any time during the competition. Any violations of this rule will result in the immediate expulsion of all members of the offending school, not just the individual team member in violation. This rule applies to team members and faculty advisors. Any use of illegal drugs or any use of alcohol by an underage person must be reported to the local law enforcement authorities for prosecution.

4. **Organizer's Authority**
   The Organizer reserves the exclusive right to revise the schedule of the competition and/or to interpret the competition rules at any time and in any manner which is required for efficient operation or safety of the competition.

5. **Ground Safety and Flight Line Safety Equipment**

   1. **No open toe shoes allowed.** All team participants, including faculty advisors and pilots, will be required to wear CLOSED toe shoes during flight testing and during flight competition.
   2. **Smoking is prohibited.** Smoking is prohibited in all competition areas.
   3. All students in all classes involved at the flight line must wear safety glasses.
   4. Micro Class must wear hard hats in addition to safety glasses at the flight line.

1.18   SAE TECHNICAL STANDARDS ACCESS

A cooperative program of SAE International's Education Board and Technical Standards Board is making some of SAE International's Technical Standards available to teams registered for any North American CDS competition at no cost. The Technical Standards referenced in the Collegiate Design Series rules, along with other standards with reference value, will be accessible online to registered teams, team members and faculty advisors.

To access, teams can follow these procedures. Once registered, a link to SAE MOBILUS will appear to access the technical standards under "Design Standards" on your team's profile page on sae.org, where all the required onsite team information is added. On SAE MOBILUS, you will have the ability to search standards either by J-number assigned or topic of interest such as brake light.

A list of accessible SAE International Technical Standards can be found in Appendix G.

2 GENERAL AIRCRAFT REQUIREMENTS

2.1 AIRCRAFT IDENTIFICATION

Team number as assigned by SAE International must be visible on both the top and bottom of the wing, and on both sides of the vertical stabilizer or other vertical surface.

1. Aircraft must be identified with the school name and address either on the outside or the inside of the aircraft.
2. Team numbers on Regular and Advanced Class aircraft shall be a minimum of 3 inches in height. Micro Class team numbers shall be a minimum of 1 inch in height.
3. The University name must be clearly displayed on the wings or fuselage.
4. The University initials may be substituted in lieu of the University name provided the initials are unique and recognizable.

The assigned aircraft numbers appear next to the school name on the "Registered Teams" page of the SAE Aero Design section of the Collegiate Design Series website at:

SAE Aero East: http://students.sae.org/cds/aerodesign/east/

SAE Aero West: http://students.sae.org/cds/aerodesign/west/

2.2 NO LIGHTER-THAN-AIR OR ROTARY WING AIRCRAFT

Competing designs are limited to fixed wing aircraft only. No lighter-than-air or rotary wing aircraft such as helicopters or auto-gyros will be allowed to compete.

2.3 EMPTY CG DESIGN REQUIREMENT AND EMPTY CG MARKINGS ON AIRCRAFT

All aircraft must meet the following Center of Gravity (CG) related requirements:

1. All aircraft must be flyable at their designated Empty CG position (no payload, ready to fly) on the submitted 2D aircraft drawing.
2. All aircraft must have the fuselage clearly marked on both sides with a classic CG symbol (Figure 2.1) that is a minimum of 0.5 inches in diameter centered at the Empty CG position, per the submitted 2D drawings. (Wing type aircraft may place the two CG markings on the bottom of the wing.)
3. The Empty CG location will be verified during Technical and Safety Inspection.
4. No empty weight flight is required.

Figure 2.1 - Center Of Gravity Symbol

2.4 GROSS WEIGHT LIMIT

Aircraft gross take-off weight may not exceed fifty-five (55) pounds.

2.5   CONTROLLABILITY

1. All aircraft must be controllable in flight.
2. If an aircraft is equipped with a wheeled landing gear, the aircraft must have some form of ground steering mechanism for positive directional control during takeoffs and landings. Aircraft may not rely solely on aerodynamic control surfaces for ground steering.

2.6   RADIO CONTROL SYSTEM

The use of a 2.4 GHz radio control system is required for all aircraft. The 2.4 GHz radio control system must have a functional fail safe system that will reduce the throttle to zero if the radio signal is lost.

2.7   SPINNERS OR SAFETY NUTS REQUIRED

All aircraft must utilize either a spinner or a rounded model aircraft type safety nut.

2.8   METAL PROPELLERS

Metal propellers are not allowed.

2.9   LEAD IS PROHIBITED

The use of lead in any portion of any aircraft (payload included) is strictly prohibited.

2.10   PAYLOAD DISTRIBUTION

The payload cannot contribute to the structural integrity of the airframe.

2.11   AIRCRAFT BALLAST

Aircraft ballast is allowed with the following conditions:

1. Ballast cannot be used in the closed payload bay or passenger cabin.
2. Ballast stations must be clearly indicated on the 2D drawings.
3. Ballast must be secured so as to avoid shifting or falling off the aircraft and causing a CG problem.
4. Ballast will not be counted as payload.

2.12   STORED ENERGY RESTRICTION

Aircraft must be powered by the engine(s)/motor on board the aircraft. No other internal and/or external forms of stored potential energy allowed.

2.13   CONTROL SURFACE SLOP

Aircraft control surfaces and linkage must not feature excessive slop. Sloppy control surfaces lead to reduced controllability in mild cases, or control surface flutter in severe cases.

2.14   SERVO SIZING

Analysis and/or testing must be described in the Design Report that demonstrates the servos are adequately sized to handle the expected aerodynamic loads during flight.

2.15 Clevis Keepers

All control clevises must have additional mechanical keepers to prevent accidental opening of the control clevis in flight.

2.16 Red Arming Plug

All electric powered aircraft MUST use a discrete and removable red arming plug to arm and disarm the aircraft propulsion system. This red arming plug must be integrated into the electrical circuit between the battery and the electronic speed controller (ESC).

1. The red arming plug must physically be located at 40% to 60% of the aircraft length from the aircraft propeller. This is to allow arming and disarming the aircraft at a safe distance from the propeller.
2. The red arming plug must be located on top of the fuselage or wing and external of the aircraft surface.
3. The location of the red arming plug must be clearly visible.
4. The non-removable portion of the arming plug interface may not have more than one male lead.
5. Disconnecting wiring harnesses to arm and disarm a system will NOT be allowed.

2.17 Repairs, Alterations, and Spares

1. The original design of the aircraft as presented in the written and oral reports must be maintained as the baseline aircraft during the course of the competition.
2. In the event of damage to the aircraft, the aircraft may be repaired provided such repairs do not drastically deviate from the original baseline design. All major repairs must inspected before the aircraft is cleared for flight.

2.18 Alteration after First Flight

Minor alterations are allowed after the first and subsequent flight attempts.

1. A penalty will be assessed ONLY if 2/3 of the ruling committee (Event Director, Head scoring judge and/or SAE staff judge) agree that there was significant modifications made from the baseline configuration.
2. If the ruling committee determines that the changes are a result of safety-of-flight, the changes will not incur penalty points. Alteration must be reported utilizing Engineering Change Request (ECR) Appendix E.

2.19 Competition Supplied Fuel

Classes that use internal combustion engine may use the competition-supplied fuel.

1. Advanced Class teams may provide their own fuel.
2. Fuel used for the Advanced Class must be acceptable for use by the AMA and the competition organizer.
3. No fuel systems with gaseous boosts in which gases other than air enter the internal combustion engine will be allowed; pressurized air is also not allowed.
4. Engines utilizing extremely hazardous fuels such as those containing tetra nitromethane or hydrazine are prohibited.

3 MISSION REQUIREMENTS AND SCORING

3.1 ROUND ATTEMPT

Teams are allowed one (1) flight attempt per round.

- **Regular and Advanced Classes:** Without violating other take-off restrictions, a team can have multiple attempts to become airborne within the team's prescribed time limit for each respective class identified in section 3.5.
- **Micro Class:** only one launch attempt is allowed per round.

3.2 ENGINE OR MOTOR RUN-UP BEFORE TAKEOFF

Aircraft may be throttled up/run up for takeoff, subject to the following conditions:

- **Advanced Class:** Use of a helper to hold the aircraft for takeoff is allowed. Helper may not push the aircraft on release.
- **Regular Class:** Use of a helper to hold the aircraft is allowed. Main wheels must be placed on the takeoff line for Regular Class. The helper may not push the aircraft upon release.
- **Micro Class:** aircraft must be run up and hand launched within the launch circle for Micro .

3.3 AIRCRAFT CONFIGURATION AT LIFTOFF AND DURING THE FLIGHT ATTEMPT

The aircraft must remain intact during takeoff, the circuit of the field and landing.

1. No parts of any kind may leave the aircraft during the flight attempt.
2. Exception: a broken prop during landing is allowed and does not invalidate the flight attempt.

3.4 COMPETITION CIRCUIT REQUIREMENTS

1. During departure and approach to landing, the pilot must not fly the aircraft in a pattern that will allow the aircraft to enter any of the no-fly zones.
2. No aerobatic maneuvers will be allowed at any time during the flight competition in any competition class. This includes but not limited to: loops, figure 8's, Immelmann, all types of rolling maneuvers and inverted flight.
3. Regular and Micro Class aircraft must successfully complete a minimum of one 360° circuit.
4. Advanced Class has no specific flight pattern. (See Advanced Class rules for details concerning the releasable payload drop mission element.)

3.5 TIME LIMITS AND MULTIPLE FLIGHTS ATTEMPTS

1. Multiple takeoff attempts are allowed within the class specific time allotment as long as the aircraft has NOT become airborne during an aborted attempt.
2. If an airborne aircraft returns to the ground after being airborne and is beyond the take-off limits, the flight attempt will be disqualified for that round.

Table 3.1: Flight Attempt Information

| Class | Time Limit (sec) | Can make multiple takeoff attempts if: | | | Definition of Takeoff is defined as the point at which: |
		Still within the Time Limit	Bounce within required take-off distance	Bounce outside the required take-off distance	
Regular	120	Yes	Yes	No	The wheels leave the starting line
Advanced	180	Yes	Yes	No	The wheels leave the starting line
Micro	60	No	No	No	The launcher is no longer in contact with the aircraft

3.6 TAKE-OFF

Takeoff direction will be determined by the Air Boss, and will selected to face into the wind if possible.

1. Regular and Advanced Class aircraft must remain on the runway during the takeoff roll.
2. Micro Class must be hand launched from the designated launch area that is a half circle with a radius of 7.5 ft.
3. Distance requirements are defined in Table 3.2.
4. Making the initial turn before passing the "distance from start before initial turn" requirement will disqualify that flight attempt. (Table 3.2)

Table 3.2: Take-Off information

Class	Take-Off Distance Limits (ft.)	Distance from start before initial turn (ft.)	Description
Regular	200 ft.	400 ft.	Aircraft must be airborne within the prescribed take-off distance.
Advanced	None	None	Aircraft will have the full use of the runway.
Micro	N/A	400 ft.	Team may use the entire launch half-circle per attempt to get the aircraft airborne. Only one (1) launch attempt per round is allowed.

3.7   LANDING

A successful landing is defined as a controlled return to the ground inside the landing zone for that class and remaining on the ground through rollout. A failed landing attempt will result in no score for the round.

3.8   LANDING ZONE

The landing zone is a predetermined fixed area for each class for the purpose of returning a flying aircraft back to the ground. See Table 3.3 for class requirements.

1. The landing zones will be visibly marked at each event site prior to the start of the competition.
2. It is the team and team pilot's responsibility to be aware of the class specific landing zone dimensions at the event site.

1. **Allowed during Landing**

   1. Controlled rollout beyond the landing zone is allowed provided the aircraft touches the ground inside the landing zone.
   2. Controlled run-off to the side of the runway within the landing zone is allowed provided the aircraft touches the ground inside the landing zone.
   3. Controlled run-off to the side of the runway beyond the landing zone is allowed provided the aircraft touches the ground inside the landing zone.

2. **Not Allowed during Landing**

   1. Touchdown outside the landing zone for that class.
   2. Uncontrolled runoff or bouncing across the boundary at the end of the landing zone is not allowed and will be judged as a failed landing attempt.
   3. Touch-and-goes are not allowed and will be judged as a failed landing attempt.
   4. Uncontrolled runoff or a bouncing run-off to the side of the runway is not allowed and will be judged as a failed landing attempt.

Table 3.3: Landing Distance Limit

Class	Landing Distance Limits (ft.)	Description
Regular	400 ft.	Aircraft must land in the same direction as takeoff within a designated landing zone.
Advanced	None	Aircraft must land in the same direction as takeoff within a designated landing zone.
Micro	200 ft.	Aircraft must land in the same direction as takeoff within a designated landing zone.

3.9 GROUNDING AN AIRCRAFT

1. An aircraft will be grounded if it is deemed non-flight-worthy or not in compliance with class rules by any SAE official, event official or a designated technical/safety inspector.
2. Until the non-flight-worthy or out of compliance condition has been addressed and has been cleared by re-inspection, the aircraft will not be allowed to fly in the competition.

3.10 NO-FLY ZONE

Each competition will have venue-specific **no-fly zones**. The no-fly zones will be defined during the all hands briefing at the event and during the pilot's briefings.

1. At no time will an aircraft enter the no-fly zones, whether under controlled flight or uncontrolled.
2. First infraction for crossing into the no-fly zone will result in an invalidated flight attempt and zero points will be awarded for that flight.
3. Second infraction will result in disqualification from the entire event and loss of all points.
4. It is the team and team pilot's responsibility to be aware of the venue-specific no-fly zones and to comply with all venue specific rules.
5. If a team is unable to directionally control their aircraft and it is headed towards or is in a no fly zone, the Judges and/or Flight boss may order the pilot to intentionally crash the aircraft to prevent it from endangering people or property. This safety directive must be followed immediately if so ordered by the officials.

3.11 FLIGHT RULES ANNOUNCEMENT

Flight rules will be explained to all teams before the flight competition begins, either during the pilots' meeting or during activities surrounding the technical inspections and oral presentations.

3.12 FLIGHT RULES VIOLATIONS

1. Violation of any flight rule may result in the team being eliminated from the competition.
2. All members of an eliminated team may be escorted from the grounds.

3.13 LOCAL FIELD RULES

In addition to competition rules, the local flying club may have additional rules in place at the event flying field.

1. Club rules will be obeyed during the flight competition.
2. In the event that club rules conflict with competition rules, it is the responsibility of the team captain and/or faculty advisor to bring attention to the conflict and follow the appeals process to resolve the conflict.

3.14 COMPETITION SCORING

A team's final, overall score is composed of scores in the following categories:

1. Technical Design Report (Design, Written and Drawing)
2. Presentation
3. Flight Score
4. Penalties

Any Penalty Points assessed during the competition will be deducted from a team's overall score.

4   DESIGN REPORT

The Design Report is the primary means in which a team conveys the story of how their aircraft is the most suited design to accomplish the intended mission. The Design Report should explain the team's thought processes and engineering philosophy that drove them to their conclusions.

Some topics that are important to cover are: selection of the overall vehicle configuration, wing planform design including airfoil selection, drag analysis including three-dimensional drag effects, aircraft stability and control, power plant performance including both static and dynamic thrust, and performance prediction. Other topics as appropriate may be included, see SAE Aero Design Report Guidelines available at www.saeaerodesign.com/go/downloads for additional comments, suggested topics and a suggested outline. For more information regarding performance prediction, a white paper by Leland Nicolai is also available at www.saeaerodesign.com/go/downloads.

4.1   SUBMISSION DEADLINES

The Technical Design Report, 2D drawing, and supplemental Tech Data Sheet (TDS) must be electronically submitted to www.saeaerodesign.com no later than the date indicated on the Action Deadlines given on the SAE International Website:

http://students.sae.org/cds/aerodesign

Neither the Organizer nor the SAE International is responsible for any lost or misdirected reports, drawings, or server routing delays. The SAE International will not receive any paper copies of the reports through regular mail or email outside of the emergency submissions email.

4.2   ORIGINAL WORK

The Technical Design Report shall be the team's original work for this competition year. Resubmissions of previous year's design reports will not be accepted. Recitation of previous year's work is acceptable if appropriately cited and credited to the original author. Plagiarism is a forbidden industry and academic practice, all references, quoted text and reused images from any source shall have appropriate citation within the text and within the Technical Design Report's Table of References providing credit to the original author and editor.

4.3 TECHNICAL DESIGN REPORT REQUIREMENTS

Technical Design Report will be 50 points (pts) of the competition score as broken down in Table 4.3.1.

1. The Technical Design Report shall not exceed thirty (30) pages, including the certificate of compliance, 2D Drawing, and the Supplemental Datasheet for each class. If the design report exceeds thirty (30) pages, the judges will only score the first thirty (30) pages.
2. The Technical Design Report shall include a Cover Page with Team Name, Team Number, and School Name and Team Member Names.
3. The Technical Design Report shall include a Certificate of Compliance signed by hand by the team's faculty advisor.
4. The Technical Design Report shall be typewritten and double-spaced. Tables, charts and graphs are exempt from this
5. The report font shall be 12 pt. proportional; or 10 char/in. non-proportional font.
6. The report margins shall be: 1" Left, 0.5" right, 0.5" top, and 0.5" bottom.
7. Each page, except the Cover Page, Certificate of Compliance, 2D Drawing and Technical Data Sheet (TDS) shall include a page number.
8. All report pages shall be ANSI A (81/2 x 11 inches) portrait-format.
9. The Technical Design Report shall include a Table of Contents, Table of Figures, Table of Tables, Table of References and Table of Acronyms.
10. The Technical Design Report shall be single-column text layout.
11. The Technical Design Report shall include one Technical Data Sheet (TDS) appropriate for the team's competition entrant class.

Table 4.3.1 Technical Design Report

	Page Count	Regular Class	Advanced Class	Micro Class
Cover Page	1	40 pts	40 pts	40 pts
Certificate of Compliance	1			
Design Report	26			
2D Drawing	1	5 pts	5 pts	5 pts
TDS: Payload Prediction	1	5 pts	-	-
TDS: Radio Link Budget (Appendix B)	1	-	5 pts	-
TDS: Aircraft Weight Build-Up Schedule (Appendix C)	1	-	-	5 pts
Total	**30**	**50 pts**	**50 pts**	**50 pts**

4.4 2D DRAWING REQUIREMENTS

1. **2D Format and Size**

   The 2D drawing must be ANSI B sized page (PDF) format (11 x 17 inches).

   1. For teams outside North America that cannot submit an ANSI B size drawings, page format size must be the closest size available to ANSI B.
   2. Drawing shall consist of one (1) page.

2. **Markings Required**

   The 2D drawing must be clearly marked with:

   1. Team number
   2. Team name
   3. School name

3. **Views Required**

   Drawings shall include at a minimum, a standard aeronautical 3-view orthographic projection arranged as described:

   1. **Left** side view, in lower left, with nose pointed left.
   2. **Top** view, above and aligned with the left side view, also with nose pointed left (wing-span break-view permitted).
   3. **Front** view aligned to side view, located in the lower right (projection view non-standard movement as noted by projection view arrows in accordance with ANSI-Y14.5M 1994).
   4. **(Regular Class Only)** Regular Class shall include an additional view, separate from the basic aircraft, illustrating the passenger cabin layout with appropriate dimensions identifying the passenger seating arrangement. Total passenger capacity shall be labeled.

4. **Dimensions Required**

   Drawing dimensions and tolerance shall be in English units, decimal notation accordance with ANSI-Y14.5M 1994 to an appropriate level of precision to account for construction tolerances (allowable variation from analyzed prediction to account for fabrication) (i.e. X.X = ± .1 in; X.XX = ± .03 in; X.XXX = ± .010 in).

   The minimum required dimensions/tolerances are: Aircraft length, width, and height

5. **Summary Data Required**

   The drawing shall contain a summary table of pertinent data to include but not limited to:

   1. Wingspan
   2. Empty weight
   3. Battery(s) capacity
   4. Motor or engine make and model
   5. Motor KV (micro and Regular Class only)
   6. Propeller manufacturer, diameter, and pitch
   7. Servo manufacturer, model number and torque specification in ounce-inches for each servo used on the aircraft. Identify servo being used at each position on the aircraft.

6. **Weight and Balance Information**
   The 2D drawing shall contain the following weight, balance and stability information:

   1. A clearly marked and labeled aircraft datum
   2. A weight and balance table containing pertinent aircraft equipment. Each item listed must show its location from the aircraft datum in inches (the moment arm), the force, and resultant moment. See www.saeaerodesign.com/go/downloads for additional information. The minimum list of pertinent equipment includes:
      a. Motor or engine
      b. Battery(s)
      c. Fuel (Advanced Class)
      d. Payload
      e. Ballast (if used)
      f. Electronics
   3. Aircraft mean aerodynamic cord, stability margin and Center of Gravity (CG) information listed below must be clearly shown on drawing.
      a. Aircraft mean aerodynamic cord
      b. Stability margin for loaded CG and empty CG
      c. Empty CG location (flightworthy)
      d. Fully loaded CG (flightworthy, with payload and fuel, if applicable)

4.5 TECH DATA SHEET: PAYLOAD PREDICTION (REGULAR CLASS ONLY)

Regular Class teams must include a total payload prediction curve as part of the technical report. The graph represents an engineering estimate of the aircraft's lift performance based on density altitude.

1. Graph of payload weight shall be linearized over the relevant range.
2. The linear equation shall be in the form of:

$$y = mX + b$$

Y = Payload weight (lbs.)
X = Density Altitude (feet)
m = Slope of the linear line
b = y-intercept.

3. Only one line and one equation may be presented on the graph. This curve may take into account predicted headwind for local conditions, rolling drag, inertia, engine and propeller performance, or any other factors that may affect takeoff performance. All these factors are allowed components of the prediction curve, but only one curve will be allowed; multiple curves to account for varying headwind conditions will not be allowed.
4. The team must provide a brief explanation of how the line was generated in the body of the report. The section of the report containing this information must be noted on the payload prediction curve.
5. Graph axes shall be in English units, decimal notation.

Payload Prediction Curve
Density Altitude

$$\text{Payload} = -0.001x + 25.2$$

(Chart: Payload (lb) on y-axis from 0 to 30; Density Altitude (ft) on x-axis from 0 to 10000 in increments of 400. Linear trend line decreasing from 25 at 0 ft to 15 at 10000 ft.)
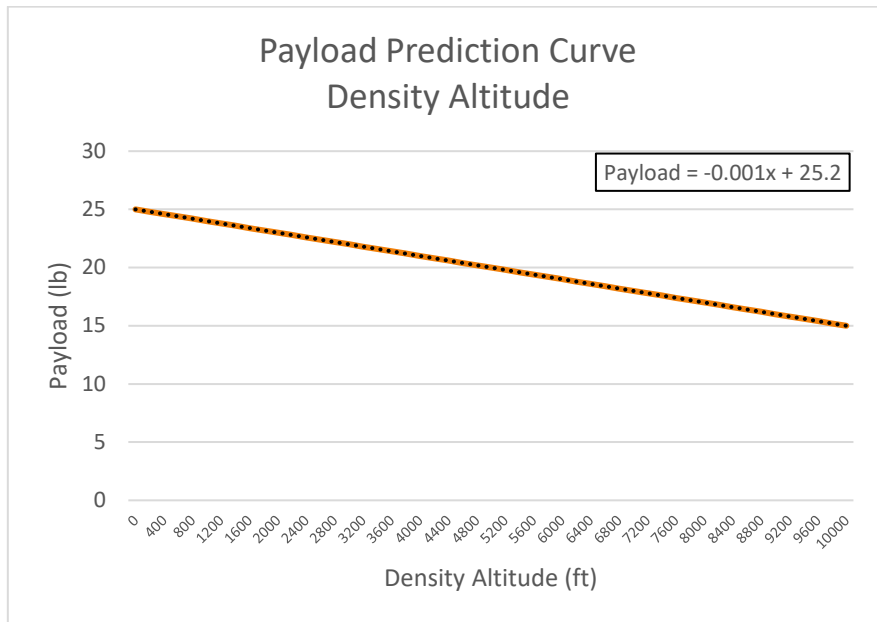
4.6 TECH DATA SHEET: RADIO LINK BUDGET (ADVANCED CLASS ONLY)

A **link budget** is an accounting of all of the gains and losses from the transmitter, through the medium (free space, cable, waveguide, fiber, etc.) to the receiver in a telecommunication system. It accounts for the attenuation of the transmitted signal due to propagation, as well as the antenna gains, feed-line and miscellaneous losses. Randomly varying channel gains and propagation fading are taken into account by adding signal margin, depending on the anticipated severity of these effects. The amount of margin required can be reduced by the use of mitigating techniques such as antenna diversity or frequency hopping.

A template for the link budget can be found in Appendix B.

4.7 TECH DATA SHEET: WEIGHT BUILDUP (MICRO CLASS ONLY)

The Micro Class Weight & Balance Build-up schedule will help teams understand the importance of managing aircraft weight to achieve safety of flight at the desired payload fraction. Each team shall supply a one (1) sheet summary list of pertinent aircraft parts and weight (lb.).

A template for the weight buildup can be found in Appendix C.

5 TECHNICAL PRESENTATION

Like all professionals, engineers must possess a well-developed ability to synthesize issues and communicate effectively to diverse audiences. The technical portion of the aero-design competition is designed to emphasize the value of an ability to deliver clear, concise and effective oral presentations. Teams can obtain a maximum technical presentation score of fifty (50) points. Presentation score shall be comprised of scores from the presenter's delivery technique and the judges' evaluation of technical content, empirical analysis, and quality visual aide.

5.1 TECHNICAL PRESENTATION REQUIREMENTS

1. Technical presentation shall last ten (10) minutes and be followed by a five (5) minute "Question and Answer" (Q&A) period.

2. Technical presentation shall be delivered in English.

3. Technical presentation shall address, but are not limited to, trade studies performed, design challenges, and manufacturing techniques.

4. Technical presentation is limited to student team members only. Non-team member pilot, faculty advisors, and/or parents can attend the technical presentation but are prohibited from participating in the setup, delivery, and/or the Q&A.

5. Assistance in the use of visual aids is advisable; Film clips, if used, may not exceed one-minute total duration; Film clips may not be accompanied by recorded narration.

6. Regular and Micro Class shall display their entry aircraft during technical presentation. Advanced Class team are exempted from the requirement to have a static display if and only if the size of the aircraft prevents entry into the room.

7. Advanced Class teams shall make every effort to bring all or a portion of their aircraft to the presentation; however, if the size of the aircraft prevents its display, adequate photographs are acceptable substitutes.

8. During the presentation and static display setup, the teams shall provide a single sheet (8.5" x 11") marketing/promotion piece to further detail aircraft's feature, capabilities, and unique design attributes.

5.2 TECHNICAL PRESENTATION PROCESS AND PROCEDURES

Each presentation room shall have a lead judge with the responsibility to ensure compliance with competition rules and schedule. Lead judge will identify a timekeeper.

1. With agreement from the speaker, the timekeeper will give the speaker a one (1) minute warning prior to the ten (10) minute limit.
2. If the team exceeds the ten (10) minute limit, the team will be assessed a five (5) point penalty for going over the time limit.
3. The presentation shall be stopped at the eleven (11) minute mark.
4. A team shall have five (5) minutes for Q&A immediately following the presentation. Questions may be asked by any judge on the panel.
5. Any time remaining or exceeding the ten (10) minutes shall be added to or subtracted from the five (5) minute Q&A.
6. Presentation Time Breakdown:

Time (Minutes)	Description
2	Setup presentation, visual aide, and/or static display
10	Perform Technical Presentation
5	Questions & Answers
3	Pack-up presentation and static display

6 TECHNICAL INSPECTION AND AIRCRAFT DEMONSTRATIONS

Technical and Safety inspection of all aircraft will be conducted using the published Technical and Safety Inspection checklists for each class for the current year. The checklists can be found at www.saeaerodesign.com/go/downloads.

Technical and Safety Inspection is the process of checking all aircraft for:

- Compliance with all General aircraft requirements.
- Compliance with all aircraft configuration requirements for their class.
- Overall safety and airworthiness.

All aircraft must pass the Technical and Safety Inspection in order to compete. It is strongly suggested that each team pre-inspect their aircraft and correct any problems using the official inspection checklist before arriving at the competition.

All required Aircraft Demonstrations will be performed at designated locations in the Technical Inspection area.

- **Regular Class** will demonstrate the ability to load and unload their aircraft per the requirements of rule 7.6.
- **Advanced Class** will demonstrate that their aircraft has proven operational ability by providing a video showing the aircraft successfully taking off, dropping a payload and landing per the requirements of rule 8.1.
- **Micro Class** will demonstrate the timed assembly of their aircraft per the requirements of rule 9.6.

6.1 AIRCRAFT CONFORMANCE TO 2D DRAWING

During Technical Inspection, the aircraft will be inspected and measured for conformance to the 2D drawing presented in the Design Report.

1. At a minimum, aircraft length, wingspan and height dimensions will be measured and compared to the 2D drawing.
2. All teams must have a hard copy of their design report with them during technical inspection.
3. Aircraft will have their actual empty CG compared to the empty CG presented in the design report 2D drawing.

6.2 FAILURE TO REPORT DESIGN CHANGES

Failure to report any design changes incorporated after Design Report submission and prior to Technical Check-in will incur a one (1) point penalty for each unreported design change discovered during technical inspection.

6.3 DEVIATIONS FROM 2D DRAWING

Any deviation in construction of the aircraft from the submitted 2D drawing, after submission of the Design Report, must be reported in writing.

1. Each design change must be documented separately using the Engineering Change Request (ECR) – a physical copy of which must be brought to the Technical and safety Inspection
2. Only one design change may be submitted per ECR form.
3. Penalty points for design changes will be assessed in accordance with the penalty guidelines in Appendix E, subject to the judges' final determination.

6.4   SAFETY AND AIRWORTHINESS OF AIRCRAFT

Technical and Safety Inspection will be also be used to assess the general safety and airworthiness aspects of each aircraft by seeking any problems that could cause an aircraft to depart controlled flight. This assessment includes but is not limited to:

1. Unintentional wing warps
2. Control surface alignment
3. Correct control surface response to radio transmitter inputs
4. Structural and mechanical soundness

6.5   INSPECTION OF SPARE AIRCRAFT AND SPARE AIRCRAFT COMPONENTS.

1. All spare aircraft and spare aircraft components (wings, fuselages and tail surfaces) must be presented for inspection.
2. Teams may submit up to two complete aircraft at Technical Inspection on Friday.
3. Additional spare aircraft and parts beyond two sets may be submitted for inspection during the event on Saturday and Sunday.

6.6   AIRCRAFT MUST MEET ALL INSPECTION REQUIREMENTS THROUGHOUT THE COMPETITION.

1. All aircraft must meet all Technical and Safety Inspection requirements throughout the competition.
2. Any official may request that an aircraft be re-inspected if a general, class configuration or safety requirement problem is seen on an aircraft at any time during the event.
3. This includes any errors or omissions made by officials during inspection.

6.7   TECHNICAL AND SAFETY INSPECTION PENALTIES

No points are available to be scored as a result of the Technical and Safety Inspection: teams may only lose points as a result of errors and problems encountered during the inspection process. Any penalties assessed during Technical Inspection will be applied to the overall competition score.

7 REGULAR CLASS DESIGN REQUIREMENTS

The objective of Regular Class is to design an aircraft that can generate revenue by carrying as much payload as possible while observing the power available requirement. Payload will consist of passengers, represented by tennis balls, and Luggage, represented by payload weights, which must be carried on each flight. Accurately predicting the lifting capacity of the aircraft and selecting the appropriate number of passenger seats is an important part of the airplane design.

7.1 AIRCRAFT DIMENSION REQUIREMENT

Regular Class aircraft are limited to a wingspan of 144 inches.

7.2 MATERIAL AND EQUIPMENT RESTRICTIONS FOR REGULAR CLASS

1. **Fiber-Reinforced Plastic (FRP)**
   The use of Fiber-Reinforced Plastic (FRP) is prohibited on all parts of the aircraft. Exceptions to this rule include: commercially available FRP motor mount, propeller, landing gear and control linkage components. Exploration of alternative materials is encouraged.

2. **Rubber bands**
   Elastic material such as rubber bands shall not be used to retain the wing or payloads to the fuselage.

3. **Stability Assistance**
   All types of gyroscopic or other stability assistance are prohibited.

7.3 AIRCRAFT SYSTEM REQUIREMENTS

1. **Electric Motor Requirements**
   The aircraft shall be propelled by a single electric motor (no multiple motors). There are **no restrictions on the make or model of the electric motor.**

2. **Gear boxes, Drives, and Shafts**
   Gearboxes, belt drive systems, and propeller shaft extensions are allowed as long as a one-to-one propeller to motor RPM is maintained. The prop(s) must rotate at motor **RPM.**

3. **Aircraft Propulsion System Battery**
   Regular Class aircraft must be powered by a commercially available Lithium-Polymer battery pack.

   1. Required: 6 cell (22.2 volt) Lithium Polymer (Li-Poly/Li-Po) battery pack. Minimum requirements for Li-Po battery: 3000 mAh, 25c
   2. Homemade batteries are NOT allowed.

4. **Power Limiter**
   All Regular Class aircraft must use a 2015 V2 or newer version 1000 watt power limiter from the official supplier, Neumotors.com.

   1. Repair and/or modifications to the limiter are prohibited.
   2. The limiter must be fully visible and easy to inspect.

3. Only battery, receiver, speed control, and limiter are allowed within the power circuit.
4. The limiter is only available at the follow link:

http://neumotors.cartloom.com/shop/item/24377

This supplier has agreed to ship worldwide to any team.

5. **Radio System Battery and Switch**
    If a separate battery is used for the radio system, the battery pack must have enough capacity to safely drive all the servos in the aircraft, taking into consideration the number of servos and potential current draw from those servos.

    1. A battery pack with a minimum capacity of 1000 mAh must be used for the radio system.
    2. The battery pack must be a LiPo or LiFE type battery.
    3. Battery voltage regulators are allowed.
    4. The battery pack must be controlled by a clearly visible and properly mounted on/off switch on the external surface of the aircraft, located at least 12" from the prop.

7.4   PAYLOAD REQUIREMENTS

1. **Types of Payload**
    Regular Class payload shall consist of two types; (1) Passengers and (2) Luggage, which must be carried in proportion to one another in the Passenger Cabin and Payload Bay respectively. Both the Passenger Cabin and Payload Bay must be designed for ease of access to both Passengers and Luggage. This will be demonstrated during the oral presentation (Reference Section 7.6 for demonstration details).

2. **Payload Bay Requirements**
    Regular Class aircraft shall have a single fully enclosed Payload Bay for carrying Luggage (see section 7.4.2) with the following additional requirements:

    1. The Payload Bay shall only contain Luggage.

    2. The Payload Bay shall fully enclose the Luggage.

    3. The Payload Bay has no restriction on size or shape.

    4. Only one Payload Bay is allowed in a Regular Class aircraft.

3. **Luggage and Luggage Support Requirements**

Luggage shall consist of a support assembly and payload plates with the following additional requirements:

1. For weight measurement and scoring, Luggage shall consist of the payload plates and support structure used to retain the weight(s) in the Payload Bay.
2. An average Luggage weight of ½ lb. or more must be carried for each Passenger carried.
3. If the Luggage weight carried does not meet the ½ lb. per passenger requirement, the excess Passengers will be counted as empty seats and the flight scored accordingly.
4. Luggage weight in excess of ¾ lbs. per passenger will not count in Luggage weight scoring.
5. There is no required configuration for the payload plates.
6. Teams must provide their own payload plates.
7. The support assembly must securely bolt together all payload plates, creating a single mass of payload. The support assembly must also securely bolt all payload plates to the structure of the aircraft to ensure that the payload luggage will not shift or come loose in flight.
8. Tape, Velcro, rubber bands, container systems and friction systems alone may not be used to retain the support assembly and/or payload plates.

4. **Passenger Payload Definition**

The Passenger* payload must consist only of unmodified tennis balls which meet or exceed the minimum size and weight specifications for Type 1 and Type 2 tennis balls as specified by the International Tennis Federation (ITF). Accordingly, the minimum tennis ball weight is 1.975 ounces and minimum ball diameter allowed is 2.57 inches. A list of accepted brands of tennis balls is given at:

http://www.itftennis.com/technical/balls/.

* Teams must provide their own Passengers.

5. **Passenger Cabin Requirements**

Regular Class aircraft must position all Passengers in a single Passenger Cabin.

1. The Passenger Cabin must position all Passengers to be tangent to the same side of a single geometric plane.
2. All Passengers must be constrained to the geometric plane within the Passenger Cabin so that they will not shift or come loose during any portion of a flight.
3. A position designed to hold a Passenger is a Seat. Passenger Seats must be in contiguous positions. Contiguous is defined as being less than 0.25 inches from the adjacent Passenger.
4. Any Passenger not in a seat after a flight will not count as revenue generated by Passengers.
5. Passengers must be in a countable configuration to be scored as a revenue generating Passenger. A countable configuration is defined as when Passengers are clearly visible and can be easily touch-counted.

6. Each Passenger carried in excess of the maximum number (as determined by Luggage weight), will not count as a revenue generating Passenger and will be scored as an empty Seat.

7.5   PASSENGER SEATING REQUIREMENTS

1. Regular **Class** aircraft must accommodate a minimum of 10 passengers and the required luggage.
2. Regular **Class** teams must document the number of passenger seats in their design per rule 4.4.3.4 at the time the design report is submitted. This seat number is used to determine passenger count and empty seats for the scoring equation.
3. Teams are allowed to reduce the number of seats in their design one time. This reduction can only be made after design report submission and before technical inspection. An Engineering Change Request defining the new seating number must be submitted on the normal ECR form. There is a one point penalty for each seat removed from the original design submission. After this ECR is submitted, the revised number of seats is then used in the scoring equation.
4. The number of passenger seats may never be increased after Design Report submission.

7.6   REGULAR CLASS PAYLOAD LOADING AND UNLOADING DEMONSTRATION

Technical Presentation for Regular Class shall demonstrate the requirement to quickly load/secure and unload both Passengers and Luggage. This is a timed activity and shall be performed by no more than two (2) members of the team within the following time constraints:

1. One (1) minute to load/secure both Luggage (5 – 7.5lbs.) and 10 passengers for flight.

   - The demonstration will start with the passengers and cargo separate from the aircraft and the aircraft in a flight-ready configuration.
   - The demonstration is considered complete when all required passengers and Luggage are loaded, secured, and the aircraft is put back in a flight-ready configuration.

2. One (1) minute to unload both Luggage (5 – 7.5lbs.) and 10 Passengers.

   - The demonstration will start with all required Passengers and Luggage loaded, secured, and the aircraft in a flight-ready configuration.
   - The demonstration will be considered complete when both the Passengers and Luggage are separate from the aircraft and the aircraft is put back in a flight-ready configuration.

This demonstration will be performed at a designated location in the Technical Inspection area on Friday.

7.7 REGULAR CLASS SCORING

In order to participate in the flight portion of the competition, each team is required to have submitted AND received a score for their Design Report and Oral Presentation.

The Final Regular Class Flight Score shall be based upon the Total Revenue earned and Total Penalty deductions received.

Scoring Equation:

$$FFS = \ Final\ Flight\ Score = \ \frac{1}{40\ N}\left[\sum_{1}^{N} FS\right]$$

Where:

$FS = Flight\ Score = \$100P + \$50C - \$100E\ for\ each\ flight$

$P = Number\ of\ seated\ Passengers\ carried\ on\ a\ flight$

$C = Luggage\ weight\ (lbs)$

$E = Number\ of\ empty\ Seats$

$N = Total\ Number\ of\ Flight\ Rounds\ During\ Competition$

All Flight Score's with a value less than zero (0) will default to zero (0).

Penalty Points

Any penalty points assessed during the competition are now deducted from a team's overall score per rule 3.14.

SAE AERO DESIGN

STATEMENT OF COMPLIANCE
Certification of Qualification

Team Name		Team Number	
School			
Faculty Advisor			
Faculty Advisor's Email			

Statement of Compliance

As Faculty Advisor, I certify that the registered team members are enrolled in collegiate courses. This team has designed, constructed and/or modified the radio controlled aircraft they will use for the SAE Aero Design 2018 competition, without direct assistance from professional engineers, R/C model experts or pilots, or related professionals.

Signature of Faculty Advisor

Team Captain Information:

Team Captain:	
Captain's E-mail:	
Captain's Phone:	

Note:
A copy of this statement needs to be included in your Design Report as page 2 (Reference Section 4.3)

Engineering Change Request (ECR)

Team Number:	
School Name:	
Team Name:	

Discovery Method	□Tech Inspection □Safety Inspection □Test Flight □Design Analysis	System Affected	□Wing (area +/-) □Fuselage (area +/-) □Horiz. Stabilizer (area +/-) □Vertical Tail (area +/-) □Engine Mount assembly	□Mechanical □Landing System □Structural □Electronics (avionics) □Payload bay Assembly

Surface Area	AREA ADDED:_____ AREA REDUCED:_____ *If surface area was impacted by the modification, specify total area added or reduced. Show calculations:*
Describe the Modification	
Reason for Modification	
Other Considerations	

*** OFFICIAL USE ONLY ***	
ECR #	

Penalty Chart Guidelines

These charts provide guidelines to possible assessment of penalty points for different design changes. Final assessment of penalty points is subject to the judges' determination.

Table D1: Penalties guidelies for for wing surface changes

Dimension	Add	Remove
Span	2pts per inch	1pt per inch
Chord	10pts per inch	5 pts per inch

Table D2: Penalty guidelines by category and size of change

Type	Small	Medium	Large
Structural	2pts	4pts	6pts
Mechanical	2pts	4pts	6pts
Electronics	1pts	2pts	3pts
Miscellaneous	1pts	3pts	5pts

APPEALS

Team Name	
Team Captain	
Collateral Points	*All appeals will require the team to post twenty five (25) points as collateral. If the appeal is successful and the action is reversed, the team will not forfeit the twenty five (25) collateral points. If the appeal is overruled, the team will forfeit the twenty five (25) collateral points* Collateral Points: 25 Sign if Agree: _____
Reason for this Appeal	
Rule Reference	*List the section(s) in the official rule that is (are) in conflict with the action(s) taken by competition official* Section:_____ Section:_____ Section:_____ Section:_____
Desire outcome	

SAE Technical Standards

The SAE Technical Standards Board (TSB) has made the following SAE Technical Standards available on line, **at no cost**, for use by Collegiate Design teams. Standards are important in all areas of engineering and we urge you to review these documents and to become familiar will their contents and use.

The technical documents listed below include both (1) standards that are identified in the rules and (2) standards that the TSB and the various rules committees believe are valuable references or which may be mentioned in future rule sets.

All Collegiate Design Series teams registered for competitions in North America have access to all the standards listed below - including standards not specific to your competition.

SAE Technical Standards included in the CDS Rules

Baja SAE
J586 - Stop Lamps for Use on Motor Vehicles Less Than 2032 mm in Overall Width
J759 - Lighting Identification Code
J994 - Alarm - Backup – Electric Laboratory Tests
J1741 - Discriminating Back-Up Alarm Standard
Clean Snowmobile Challenge
J192 - Maximum Exterior Sound Level for Snowmobiles
J1161 - Sound Measurement – Off-Road Self-Propelled Work Machines Operator-Work Cycle
Formula Hybrid
J1318 - Gaseous Discharge Warning Lamp for Authorized Emergency, Maintenance and Service Vehicles
J1673 - High Voltage Automotive Wiring Assembly Design
Formula SAE
SAE 4130 steel is referenced but no specific standard is identified
SAE Grade 5 bolts are required but no specific standard is identified
Supermileage
J586 - Stop Lamps for Use on Motor Vehicles Less Than 2032 mm in Overall Width

SAE Technical Standards for Supplemental Use

Standards Relevant to Baja SAE
J98 – Personal Protection for General Purpose Industrial Machines – Standard
J183 – Engine Oil Performance and Engine Service Classification - Standard
J306 – Automotive Gear Lubricant Viscosity Classification - Standard
J429 – Mechanical and Material Requirements for Externally Threaded Fasteners – Standard

J512 – Automotive Tube Fittings - Standard

J517 – Hydraulic Hose - Standard

J1166 – Sound Measurement – Off-Road Self-Propelled Work Machines Operator-Work Cycle

J1194 – Rollover Protective Structures (ROPS) for Wheeled Agricultural Tractors

J1362 – Graphical Symbols for Operator Controls and Displays on Off-Road Self-Propelled Work Machines - Standard

J1614 – Wiring Distribution Systems for Construction, Agricultural and Off-Road Work Machines

J1703 - Motor Vehicle Brake Fluid - Standard

J2030 – Heavy Duty Electrical Connector Performance Standard

J2402 – Road Vehicles – Symbols for Controls, Indicators and Tell-Tales – Standard

Standards Relevant to Clean Snowmobile Challenge

J44 – Service Brake System Performance Requirements – Snowmobiles - Recommended Practice

J45 – Brake System Test Procedure – Snowmobiles – Recommended Practice

J68 – Tests for Snowmobile Switching Devices and Components - Recommended Practice

J89 – Dynamic Cushioning Performance Criteria for Snowmobile Seats - Recommended Practice

J92 – Snowmobile Throttle Control Systems – Recommended Practice

J192 – Maximum Exterior Sound Level for Snowmobiles - Recommended Practice

J288 – Snowmobile Fuel Tanks - Recommended Practice

J1161 – Operational Sound Level Measurement Procedure for Snowmobiles - Recommended Practice

J1222 – Speed Control Assurance for Snowmobiles - Recommended Practice

J1279 – Snowmobile Drive Mechanisms - Recommended Practice

J1282 – Snowmobile Brake Control Systems - Recommended Practice

J2567 – Measurement of Exhaust Sound Levels of Stationary Snowmobiles - Recommended Practice

Standards Relevant to Formula SAE

J183 – Engine Oil Performance and Engine Service Classification - Standard

J306 – Automotive Gear Lubricant Viscosity Classification - Standard

J429 – Mechanical and Material Requirements for Externally Threaded Fasteners – Standard

J452 - General Information – Chemical Compositions, Mechanical and Physical Properties of SAE Aluminum Casting Alloys – Information Report

J512 – Automotive Tube Fittings - Standard

J517 – Hydraulic Hose - Standard

J637 – Automotive V-Belt Drives – Recommended Practice

J829 – Fuel Tank Filler Cap and Cap Retainer

J1153 - Hydraulic Cylinders for Motor Vehicle Brakes – Test Procedure

J1154 – Hydraulic Master Cylinders for Motor Vehicle Brakes - Performance Requirements - Standard

J1703 - Motor Vehicle Brake Fluid - Standard

J2045 – Performance Requirements for Fuel System Tubing Assemblies - Standard

J2053 – Brake Master Cylinder Plastic Reservoir Assembly for Road Vehicles – Standard

Standard Relevant to Formula Hybrid

J1772 – SAE Electric Vehicle and Plug in Hybrid Conductive Charge Coupler

Standard Relevant to all CDS Competitions

J1739 – Potential Failure Mode and Effects Analysis in Design (Design FMEA) Potential Failure Mode and Effects Analysis in Manufacturing and Assembly Processes (Process FMEA) and Potential Failure Mode and Effects Analysis for Machinery (Machinery FMEA)

B List of Aerodynamics Equations and Variables

AERODYNAMIC VALUES

Lift

$$L = \tfrac{1}{2}\rho V^2 S C_L = Q S C_L$$

In Steady/Cruise Flight:

$$L = W$$

In Steady Climb:

$$L = W\cos\gamma$$

In Level Turn:

$$L = \frac{W}{\cos\phi} = \frac{WV^2}{gr\sin\phi}$$

With Downwash Effects:

$$L = L'\cos\alpha_i$$

Drag

$$D = \tfrac{1}{2}\rho V^2 S C_D = Q S C_D$$

In Steady/Cruise Flight:

$$D = T$$

In Steady Climb:

$$D = T - W\sin\gamma$$

In Level Turn:

$$D = T$$

L/D Ratio (Takeoff, cruise, landing)

$$\frac{L}{D} = \frac{C_L}{C_D}$$

Coefficient of Lift

General:

$$C_L = \frac{W}{QS} = \frac{L}{\tfrac{1}{2}\rho V^2 S} = \frac{L}{QS}$$

2-D Airfoil:

$$C_l = \frac{L}{\tfrac{1}{2}\rho V^2 c} = \frac{L}{Qc} = C_{l_0} + a_0\alpha = a_0(\alpha - \alpha_{0L})$$

2-D Airfoil at Zero Angle of Attack:

$$C_{l_0} = -\,a_0\alpha_{0L}$$

2-D Wing with Downwash Effects:

$$C_l = a_0(\alpha_{eff} - \alpha_{0L})$$

Coefficient of Drag

2-D Airfoil:

$$C_d = \frac{D}{\tfrac{1}{2}\rho V^2 c} = \frac{D}{Qc}$$

3-D Drag Coefficient/Polar = Parasitic + Induced Drag:

$$C_D = \frac{D}{\tfrac{1}{2}\rho V^2 S} = \frac{D}{QS}$$

$$C_D = C_{D_{0L}} + C_{D_i} = C_{D_{0L}} + K C_L^2 = C_{D_{0L}} + K\left(\frac{W}{QS}\right)^2$$

Induced Drag (from Downwash)

$$D_i = L'\sin\alpha_i = L\frac{C_L}{\pi AR} = QS\frac{C_L^2}{\pi ARe} = QSC_{D_i}$$

Induced Drag Coefficient

$$C_{D_i} = \frac{C_L^2}{\pi ARe} = KC_L^2$$

Induced Drag Parameter

$$K = \frac{1}{\pi e(AR)}$$

Skin Friction Coefficient

$$C_f = \frac{\tau_w}{\frac{1}{2}\rho V^2}$$

Pitch Moment

$$M = \sum_{i=0}^{n} m_i l_i$$

Pitch Moment Coefficient (about leading edge)
    2-D Airfoil:

$$C_m = \frac{M}{\frac{1}{2}\rho V^2 c^2} = \frac{M}{Qc^2}$$

Stall Speed

$$V_{stall} = \sqrt{\frac{2W}{\rho S C_{L_{max}}}}$$

AIRCRAFT PROPERTIES
Aircraft Weight

$$W = mg$$

(Center of Gravity)

$$CG = \frac{M}{m_{total}}$$

Center of Lift

$$CL = \frac{\sum_{i=0}^{n} L_i l_i}{L_{total}}$$

Oswald Efficiency Factor
    For Planes with AR<25:

$$e = 1.78(1 - 0.045AR^{0.68}) - .64$$

Required Thrust
    In Steady/Cruise Flight:

$$T_{req} = D = QSC_{D_{0L}} + \frac{KS}{Q}\left(\frac{W}{S}\right)^2$$

Minimum Velocity at Cruise

$$V_{MT} = \sqrt{\frac{2}{\rho}\left(\frac{W}{S}\right)\sqrt{\frac{K}{C_{D_{0L}}}}}$$

T/W Ratio (Takeoff, cruise, landing)

$$\frac{T}{W} = \left(\frac{550\eta_p}{V}\right)\left(\frac{P}{W}\right) = \frac{QC_{D_0}}{(W/S)} + \frac{(W/S)}{\pi(AR)eQ}$$

$$\left(\frac{T}{W}\right)_{cruise} = \left(\frac{L}{D}\right)^{-1}_{cruise}$$

Aerodynamic Center = c/4

Location on 2-D Airfoil Where:

$$\frac{dC_{m_{ac}}}{d\alpha} = 0$$

Center of Pressure

Location on 2-D Airfoil Where:

$$M_{cp} = 0$$

WING GEOMETRY

Aspect Ratio

$$AR = \frac{b}{c_g} = \frac{b^2}{S}$$

Wetted Aspect Ratio

$$AR_{wet} = \frac{b^2}{S_{wet}} = \frac{AR}{S_{wet}/S}$$

Mean Geometric Chord: Equivalent Chord of a rectangular wing w/ same span & area

General:

$$c_g = \frac{2}{b} \int_{0}^{b/2} c(y)dy$$

Rectangular Wing:

$$c_g = \frac{S}{b}$$

Straight Tapered Wing:

$$c_g = \frac{c_r}{2}(1 + \lambda)$$

Mean Aerodynamic Chord: Equivalent Chord of a rectangular wing with same pitch-moment aerodynamic characteristics

General:

$$\bar{c} = \frac{2}{S} \int_{0}^{b/2} [c(y)]^2 dy$$

Straight Tapered Wing:

$$\bar{c} = \frac{2}{3}c_r \frac{1+\lambda+\lambda^2}{1+\lambda}$$

Taper Ratio

$$\lambda = \frac{c_t}{c_r}$$

Wing Sweep Angle

Calculate at chord location n using known Sweep Angle at chord location m:

$$tan\Lambda_n = tan\Lambda_m - \frac{4}{AR}[(n-m)\frac{1-\lambda}{1+\lambda}]$$

Wing Loading = W/S (Takeoff, cruise, landing)

Horizontal and Vertical Stabilizer/Tail Area

For an ideal tail volume: $V_v = 0.02 \dots 0.05$

$$V_v = \frac{S_v l_v}{Sb}$$

For an ideal tail volume: $V_h = 0.30 \dots 0.60$

$$V_h = \frac{S_h l_h}{Sc}$$

FLIGHT PROPERTIES

Reynold's Number

$$Re = \frac{\rho V c}{\mu_\infty}$$

Dynamic Pressure

$$Q = \tfrac{1}{2}\rho V^2$$

Angle of Attack

Zero-Lift Angle of Attack:

$$\alpha_{0L} = -\frac{C_{l_0}}{a_0}$$

Induced/Downwash Angle of Attack:

$$\alpha_i = -\frac{w}{V} = \frac{C_L}{\pi AR}$$

Effective Angle of Attack:

$$\alpha_{eff} = \alpha - \alpha_i$$

Lift/Angle Curve Slope

2-D Airfoil:

$$a_0 = \frac{dC_l}{d\alpha}$$

3-D Wing:

$$a = \frac{dC_L}{d\alpha} = \frac{a_0}{1 + \frac{a_0}{\pi AR e_w}}$$

Rate of Climb

$$(RC) = V \sin\gamma = \frac{(T-D)V}{W} \approx V\left(\frac{T}{W} - \frac{Q C_{D_0}}{W/S} - \frac{W}{S}\frac{K}{Q}\right)$$

Variables

a = lift-curve slope [1/radians]

AR = wing aspect ratio [unitless]

AR_{wet} = wetted aspect ratio [unitless]

b = wingspan [m]

α = angle of attack [radians]

α_{eff} = effective angle of attack [radians]

α_i = induced/downwash angle of attack [radians]

α_{0L} = zero-lift angle of attack [radians]

c = wing chord length [m]

$\bar{c}$ = Mean Aerodynamic Chord [m]

C_D = Coefficient of Drag [unitless]

C_{D_i} = Induced Drag Coefficient [unitless]

$C_{D_{0L}}$ = Zero-Lift Drag Coefficient [unitless]

C_f = Skin Friction Coefficient [unitless]

c_g = Mean Geometric Chord [m]

C_L = Coefficient of Lift [unitless]

C_{L_0} = Zero Angle of Attack Coefficient of Lift [unitless]

C_M = Coefficient of Pitch Moment [unitless]

$C_{M_{ac}}$ = Coefficient of Pitch Moment at Aerodynamic Center [unitless]

c_r = chord of wing root [m]

c_t = chord of wing tip [m]

CG = Center of Gravity

D = drag force [N]

D_i = induced drag force [N]

e = Oswald efficiency factor, must be <1 [unitless]

γ = climb/pitch angle [degrees]

Λ_n = Sweep Angle at chord location "n" [radians]

g = gravitational constant (9.81) [m/s^2]

L = lift force [N]

L' = effective lift force from downwash effects [N]

l = length

l_v = vertical tail moment arm

l_h = horizontal tail moment arm

λ = taper ratio [unitless]

M = pitch moment [N•m]

M_{ae} = pitch moment at Aerodynamic Center [N•m]

M_{cp} = pitch moment at Center of Pressure [N•m]

M = mass [kg]

η_p = propulsive efficiency

μ_∞ = kinematic viscosity of the air [N•s/m^2]

K = Induced Drag Parameter [unitless]

ϕ = turn angle [degrees]

P = power [kg•m^2/s^{-3}]

Q = Dynamic Pressure [kg/m•s^2]

r = radius of turn [m]

Re = Reynold's Number [unitless]

ρ = air density [kg/m^3]

S = wing area [m^2]

S_h = horizontal tail area

S_{wet} = total exposed surface area [m^2]

S_v = vertical tail area

T = thrust force [N]

τ_w = Wall Shear Stress [pa]

V = airspeed/flight velocity [m/s]

V_{stall} = stall speed [m/s]

V_v = vertical tail volume

w = downwash force [N]

W = total aircraft weight [N]

y = distance along wing from leading edge to trailing edge

C Hobby Plane Spreadsheet

INPUTS: DESIRED FLIGHT AND AERODYNAMIC PROPERTIES FOR LEVEL FLIGHT OR STEADY FLIGHT

Flight Properties		
altitude (h)	10	m
velocity (v)	10	m/s
Angle of Climb (gamma)	0	deg
	0	rad

Aircraft Properties		
Weight estimate (W)	13.73	N
root chord (cr)	0.2413	m
tip chord (ct)	0.2413	m
Wingspan (b)	1.555	m
Surface Area (S)	0.3752215	m^2
Aspect Ratio (AR)	6.44426026	
Taper Ratio	1	
Angle of Incidence	0	deg
Elevator Surface Area	0.07	m^2
Rudder Surface Area	0.026	m^2
Total Control Surface Area	0.4712215	m^2

same as MAC and Mean Geometric Chord for a rectangular wing

KEY	
Desired flight parameter	
Measured value	

OUTPUTS: REQUIRED AIRCRAFT PROPERTIES FOR LEVEL FLIGHT OR STEADY CLIMB

Aerodynamic Forces at Steady Flight	
Lift at Level Flight (L)	13.73 N
Lift at Steady Climb (L)	13.73 N
Drag (D)	0.77195 N
Induced Drag (Di)	0.377410227
L/D Ratio	17.78612604
T/W Ratio	0.056223598
Required Thrust (T)	0.77195 N
T *(Alternate Equation)	0.77195 N
Required Thrust at Climb (T)	0.77195 N

Other Properties at Level Flight	
Dynamic Pressure (q)	61.1911837
Reynold's Number	165069.118
Oswald Efficiency Factor	0.85563889
Min. Velocity at Cruise	9.88964536
Induced AoA (alpha-i)	0.0235198 rad
	1.34758533 deg
Effective AoA (alpha-eff)	-0.0235198 rad
	-1.3475853 deg
Rate of Climb (RC)	0 m/s
RC *(Alternate Equation)	0 m/s

Coefficients at Level Flight	
Lift Coeff. at Level (Cl)	0.47616403
Drag Coeff. (Cd)	0.02677165
Induced Drag Param. (K)	0.057728
Induced Drag Coeff. (Cdi)	0.0130888
Zero-Lift Drag Coeff. (Cd0L)	0.01368286

INPUTS: DESIRED FLIGHT AND AERODYNAMIC PROPERTIES FOR LEVEL FLIGHT OR STEADY FLIGHT

Flight Properties		
altitude (h)	10	m
velocity (v)	15	m/s
Angle of Climb (gamma)	10	deg
	0.174532925	rad

Aircraft Properties		
Weight estimate (W)	13.73	N
root chord (cr)	0.2413	m
tip chord (ct)	0.2413	m
Wingspan (b)	1.555	m
Surface Area (S)	0.3752215	m^2
Aspect Ratio (AR)	6.44426026	
Taper Ratio	1	
Angle of Incidence	0	deg
Elevator Surface Area	0.07	m^2
Rudder Surface Area	0.026	m^2
Total Control Surface Area	0.4712215	m^2

same as MAC and Mean Geometric Chord for a rectangular wing

KEY	
Desired flight parameter	
Measured value	

OUTPUTS: REQUIRED AIRCRAFT PROPERTIES FOR LEVEL FLIGHT OR STEADY CLIMB

Aerodynamic Forces at Steady Flight	
Lift at Level Flight (L)	13.73 N
Lift at Steady Climb (L)	13.52141045 N
Drag (D)	1.249855 N
Induced Drag (Di)	0.167737878
L/D Ratio	10.81838329
T/W Ratio	0.092435253
Required Thrust (T)	1.249855 N
T *(Alternate Equation)	1.249855 N
Required Thrust at Climb (T)	3.634044479 N

Other Properties at Level Flight	
Dynamic Pressure (q)	137.680163
Reynold's Number	247603.677
Oswald Efficiency Factor	0.85563889
Min. Velocity at Cruise	9.41196879
Induced AoA (alpha-i)	0.01045324 rad
	0.59892681 deg
Effective AoA (alpha-eff)	0.16407968 rad
	9.40107319 deg
Rate of Climb (RC)	2.60472267 m/s
RC *(Alternate Equation)	2.60472267 m/s

Coefficients at Level Flight	
Lift Coeff. at Level (Cl)	0.21162846
Drag Coeff. (Cd)	0.01926474
Induced Drag Param. (K)	0.057728
Induced Drag Coeff. (Cdi)	0.00258544
Zero-Lift Drag Coeff. (Cd0L)	0.0166793

INPUTS: DESIRED FLIGHT AND AERODYNAMIC PROPERTIES FOR LEVEL FLIGHT OR STEADY FLIGHT

Flight Properties		
altitude (h)	10	m
velocity (v)	20	m/s
Angle of Climb (gamma)	0	deg
	0	rad

Aircraft Properties		
Weight estimate (W)	13.73	N
root chord (cr)	0.2413	m
tip chord (ct)	0.2413	m
Wingspan (b)	1.555	m
Surface Area (S)	0.3752215	m^2
Aspect Ratio (AR)	6.44426026	
Taper Ratio	1	
Angle of Incidence	0	deg
Elevator Surface Area	0.07	m^2
Rudder Surface Area	0.026	m^2
Total Control Surface Area	0.4712215	m^2

Mean Aerodynamic Chord, Mean Geometric Chord

KEY	
Desired flight parameter	
Measured value	

OUTPUTS: REQUIRED AIRCRAFT PROPERTIES FOR LEVEL FLIGHT OR STEADY CLIMB

Aerodynamic Forces at Steady Flight		
Lift at Level Flight (L)	13.73	N
Lift at Steady Climb (L)	13.73	N
Drag (D)	1.78656	N
Induced Drag (Di)	0.094352557	
L/D Ratio	7.685160308	
T/W Ratio	0.130120903	
Required Thrust (T)	1.78656	N
T *(Alternate Equation)	1.78656	N
Required Thrust at Climb (T)	1.78656	N

Other Properties at Level Flight		
Dynamic Pressure (q)	244.764735	
Reynold's Number	330138.237	
Oswald Efficiency Factor	0.85563889	
Min. Velocity at Cruise	9.71862922	
Induced AoA (alpha-i)	0.00587995	rad
	0.33689633	deg
Effective AoA (alpha-eff)	-0.00588	rad
	-0.3368963	deg
Rate of Climb (RC)	0	m/s
RC *(Alternate Equation)	0	m/s

Coefficients at Level Flight	
Lift Coeff. at Level (Cl)	0.11904101
Drag Coeff. (Cd)	0.01548972
Induced Drag Param. (K)	0.057728
Induced Drag Coeff. (Cdi)	0.00081805
Zero-Lift Drag Coeff. (Cd0L)	0.01467167

Atmospheric Conditions and Constants

Standard (Sea Level)		
h		m
T	288.16	K
P	101325	N/m^2
p	1.225	kg/m^3
a	340.2979	m/s
mu_inf	0.00001789	N sec/m^2

Constants		
Gamma	1.4	
R	287	J/kg-K
Cp	1005	J/kg-K
Cv	717.857143	J/kg-K
mw	0.0288	kg/mol
temp grad.	-0.0065	K/m
g	9.81	m/s^2

For Input Altitude		
h	10	m
T	288.095	K
P	101204.8672	N/m^2
p	1.223823675	kg/m^3
a	340.2685528	m/s speed of sound
mu	0.00001789	N sec/m^2 viscosity

D Thrust Calculation MATLAB Script

```matlab
S = 6; %Cell Count
v = S*3.7; %Voltage
V = [.75*v:0.1:v];
K = 412; %KV value of the Motor
R = K*V; %Prop RPM
D = 16; %Prop Diameter in Inches
P = 8; %Prop Pitch in Inches
V0 = 0; %Forward Flight Speed in M/s

F = 0.00000004392399.*R.*((D^3.5)/(sqrt(P))).*((0.000423333).*(R).*(P)-(V0)); %in Newtons
Thrust = F/9.81; %in kilograms

plot(V,F/9.81,'r-','LineWidth',2.0);
xlabel_str = ['Voltage'];
xlabel(xlabel_str);
ylabel_str = ['Thrust in Kg'];
ylabel(ylabel_str);
title_str = ['16x8 Max Thrust in Kg vs V_b_a_t_t'];
title(title_str);
hold on;

D = 18;
P = 8;
F = 0.00000004392399.*R.*((D^3.5)/(sqrt(P))).*((0.000423333).*(R).*(P)-(V0)); %in Newtons

plot(V,F/9.81,'b-','LineWidth',2.0);
xlabel_str = ['Voltage'];
xlabel(xlabel_str);
ylabel_str = ['Thrust in Kg'];
ylabel(ylabel_str);
title_str2 = ['18x8 Max Thrust in Kg vs V_b_a_t_t'];
title(title_str);
```

E List of Stability and Controls Equations and Variables

Geometric Calculations:

Taper Ratio:

$$\lambda = c_{\text{tip}}/c_{\text{root}}$$

Surface Area:

$$S = \tfrac{1}{2}bc_{\text{root}}(1 + \lambda)$$

Aspect ratio:

$$AR = b^2/S.$$

Mean chord:

$$\bar{c} = \frac{2}{3}c_{\text{root}}\frac{1 + \lambda + \lambda^2}{1 + \lambda}$$

Sweep angle:

$$\Lambda = \tan^{-1}\left(\tan\Lambda_{\text{LE}} - \frac{1 - \lambda}{AR(1 + \lambda)}\right)$$

Lift curve slope:

$$a_{wb} = \frac{2\pi(AR)}{2 + \sqrt{\frac{(AR)^2(1 - Mach^2)}{k^2}\left(1 + \frac{\tan^2\Lambda}{(1 - Mach^2)}\right) + 4}},$$

$$\text{where } k := \begin{cases} 1 + (AR)(1.87 - 2.33 \times 10^{-4}\Lambda)/100, & \text{for } (AR) < 4, \\ 1 + (8.2 - 2.3\Lambda - (AR)(0.22 - 0.153\Lambda)/)100, & \text{for } (AR) \geqslant 4. \end{cases}$$

Neutral point:

$$h_n := h_{n_{wb}} + \frac{a_t}{\bar{a}}\bar{V}_H\left(1 - \frac{\partial\varepsilon}{\partial\alpha}\right)$$

Lift stability derivative with respect to angle of attack:

$$\bar{a} := a_{wb}\left[1 + \frac{a_t}{a_{wb}}\frac{S_t}{S}\left(1 - \frac{\partial\varepsilon}{\partial\alpha}\right)\right]$$

Horizontal tail volume coefficient:

$$\bar{V}_H := \frac{\bar{\ell}_t S_t}{\bar{c}S}$$

Downwash derivative:

$$\frac{\partial\varepsilon}{\partial\alpha} := 4.44\sqrt{1 - Mach^2}\left(\left(\frac{1}{(AR)} - \frac{1}{1+(AR)^{1.7}}\right)\left(\frac{10-3\lambda}{7}\right)\left(\frac{1-(\bar{\ell}_{tv}/b)}{(2\bar{\ell}_t/b)^{0.33}}\right)\sqrt{\cos\Lambda}\right)^{1.19}$$

Variables:

b = wing span

$\bar{c}$ = mean aerodynamic chord of the wing

$H_{n,wb}$ = wing-body aerodynamic center

a_{wb} = wing-body lift curve slope

a_t = horizontal tail lift curve slope

AR = wing Aspect Ratio

S = wing surface area

S_t = horizontal tail surface area

$\frac{\partial\varepsilon}{\partial\alpha}$ = downwash derivative

$\bar{V}_H$ = horizontal tail volume coefficient

$\bar{a}$ = wing-tail effective lift curve slope

$\bar{l}_t$ = horizontal distance between the wing and the tail aerodynamic center

l_t = horizontal distance between center of mass and tail aerodynamic center

$\bar{l}_{tv}$ = vertical distance between the wing and the tail aerodynamic center

λ = taper ratio

Λ = sweep angle

F   Static Stability MATLAB Script

```matlab
%% Inputs
b_w       = 3.5;    %wingspan in m
w_rc      = 0.751;  %wing chord at root in m
w_tc      = 0.3755; %wing chord at tip in m
cbar_w    = 0.6795; %MAC of wing in m
b_f       = 0.225;  %Fuselage horizontal length in m
    %(what span of the wing is on the fuselage)
b_HT      = 1.60;   %Horizontal tail span in m
HT_rc     = 0.50;   %HT chord at root in m
HT_tc     = 0.25;   %HT chord at tip in m
l_LE_HT   = 2.6;
    %distance from wing LE to horizontal tail LE in m (moment arm)
lbar_HTv = 0.05;    %vertical distance between wing and horizontal tail
velocity = 10;      %trim airspeed in m/s^2
SM_opt   = 7;       %desired static margin around 15 percent
CG       = 0.63;    %dimesnional CG from wing LE in m
Vbar_V   = 0.1;     %Vertical tail volume coefficient

%#ok<*NOPRT>
%#ok<*NASGU>
%% Geometry calculations
%{
%when wing and HT have straight taper from LE, then:
%leading edge sweep angle of wing and HT in radians are:
Lambda_LEw    = atan(b_w/(c_rw-c_tw));
    %leading edge sweep angle of wing in radians
Lambda_LEt    = atan(b_t/(c_rt-c_tt));
    %leading edge sweep angle of HT in radians
%}
%%{
%with wing starting taper at halfway
%HT having straight taper from LE
Lambda_LEw    = atan((b_w/2)/(w_rc-w_tc));
    %leading edge sweep angle of wing in radians
Lambda_LEHT   = atan(b_HT/(HT_rc-HT_tc));
    %leading edge sweep angle of HT in radians
%%}
lambda_w      = w_tc / w_rc;
    %taper ratio of the wing
lambda_HT     = HT_tc / HT_rc;
    %taper ratio of the HT
%S_w           = 0.5 * b_w * c_rw * (1 + lambda_w);
    %wing surface area
S_w           = (w_rc*b_w/2) + (0.5 * (b_w/2) * w_rc * (1 + lambda_w));
    %surface area of the half tapered wing
S_HT          = 0.5 * b_HT * HT_rc * (1 + lambda_HT);
    %HT surface area
AR_w          = b_w^2 / S_w;
    %wing aspect ratio
AR_t          = b_HT^2 / S_HT;
    %HT aspect ratio
%{
%wing with a taper at halfspan
cbar_w_tp     = (2/3) * w_rc * ((1+lambda_w+lambda_w^2)/(1+lambda_w));
    %wing mean chord (tapered part)
cbar_w_sp     = w_rc;
    %wing mean chord of the straight part
cbar_w        = (cbar_w_tp+cbar_w_sp)/2
    %wing mean chord
```

```matlab
%}
cbar_HT         = (2/3) * HT_rc * ((1+lambda_HT+lambda_HT^2)/(1+lambda_HT));
    %HT mean chord
ac_w            = cbar_w/4;
    %wing aerodynamic center for low speed and thin airfoils
ac_t            = cbar_HT/4;
    %HT aerodynamic center (distance from HT LE)
lbar_HT         = l_LE_HT - ac_w + ac_t;
    %horizontal distance between wing ac and HT ac (ac to ac moment arm)
LambdaAngle_w  = ...
    atan(tan(Lambda_LEw)-((1 - lambda_w)/(AR_w*(1+lambda_w))));
    %sweep angle from wing ac
LambdaAngle_t  = ...
    atan(tan(Lambda_LEHT)-((1 - lambda_HT)/(AR_t*(1+lambda_HT))));
    %sweep angle from HT ac

%% Speed
soundspeed      = 340.29;
    %speed of sound at sea level (close estimation for our case)
mach            = velocity/soundspeed;

%% lift curve slopes and Downwash
if(AR_w>=4)
    %find k of wing
    kw          = ...
        1+(8.2-(2.3*LambdaAngle_w) ...
        -((AR_w)*(0.22-0.153*LambdaAngle_w)))/100;
else
    kw          =(1+(AR_w*(1.87-(2.33e-4)*LambdaAngle_w)));
end

if(AR_t>=4)
    %find k of HT
    kt          = ...
        1+(8.2-(2.3* LambdaAngle_t) ...
        -((AR_t)*(0.22-0.153* LambdaAngle_t)))/100;
else
    kt          = ...
        (1+(AR_t*(1.87-(2.33e-4)* LambdaAngle_t)));
end
a_wb            = ...
    ((2*(pi)*AR_w)/(2+sqrt(((AR_w^2)*(1-(mach^2))/kw^2)) ...
    *(1+(tan(LambdaAngle_w))^2/(1-mach^2)))+4);
    %lift curve slope for the wing-body
a_t             = ...
    ((2*(pi)*AR_t)/(2+sqrt(((AR_t^2)*(1-(mach^2))/kt^2)) ...
    *(1+(tan(LambdaAngle_t))^2/(1-mach^2)))+4);
    %lift curve slope for the HT
downwash_deriv = ...
    4.44*sqrt(1-(mach^2))*(((1/AR_w)-(1/(1+AR_w^1.7))) ...
    *((10-3*LambdaAngle_w)/7)*((1-lbar_HTv/b_w) ...
    /((2*lbar_HT/b_w)^0.33))*cos(LambdaAngle_w))^1.19;
    %downwash derivative
%% Neutral Point
a_bar           = a_wb*(1+(a_t/a_wb)*(S_HT/S_w)*(1-downwash_deriv));
    %wing-HT effective lift curve slope
Vbar_H          = (lbar_HT*S_HT)/(cbar_w*S_w)
    %HT volume ratio
Hnwb            = 0.25;
```

```matlab
                %assumed to be 0.25 (standard assumption)
Hn              = Hnwb+(a_t/a_bar)*(Vbar_H)*(1-downwash_deriv);
    %Calcuate non-dimensional neutral point
NP              = Hn*cbar_w + (w_rc-cbar_w);
    %dimensional Neutral Point from wing LE
%% Longitudinal Static Stabiltiy
NP_percentage   = Hn * 100
    %neutral point percentage of mean chord
CG              = cbar_w - (w_rc - CG);
    %actual CG from the  leading edge of the MAC
CG_percentage   = (CG/cbar_w)*100
    %actual CG percentage of mean chord
SM_percentage   = NP_percentage - CG_percentage
    %if we have the actual CG we can calculate the actual static margin
CG_opt_prctg    = NP_percentage - SM_opt;
    %CG percentage of mean chord
CG_optimal      = (CG_opt_prctg/100)*cbar_w  + (w_rc-cbar_w)
    %dimensional location of desired CG with desired SM from wing LE
opt_Stability   = [NP_percentage, CG_opt_prctg, SM_opt]
    %Optimal stability with given SM
act_Stability   = [NP_percentage, CG_percentage, SM_percentage]
    %Actual stabiltiy with given CG
%% Vertical Tail sizing with given volume coefficient
VT_rc           = 1.25*HT_rc;
    %conventional config. typical root chord size for transport design
x               = 0.75*(VT_rc -HT_rc);
    %distance between ac_HT and ac_VT
lbar_VT         = lbar_HT - x;
    %VT moment arm as trailing edges of the tails align to reduce wake
l_VT            = lbar_HT - (VT_rc - HT_rc);
    %VT moment arm from LE to LE
S_VT            = Vbar_V*S_w*b_w/lbar_VT;
    %VT surface area
VT_tc           = 0.75*HT_rc;
    %typical conventional config. tip chord for transport
lambda_VT       = VT_tc / VT_rc;
    %taper ratio of the VT
b_VT            = S_VT/(VT_rc*(1+lambda_VT));
    %VT span
VT_size         = [b_VT, VT_rc, VT_tc];
    %VT size in order is span, root chord, and tip chord
%% Elavators Size
S_El            = 0.40*S_HT;
    %Typical area of the elevators
b_El            = b_HT;
    %Elvators span to be the same length as the HT span
El_c            = S_El/b_El;
    %non-tapered chord lenght of the elvators
El_size_both    = [b_El, El_c];
%% Rudder Size
S_Rd            = 0.35*S_VT;
    %Typical area of the Rudder
b_Rd            = b_VT;
    %Rudder to span across all of the VT
Rd_c            = S_Rd/b_Rd;
    %non_tapered rudder chord lenght
Rd_size         = [b_Rd, Rd_c];
%% Ailerons Size
b_hw_f          = (b_w/2)-(b_f/2);
```

```matlab
    %The span of halfwing from fuselage
b_Al            = 0.40*b_hw_f;
    %Typical span of an aileron
Al_c            = 0.25*cbar_w;
    %Typical chord lenght of the ailerons
S_Al            = 2*Al_c*b_Al;
    %Area of both Ailerons
S_Al_percent    = S_Al/S_w;
    %Ailerons area percentage of the wing area
Al_size_each    = [b_Al, Al_c];
%% Flaps size
b_Fl            = 0.55*b_hw_f;
    %Typical span of a flap
Fl_c            = 0.25*cbar_w;
    %Typical chord length of the flaps
S_Fl            = 2*Fl_c*b_Fl;
    %area of the flaps
S_Fl_percent    = S_Fl/S_w;
    %Flaps area percentage of the wing area
Fl_size_each    = [b_Fl, Fl_c];
%{
%wingspan remaining for the fuselage after implementing Flaps and Ailerons
b_w_rem         = 2*(b_Al+b_Fl);
    %remaining of the wingspan for the fuselage
b_w_rem_ratio   = b_w_rem/b_w;
    %Span remaining ratio
%}
```

G   List of Propulsion eCalc Simulator Equations

Thrust Calculations in eCalc By McCormick Methods

Equations

Power-Thrust Calculations

Setup

$W = 48\ [lb_f]$	All-up weight of Aircraft
$N_{motor} = 1$	Number of motors
$n = 0.85$	Average motor efficiency
$RPM = 8000$	Estimated max RPM

Battery

$V = 50$	Selected motor voltage in volts
$N_{Batt} = 2$	Number of batteries in parallel
$C = 6600\ [mAh]$	Battery capacity

Propeller

$D = 22\ [in]$	Propeller Diameter
$Pitch = 12\ [in]$	Propeller Pitch
$A = 0.25 \cdot \pi \cdot D^2$	Propeller sweep area in square inches
$A_{ft} = A \cdot \left|0.0069444444 \frac{ft^2}{in^2}\right|$	Propeller sweep area in square feet

Full Throttle

$PL = \frac{P_{in} \cdot n}{A_{ft}}$	Power loading equation
$TL = 8.6859 \cdot PL^{-.3107} \cdot [lbf/hp]$	Thrust loading equation
$Thrust = TL \cdot (P_{in} \cdot n)$	Thrust per motor
$P_{in\ Watt} = P_{in} \cdot \left|745.7 \cdot \frac{W}{hp}\right|$	Power input to motor in watts
$I_{tot} = I_{motor} \cdot N_{motor}$	Current of motor

Endurance

$t_{flight} = \frac{60 \cdot (C/1000) \cdot N_{Batt}}{I_{tot}}$	Total flight time

H List of Structural Equations and Variables

Cantilever Beam Deflection for Wingtip Estimation:

$$\delta = \frac{Pl^3}{EI}$$

Wingtip Deflection:

$$\delta = \left(\frac{PW_{fuse}}{EI_0}\right)\left(\frac{b^3}{96}\right)\left(\frac{1+2\lambda}{1+\lambda}\right)$$

Landing Gear Loading Factor:

$$\eta_{LG} = \frac{\frac{1}{2}\frac{V_s^2}{g} - \frac{\eta_t K_t X_t^2}{2W} + (1 - \frac{L}{W})(X_t + X_s)}{\eta_s X_s}$$

Angle of Twist:

$$\theta = \frac{G_c J}{TL}$$

Maximum Torque:

$$\tau_{max-twist}(x) = \frac{M_p(x)}{G_c J}$$

Factor of Safety:

$$FoS = \frac{yield\ stress}{working\ stress}$$

Variables:

δ = deflection [m]

P = applied load [N]

l = length [m]

E = Elastic Modulus [Pa]

I = Moment of Inertia [kg • m^2]

I Takeoff Distance MATLAB Script

```matlab
clear variables; clc;

%%%%%%%%%%%%%%%%%%%%%%%%%%%%%%%%%%%%%%%%%%%%%%%%%%%%%%%%%%%%%%%%%%%%%%%%

%%%Derived from Aircraft Performance and Design
%%%%by John D. Anderson, Jr. (1998)

%%%%%%%%%%%%%%%%%%%%%%%%%%%%%%%%%%%%%%%%%%%%%%%%%%%%%%%%%%%%%%%%%%%%%%%%

%% Plane Parameters

%The Plane
W = 45 * 4.44822;          %Weight: Convert lbs to N
ptc_deg = 0;               %Wing angle of incidence in degrees
ptc = ptc_deg * (pi/180);  %Wing incidence in radians
m = W / 9.81;              %mass of the plane in kg
fuselage_width = 0.2;      %meters
%T = 41.1 - 0.131 * V - 0.0468 * V^2;        %%Exponential Thrust Curve
%in the form k1 - k2 * V + k3 * V^2
k1 = 41.1;
k2 = 0.131;
k3 = -0.0468;


%The Wing
S = 2.3;                   %Wing area in m^2
b = 3.6;                   %Wingspan in m
CL_max = 1.9;              %Max. Lift Coefficient from XFLR5
CD_0 = 0.1;                %0-Lift Drag Coefficient from XFLR5
wing_height = 0.39;        %m off ground (for ground effect)
lift_slope_deg = 0.084;    %from XFLR5, in 1/deg
CL_0 = 0.631;              %0-angle Lift Coefficient from XFLR5
CL = lift_slope_deg * ptc_deg + CL_0;   %Calculate CL based on AoA
AR = b^2 / S;              %Wing Aspect Ratio
WS = W / S;                %Wing Loading, N/m^2
K = 0.0697;                %Drag value from XFLR5

%%Flap Deflection Constant: Estimates from textbook
K_uc = 5.81 * 10^(-5);     %No flap deflection
%K_uc = 4.5 * 10^(-5);     %Some flap deflection
%K_uc = 3.16 * 10^(-5);    %Maximum flap deflection

%The Environment
rho = 1.225;               %Air density in kg/m^3
mu_r = 0.04;               %Friction coeff. of runway
G = (16 * (wing_height / b))^2 / (1 + (16 * (wing_height / b))^2);
       %%%ground effect factor
g = 9.81;                  %gravitational constant


%%%%%%%%%%%%%%%%%%%%%%%%%%%%%%%%%%%%%%%%%%%%%%%%%%%%%%%%%%%%%%%%%%%%%%%%
%% Find Velocity Conditions

V_stall = sqrt( (2*W) / (rho*S*CL_max) );     %Stall velocity in m/s
V_TO = 1.1 * V_stall;                         %Takeoff velocity in m/s

%Evaluated at 0.7 V_inf
V_inf = 0.7 * V_TO;                           %m/s (avg. speed)
T_approx = k1 - k2 * V_inf + k3 * V_inf^2;    %N (avg. Thrust)
```

```matlab
%% Flap Deflection

delta_CD_0 = (W/S) * K_uc * m^(-0.215);          %%No flap deflection


%% Find K_A and K_T

K_T = (T_approx/W - mu_r);

k_3 = 3*K/4
k_1 = (1/3) * k_3;

K_A = -(rho/(2*WS)) * (CD_0 + delta_CD_0 + (k_1 + G * k_3) * CL^2 - mu_r * CL);

%%%%%%%%%%%%%%%%%%%%%%%%%%%%%%%%%%%%%%%%%%%%%%%%%%%%%%%%%%%%%%%%%%%%%%%%%%%
%% Solve for Takeoff Distance S_G

N = 1; %Constant For small aircraft

S_G = (1/(2*g*K_A)) * log(1 + (K_A/K_T) * V_TO^2) + N * V_TO; %%m distance
S_G_feet = S_G * 3.28084;


fprintf("Wing Area:        " + S +          "        m^2 \n")
fprintf("Wing Incidence:    " + ptc_deg +  "          deg \n")
fprintf("Takeoff Distance:  " + S_G_feet + " ft \n")
```

J Longitudinal Dynamic Stability MATLAB Script

```matlab
function long_dynamical_stability(u0, theta0, m, CG, I_y, b_w, b_t, c_tw, c_rw, c_tt, c_rt,↵
Lambda_LEw, Lambda_LEt, l_LE, lbar_tv)
%Inputs in order are: trim airspeed, trim pitchangle, mass, CG point behind
%wing LE, moment of inertia about y-axis with origin at CG
%The static stability inputs in order are defined as: wingspan, tailspan,
%chord lengths at tip and root, leading edge sweep angle of wing and tail,
%distance from wing LE to horizontal tail LE,
%and vertical distance between wing and tail.
%All in SI units

%constants,geometry calculations, and values from static stability code
rho          = 1.225;  %density at sea level
soundspeed = 340.29; %speed of sound at sea level
g            = 9.81;

lambda_w      = c_tw / c_rw;                                                %taper ratio of the↵
wing
lambda_t      = c_tt / c_rt;                                                %taper ratio of the↵
tail
S_w           = 0.5 * b_w * c_rw * (1 + lambda_w);                          %wing surface area
S_t           = 0.5 * b_t * c_rt * (1 + lambda_t);                          %tail surface area
AR_w          = b_w^2 / S_w;                                                %wing aspect ratio
AR_t          = b_t^2 / S_t;                                                %tail aspect ratio
c_barw        = (2/3) * c_rw * ((1+lambda_w+lambda_w^2)/(1+lambda_w));      %wing mean chord
c_bart        = (2/3) * c_rt * ((1+lambda_t+lambda_t^2)/(1+lambda_t));      %tail mean chord
ac_w          = c_barw/4;                                                   %wing aerodynamic↵
center for low speed and thin airfoils
ac_t          = c_bart/4;                                                   %tail aerodynamic↵
center (distance from tail LE)
LambdaAngle_w = atan(tan(Lambda_LEw)-((1 - lambda_w)/(AR_w*(1+lambda_w)))); %sweep angle from↵
wing ac
LambdaAngle_t = atan(tan(Lambda_LEt)-((1 - lambda_t)/(AR_t*(1+lambda_t)))); %sweep angle from↵
tail ac

%distances
lbar_t        = l_LE - ac_w + ac_t;    %horizontal distance between wing ac and tail ac

soundspeed    = 340.29;                %speed of sound at sea level
mach          = u0/soundspeed;

if(AR_w>=4)                                                                 %find k of wing
    kw = 1+(8.2-(2.3*LambdaAngle_w)-((AR_w)*(0.22-0.153*LambdaAngle_w)))/100;
else
    kw =(1+(AR_w*(1.87-(2.33e-4)*LambdaAngle_w)));
end

if(AR_t>=4)                                                                 %find k of tail
    kt = 1+(8.2-(2.3* LambdaAngle_t)-((AR_t)*(0.22-0.153* LambdaAngle_t)))/100;
else
    kt =(1+(AR_t*(1.87-(2.33e-4)* LambdaAngle_t)));
end
a_wb = ((2*(pi)*AR_w)/(2+sqrt(((AR_w^2)*(1-(mach^2)))/kw^2))*(1+(tan(LambdaAngle_w))^2/(1-↵
mach^2)))+4); %lift curve slope for the wing-body
a_t  = ((2*(pi)*AR_t)/(2+sqrt(((AR_t^2)*(1-(mach^2)))/kt^2))*(1+(tan(LambdaAngle_t))^2/(1-↵
mach^2)))+4); %lift curve slope for the tail

downwash_deriv = 4.44*sqrt(1-(mach^2))*(((1/AR_w)-(1/(1+AR_w^1.7)))*((10-3*LambdaAngle_w)/7)*↵
((1-lbar_tv/b_w)/((2*lbar_t/b_w)^0.33))*cos(LambdaAngle_w))^1.19;
a_bar         = a_wb*(1+(a_t/a_wb)*(S_t/S_w)*(1-downwash_deriv));           %wing-tail↵
```

```
effective lift curve slope
Vbar_H         = (lbar_t*S_t)/(c_barw*S_w);                    %Horizontal tail↵
volume ratio
Hnwb           = 0.25;                                         %assumed to be 0.25↵
(standard assumption)
Hn             = Hnwb+(a_t/a_bar)*(Vbar_H)*(1-downwash_deriv); %Calcuate neutral↵
point ratio

e        = 0.8 ; %oswald efficiency factor, around 0.7 to 0.9 for our numbers of AR and CD0
Cw0      = (m*g)/(0.5*rho*(u0^2)*S_w);
CL_0     = Cw0; %trim lift coefficient
CD0      = ; %zero lift drag coefficient, maybe needs to be an input
CD_0     = CD0 + ((CL_0^2)/(pi*AR_w*e)); %trim drag coefficient

l_t  = l_LE - CG + ac_t; %horizontal distance between CG and tail ac

%nondimensional stability derivatives (retrieve from chapter 5 of dynamcis
%of fligth stabiltiy and control by Etkin and Reid OR Prof. Cowlagi's
%notes

Cx_u         = ;
Cx_alpha     = ;
Cx_alphadot  = ;
Cx_q         = ;

Cz_u         = ;
Cz_alpha     = ;
Cz_alphadot  = ;
Cz_q         = ;

Cm_u         = ;
Cm_alpha     = ;
Cm_alphadot  = ;
Cm_q         = ;

%Longitudinal dimensional stability derivatives

X_u    = ;
X_w    = ;
X_q    = ;
X_wdot = ;

Z_u    = ;
Z_w    = ;
Z_q    = ;
Z_wdot = ;

M_u    = ;
M_w    = ;
M_q    = ;
M_wdot = ;

%eigenvalue calculation

A_long = ; %state vector of [delta V, delta alpha, q, delta theta]

lambda = eig(A_long) %eigenmatrix

%with lambda = n +- omega i
```

```
%t = 0.0105;
%T = t*2*pi/omega %period
%t_half = -t*0.69315/n %half life
%N_half = t_half /T %cycles

end
```

K Longitudinal Trim Control MATLAB Script

```matlab
%% Inputs
W         = 45*(1/2.2);  %Weight in kg
b_w       = 3.5;         %wingspan in m
w_rc      = 0.751;       %wing chord at root in m
w_tc      = 0.3755;      %wing chord at tip in m
cbar_w    = 0.6795;      %MAC of wing in m
b_HT      = 1.6;         %Horizontal tail span in m
HT_rc     = 0.50;        %HT chord at root in m
HT_tc     = 0.25;        %HT chord at tip in m
l_LE_HT   = 2.6;
    %distance from wing LE to horizontal tail LE in m (moment arm)
lbar_HTv = 0.05;         %vertical distance between wing and horizontal tail
velocity = 8.5;          %trim airspeed in m/s^2
CG        = 0.63;        %dimesnional CG from wing LE
CG_ratio = (CG/cbar_w);  %non-dimensional CG ratio of MAC
Cm_0      = -0.55;       %non-dimensional moment at zero lift
CL_0      = 0.80;        %non-dimensional lift at zero alpha
i_HT      = -3;          %Horizontal tail incidence angle in degrees
a_e       = 2.72;        %elevator lift effectiveness
%#ok<*NOPRT>
%#ok<*NASGU>
%% Geometry Calculations
%Wing starting taper at halfway
Lambda_LEw     = atan((b_w/2)/(w_rc-w_tc));
    %leading edge sweep angle of wing in radians
%HT having straight taper from LE
Lambda_LEHT    = atan(b_HT/(HT_rc-HT_tc));
    %leading edge sweep angle of HT in radians
lambda_w        = w_tc / w_rc;
    %taper ratio of the wing
lambda_HT       = HT_tc / HT_rc;
    %taper ratio of the HT
%S_w            = 0.5 * b_w * w_rc * (1 + lambda_w);
    %wing surface area with straight LE taper and straight TE
S_w            = (w_rc*b_w/2) + (0.5 * (b_w/2) * w_rc * (1 + lambda_w));
    %surface area of the half tapered wing
S_HT           = 0.5 * b_HT * HT_rc * (1 + lambda_HT);
    %HT surface area
AR_w           = b_w^2 / S_w;
    %wing aspect ratio
AR_t           = b_HT^2 / S_HT;
    %HT aspect ratio
%{
%wing with a taper at halfspan
cbar_w_tp      = (2/3) * w_rc * ((1+lambda_w+lambda_w^2)/(1+lambda_w));
    %wing mean chord (tapered part)
cbar_w_sp      = w_rc;
    %wing mean chord of the straight part
cbar_w         = (cbar_w_tp+cbar_w_sp)/2
    %wing mean chord
%}
cbar_HT        = (2/3) * HT_rc * ((1+lambda_HT+lambda_HT^2)/(1+lambda_HT));
    %HT mean chord
ac_w           = cbar_w/4;
    %wing aerodynamic center for low speed and thin airfoils
ac_t           = cbar_HT/4;
    %HT aerodynamic center (distance from HT LE)
lbar_HT        = l_LE_HT - ac_w + ac_t;
    %horizontal distance between wing ac and HT ac (ac to ac moment arm)
```

```matlab
LambdaAngle_w  = ...
    atan(tan(Lambda_LEw)-((1 - lambda_w)/(AR_w*(1+lambda_w))));
    %sweep angle from wing ac
LambdaAngle_t  = ...
    atan(tan(Lambda_LEHT)-((1 - lambda_HT)/(AR_t*(1+lambda_HT))));
    %sweep angle from HT ac
%% Mach and Density
rho         = 1.225; %density at sea level in kg/m^3
%{
%ENGLISH ENGINEERING UNIT OUTPUT
%{
a       = (-6.5e-3)*(9/5)*(0.3048/1); %temp. gradiet in R/ft
temp_sl = 518.69;                     %sea level temp. in R
R       = 53.3533;                    %specific gas const. in lbf*ft/(lb*R)
g       = 32.174;                     %gravity accel. in ft/s^2
rho_sl  = 1.225*0.062428;             %sea level density in lb/ft^3
h_lim   = 11000*(1/0.3048);           %trophosphere ceiling limit in ft
%}

%INTERNATIONAL SYSTEM UNITS OUTPUT
%%{
a            = -6.5e-3;
    %temp. gradiet in K/m
temp_sl      = 288.16;
    %sea level temp. in K
R            = 287;
    %specific gas constant in J/(kg*K)
g            = 9.81;
    %gravity accel. in m/s^2
rho_sl       = 1.225;
    %sea level density in kg/m^3
h_lim        = 11000;
    %trophosphere ceiling limit in m
%%}

%standard atmosphere in Troposphere and Tropopause
if (h>=h_lim)
    %Tropopause temp. and density
    temp       = temp_sl+ a*h_lim;
    %temp. wrt height
    const      = g/(R*temp);
    rho        = rho_sl*((temp_sl+ a*h_lim)/temp_sl)^(-1-g/(a*R))* ...
        exp(const*h_lim-const*h);
    %density wrt height
else
    %Troposphere temp. and density
    temp       = temp_sl+ a*h;
    %temp. wrt height
    temp_r     = temp/temp_sl;
    %temp. ratio
    rho        = rho_sl*temp_r^(-1-g/(a*R));
    %density wrt height
end
%}
soundspeed = 340.29;
    %speed of sound at sea level (close estimation for our case)
mach       = velocity/soundspeed;
%% Lift Curve Slopes and Downwash
if(AR_w>=4)
```

```matlab
    %find k of wing
    kw          = ...
        1+(8.2-(2.3*LambdaAngle_w) ...
        -((AR_w)*(0.22-0.153*LambdaAngle_w)))/100;
else
    kw          =(1+(AR_w*(1.87-(2.33e-4)*LambdaAngle_w)));
end
if(AR_t>=4)
    %find k of HT
    kt          = ...
        1+(8.2-(2.3* LambdaAngle_t) ...
        -((AR_t)*(0.22-0.153* LambdaAngle_t)))/100;
else
    kt          = ...
        (1+(AR_t*(1.87-(2.33e-4)* LambdaAngle_t)));
end
a_wb            = ...
    ((2*(pi)*AR_w)/(2+sqrt(((AR_w^2)*(1-(mach^2)))/kw^2)) ...
    *(1+(tan(LambdaAngle_w))^2/(1-mach^2)))+4);
    %lift curve slope for the wing-body
a_HT            = ...
    ((2*(pi)*AR_t)/(2+sqrt(((AR_t^2)*(1-(mach^2)))/kt^2)) ...
    *(1+(tan(LambdaAngle_t))^2/(1-mach^2)))+4);
    %lift curve slope for the HT
downwash_deriv = ...
    4.44*sqrt(1-(mach^2))*(((1/AR_w)-(1/(1+AR_w^1.7))) ...
    *((10-3*LambdaAngle_w)/7)*((1-lbar_HTv/b_w) ...
    /((2*lbar_HT/b_w)^0.33))*cos(LambdaAngle_w))^1.19;
    %downwash derivative
abar            = a_wb*(1+(a_HT/a_wb)*(S_HT/S_w)*(1-downwash_deriv));
    %wing-HT effective lift curve slope
%% non-Dimensional Lift
downwash_0      = 0;
i_HT_rad        = i_HT*pi/180;
CL_alpha        = abar;
CL_delta_e      = (S_HT/S_w)*a_e;
%CL_0            = CL_0_w + a_HT*(S_HT/S_w)*(i_HT_rad-downwash_0);
%CL             = CL_0 + CL_alpha * alpha_w + CL_delta_e * delta_e;
%% non-Dimensional Moment
Vbar_HT         = (lbar_HT*S_HT)/(cbar_w*S_w); %HT volume ratio
ac_w_ratio      = ac_w/cbar_w; %aerodynamic center ratio of MAC (0.25)
%Cm_0            = Cm_ac_w + CL_0*(CG - ac_w);
Cm_alpha        = CL_alpha*(CG_ratio - ac_w_ratio) ...
    - Vbar_HT*a_HT*(1-downwash_0);
Cm_delta_e      = CL_delta_e*(CG_ratio - ac_w_ratio) - Vbar_HT*a_e;
%Cm             = Cm_0 + Cm_alpha * alpha_w + Cm_delta_e * delta_e;
%% Trim Angles
L               = W;
Q               = 0.5*rho*velocity^2;
CL_trim         = L/(Q*S_w);
Cm_trim         = 0;

A               = [Cm_alpha, Cm_delta_e; CL_alpha, CL_delta_e];
B               = [Cm_trim - Cm_0; CL_trim - CL_0];
%A              = [CL_alpha, CL_delta_e; Cm_alpha, Cm_delta_e];
%B              = [CL_trim - CL_0; Cm_trim - Cm_0];
trim_angles     = A\B *(180/pi);
    %Angle of attack and Elevator angle at trim
%% Cm vs alpha plot
```

```matlab
%plot with delta_e = 0 and delta_e_trim

delta_e0     = 0;
delta_e5     = 5 * (pi/180);
delta_e10    = 10 * (pi/180);
delta_en5    = -5 * (pi/180);
delta_en10   = -10 * (pi/180);
delta_e_trim = trim_angles(2,1) * (pi/180);

alpha_w_rec  = [];
Cm_trim_rec  = [];
Cm_de0_rec   = [];
Cm_de5_rec   = [];
Cm_de10_rec  = [];
Cm_den5_rec  = [];
for alpha_w  = -10:0.1:15
alpha_w_rad  = alpha_w * pi/180;
Cm_trim      = Cm_0 + Cm_alpha * alpha_w_rad + Cm_delta_e * delta_e_trim;
Cm_de0       = Cm_0 + Cm_alpha * alpha_w_rad + Cm_delta_e * delta_e0;
Cm_de5       = Cm_0 + Cm_alpha * alpha_w_rad + Cm_delta_e * delta_e5;
Cm_de10      = Cm_0 + Cm_alpha * alpha_w_rad + Cm_delta_e * delta_e10;
Cm_den5      = Cm_0 + Cm_alpha * alpha_w_rad + Cm_delta_e * delta_en5;
alpha_w_rec  = cat(1, alpha_w_rec,alpha_w);
Cm_trim_rec  = cat(1, Cm_trim_rec,Cm_trim);
Cm_de0_rec   = cat(1, Cm_de0_rec,Cm_de0);
Cm_de5_rec   = cat(1, Cm_de5_rec,Cm_de5);
Cm_de10_rec  = cat(1, Cm_de10_rec,Cm_de10);
Cm_den5_rec  = cat(1, Cm_den5_rec,Cm_den5);
end
plot(alpha_w_rec, Cm_trim_rec, alpha_w_rec, Cm_de0_rec, ...
     alpha_w_rec, Cm_de5_rec, alpha_w_rec, Cm_de10_rec, ...
     alpha_w_rec, Cm_den5_rec, 'LineWidth', 2); grid on; hold on;
xlabel('\alpha (degree)'); ylabel ('C_m')
title('non-dimensional moment vs Angle of Attack')
plot([trim_angles(1,1)], [0], '.', 'MarkerSize', 30);
xL = xlim;
yL = ylim;
line([0 0], yL);  %x-axis
line(xL, [0 0]);  %y-axis
legend('Trim \delta_e' , '\delta_e = 0' , '\delta_e = 5' ,...
     '\delta_e = 10' , '\delta_e = -5', 'Trim \alpha')
```

L   Propulsion Pre-Testing Checklists

Pre-Test Checklist			V=(22/25)*F	F=(25/22)*V
			Airspeed?	Freq. Set
Motor................. ....Secure			5 m/s	5.68 Hz
Prop...................... ....Secure			6 m/s	6.82 Hz
Ports.................... ....Closed/Secure			7 m/s	7.95 Hz
Water................... ....Open			8 m/s	9.09 Hz
Air........................ ....Open			9 m/s	10.23 Hz
Power.................. ....On			10 m/s	11.36 Hz
Temp. Set............ ....On			11 m/s	12.50 Hz
			12 m/s	13.64 Hz
Test Run Up			13 m/s	14.77 Hz
Pre-Test List......... ....Complete			14 m/s	15.91 Hz
Motor.................... ....Wired			15 m/s	17.05 Hz
Reciever............... ....Powered			16 m/s	18.18 Hz
Transmitter.......... ....On and Armed			17 m/s	19.32 Hz
Prop Direction...... ....Correct			18 m/s	20.45 Hz
Local Light............ ....On/Green			19 m/s	21.59 Hz
Frequency set...... ....____ Selected/Indicated			20 m/s	22.73 Hz
Temp. Set............. ....Set			21 m/s	23.86 Hz
Testers Ready....... ....Ready			22 m/s	25.00 Hz
Ready to Test....... ....Run Test			23 m/s	26.14 Hz
			24 m/s	27.27 Hz
Tunnel Shutdown			25 m/s	28.41 Hz
Test.................... ....Complete			26 m/s	29.55 Hz
Local Button......... ....Pressed			27 m/s	30.68 Hz
Coast Stop............ ....Stop			28 m/s	31.82 Hz
Temp. Set............. ....Off			29 m/s	32.95 Hz
Water................... ....Closed			30 m/s	34.09 Hz
Air....................... ....Closed			31 m/s	35.23 Hz
Power.................. ....Off			32 m/s	36.36 Hz
Ports.................... ....Open			33 m/s	37.50 Hz
Prop..................... .... Removed			34 m/s	38.64 Hz
Motor................... .... Removed			35 m/s	39.77 Hz
Ports.................... ....Closed/Secured				

Testing Checklists

M   Required Thrust MATLAB Script

```matlab
clear variables; close all; clear windows; clc;

%%%%Inputs%%%%
W = 50 * 4.44822;    %%N
W_low = 45 * 4.44822;
W_high = 55 * 4.44822;
b = 3.5;              %%m
S = 2.3;
CD_0 = 0.044;
CD_0low = 0.03;
%eff = .08;
K = 0.8;
T_max = 100;         %%N
CL_max = 1.2;        %%at 0 angle of attack


%%%%Constants%%%%
g = 9.81;            %%m/s^2
rho = 1.225;         %%kg/m^3
temp = 288.16;       %%K



%%%%%%%%%%%%%%%%%%%%%%%%%%%%%%%%%%%%%%%%%%%%%%%%%%%%%%%%%%%%%%%%%%%%%%%%%%%%%%
%%%%Plane Parameters%%%%
AR = b^2/S;
%K = 1/(pi * eff * AR);
WingLoading = W_low/S;                %%N/m^2
V_stall = sqrt(WingLoading / (.5 * rho * CL_max));
fprintf("Stall Velocity:        " + V_stall +          "        m/s \n")
fprintf("Takeoff Velocity:         " + 1.2*V_stall +      "        m/s \n")


syms V

%%%%%%%%%%%%%%%%%%%%%%%%%%%%%%%%%%%%%%%%%%%%%%%%%%%%%%%%%%%%%%%%%%%%%%%%%%%%%%
%%%%Level Trim%%%%
%%T=D, L=W
V_0 = 8;             %%m/s
V_f = 35;            %%m/s

%%Lift, Drag, Lift-to-Drag
CL = W / (0.5 * rho * V^2 * S);
CL_low = W_low / (0.5 * rho * V^2 * S);
CL_high = W_high / (0.5 * rho * V^2 * S);


%%varying weight
CD = CD_0 + K * CL^2;
CD_low = CD_0 + K * CL_low^2;
CD_high = CD_0 + K * CL_high^2;
D = 0.5 * rho * V^2 * S * CD;
D_low = 0.5 * rho * V^2 * S * CD_low;
D_high = 0.5 * rho * V^2 * S * CD_high;

%Plot CD vs. V
figure()
fplot([D_high D D_low], [V_0 V_f])
title("Drag = Thrust vs. Velocity at Trim");
xlabel("V (m/s)");
```

```matlab
ylabel("Thrust, Drag (N)");
legend("W = 55 lbs", "W = 50 lbs", "W = 45 lbs");


%%Varying drag coeff
CD_lowd = CD_0low + K * CL^2;
D_lowd = 0.5 * rho * V^2 * S * CD_low;
%Plot CD vs. Vfigure()
fplot([D D_lowd], [V_0 V_f])
title("Drag = Thrust vs. Velocity at Trim");
xlabel("V (m/s)");
ylabel("Thrust, Drag (N)");
legend("W = 50 lbs, CD_0 = 0.044", "W = 50 lbs, CD_0 = 0.03");

LD = CL / CD;
LD2 = W / D;
%%Plot L/D vs. V
figure()
fplot([LD LD2], [V_0 V_f])
title("Lift-to-Drag Ratio vs. Velocity at Trim");
xlabel("V (m/s)");
ylabel("L/D");

LD_max = sqrt(1/(4 * CD_0 * K));
fprintf("L/D Max:          " + LD_max +         "        \n")
V_minthrust = sqrt(2*W*sqrt(K/CD_0)/(rho*S));
CL_cruise = W / (0.5 * rho * V_minthrust^2 * S);
CD_cruise = CD_0 + K * CL_cruise^2;
fprintf("Minimum Required Thrust Cruise Velocity:        " + V_minthrust +        "       m/s↙
\n")

%%Min Required Thrust
T_min = W/LD_max;
fprintf("Minimum Required Thrust at Cruise:         " + T_min +         "       N \n")
```

N   Results for Propulsion Upgrade eCalc Tests

Hacker A60-16L V4 with a 22x10 prop (From the Hacker Motor Provided eCalc)													
Propeller	Throttle	Current (DC)	Voltage (DC)	el. Power	Efficiency	Thrust		Spec. Thrust		Pitch Speed		Speed Level	
rpm	%	A	V	W	%	g	oz	g/W	oz/W	km/h	mph	km/h	mph
1000	13	0.5	47.1	21.5	48.4	239	10.4	13.7	0.48	15	9	-	-
1500	20	1.1	47	52.3	67	660	23.3	12.6	0.44	23	14	-	-
2000	26	2.3	47	107.1	77.6	1174	41.4	11	0.39	30	19	-	-
2500	33	401	47	194	83.6	1834	64.7	9.5	0.33	38	24	-	-
3000	40	6.9	46.9	321.4	87.3	2641	93.2	8.2	0.29	46	28	-	-
3500	47	0.6	46.8	497.5	89.5	3595	126.8	7.2	0.25	53	33	-	-
4000	54	15.7	46.7	730.8	91	4695	165.6	6.4	0.23	61	38	51	31
4500	61	22.1	46.5	1030	91.9	5942	209.6	5.8	0.2	69	43	66	41
5000	68	30.3	46.4	1403	92.5	7336	258.8	5.2	0.18	76	47	73	46
5500	76	40.4	46.1	1860.4	92.9	8877	313.1	4.8	0.17	84	52	81	50
6000	**83**	**52.6**	**45.8**	**2409.2**	**93.1**	**10564**	**372.6**	**4.4**	**0.15**	**91**	**57**	**88**	**55**
6500	**91**	**67.3**	**45.5**	**3058.9**	**93.3**	**12398**	**437.3**	**4.1**	**0.14**	**99**	**62**	**86**	**59**
7000	99	84.8	45.1	3818.4	93.3	14379	507.2	3.8	0.13	107	66	103	64
7042	100	86.5	45	3891	93.2	14551	513.3	3.7	0.13	107	67	103	64

Hacker A60-18L V4 with a 22x10 prop (From the Hacker Motor Provided eCalc)													
Propeller	Throttle	Current (DC)	Voltage (DC)	el. Power	Efficiency	Thrust		Spec. Thrust		Pitch Speed		Speed Level	
rpm	%	A	V	W	%	g	oz	g/W	oz/W	km/h	mph	km/h	mph
800	12	0.3	47.1	14.1	37.8	188	6.6	13.4	0.47	12	8	-	-
1200	18	0.7	47	31.5	56.9	423	14.9	13.4	0.47	18	11	-	-
1600	24	1.3	47	61.2	69.5	751	26.5	12.3	0.43	24	15	-	-
2000	30	2.3	47	107.1	77.5	1174	41.4	11	0.39	30	19	-	-
2400	36	3.7	47	173.6	82.7	1690	59.6	9.7	0.34	37	23	-	-
2800	42	5.6	46.9	264.8	86.1	2301	81.2	8.7	0.31	43	27	-	-
3200	48	8.2	46.9	384.9	88.4	3005	106	7.8	0.28	49	30	-	-
3600	54	11.5	46.8	538.2	90	3803	134.1	7.1	0.25	55	34	-	-
4000	61	15.6	46.7	729.1	91.2	4695	165.6	6.4	0.23	61	38	51	31
4400	67	20.7	46.6	961.9	92	5681	200.4	5.9	0.21	67	42	65	40
4800	73	26.7	46.4	1240.9	92.6	6761	238.5	5.4	0.19	73	45	71	44
5200	80	34	46.3	1570.6	93	7935	279.9	5.1	0.18	79	49	76	47
5600	87	42.5	46.1	1955.4	93.3	9202	324.6	4.7	0.17	85	53	82	51
6000	**93**	**52.4**	**45.8**	**2399.8**	**93.5**	**10564**	**372.6**	**4.4**	**0.16**	**91**	**57**	**88**	**55**
6375	100	63.1	45.6	2875.7	93.6	11925	420.6	4.1	0.15	97	60	94	58

Hacker A60-14L V4 with a 22x10 prop (From the Hacker Motor Provided eCalc)													
Propeller	Throttle	Current (DC)	Voltage (DC)	el. Power	Efficiency	Thrust		Spec. Thrust		Pitch Speed		Speed Level	
rpm	%	A	V	W	%	g	oz	g/W	oz/W	km/h	mph	km/h	mph
1200	14	0.7	47	31.7	56.6	423	14.9	13.3	0.47	18	11	-	-
1800	21	1.8	47	82.3	73.6	951	33.5	11.6	0.41	27	17	-	-
2400	28	3.7	47	174.5	82.3	1690	59.6	9.7	0.34	37	23	-	-
3000	35	6.9	46.9	322.8	86.9	2641	93.2	8.2	29	46	28	-	-
3600	42	11.6	46.8	541.8	89.4	3803	134.1	7	0.25	55	34	-	-
4200	50	18.2	46.6	846.2	90.9	5176	182.6	6.1	0.22	64	40	60	37
4800	57	27	46.4	1251.1	91.8	6761	238.5	5.4	0.19	73	45	71	44
5400	65	38.4	46.2	1771.7	92.3	8557	301.8	4.8	0.17	82	51	79	49
600	**73**	**52.9**	**45.8**	**2423.4**	**92.6**	**10564**	**372.6**	**4.4**	**0.15**	**91**	**57**	**88**	**55**
6600	**82**	**71**	**45.4**	**3222**	**92.7**	**12782**	**450.9**	**4**	**0.14**	**101**	**63**	**97**	**60**
7200	90	93.3	44.9	4183.2	92.7	15212	536.6	3.6	0.13	110	68	106	66
7800	100	120.5	44.2	5323.3	92.6	17853	629.7	3.4	0.12	119	74	115	71
7811	100	121.2	44.2	5355.3	92.5	17904	631.5	3.3	0.12	119	74	115	71